Characterization of Repulsive Slit / Robo Signalling in Neural Crest Cell Migration and Sensory Axon Guidance in the Chicken Embryo

---

Dissertation

zur

Erlangung der naturwissenschaftlichen Doktorwürde
(Dr. sc. nat)

vorgelegt der

Mathematisch-naturwissenschaftlichen Fakultät

der

Universität Zürich

von

Marc Debrunner

von

Winterthur ZH

Promotionskomitee

Prof. Dr. Esther T. Stoeckli (Leitung der Dissertation)
Prof. Dr. Stephan Neuhauss
Prof. Dr. Dieter Zimmermann

Zürich, 2010

Table of Contents

1. Summary

Extracellular Slits and their transmembrane receptors, the Robos, represent a well characterized repulsive guidance system which is involved in different processes of axon guidance and migration of cells in invertebrates and vertebrates. In my dissertation, we dissected the role of Slits and Robos in axon guidance of sensory and motoneurons and their involvement in early neural crest cell migration. Robo1 and Robo2 are expressed in migrating neural crest cells, DRGs, motoneurons and interneurons of the spinal cord. Robo3 is only expressed in interneurons of the spinal cord. Slits are expressed along the migratory path of neural crest cells and the trajectories of sensory and motor axons. Downregulation of Robo1, Robo2 and members of the Slit family led to ectopic neural crest cells within the posterior part of the sclerotome and the dermomyotome and to perturbed formation of DRGs, dorsal roots and peripheral sensory branches as well as motoneurons. The metameric segregation was disturbed, DRGs and dorsal roots were elongated and fused and peripheral branches defasciculated. Overexpression of human and mouse Slits resulted in smaller DRGs and in the almost complete lack of dorsal roots and peripheral sensory branches as well as motoneurons. All three Slits strongly repelled DRG neurites *in vitro* and *in vivo*. Furthermore, we analysed the targeting of a subpopulation of nociceptive and proprioceptive sensory collaterals using Fast DiI as a tracer. Nociceptive collaterals showed pathfinding errors in embryos with impaired Robo1, Robo2, Slit1 and Slit3. Proprioceptive collaterals were severely affected only in Slit3 deficient embryos. Boundary cap cell clustering at the DREZ was affected in Robo1, Robo2 and Slit1-3 deficient embryos. The clusters were not properly segregated and aligned at the DREZ in the anterior and posterior somitic compartment. Thus, my results provide new insight in the function of Slit / Robo signalling in neural crest cell migration and in the development of the peripheral nervous system.

2. Zusammenfassung

Slits, extrazellulär sezernierte Glykoproteine, und ihre Transmembranrezeptoren, die Robos (Roundabouts), spielen eine wichtige Rolle als Wegweisermoleküle während der Entwicklung des peripheren und zentralen Nervensystems in Wirbellosen und Wirbeltieren und sind meistens hoch konserviert zwischen den Spezies. Die Familie der Robos setzt sich aus vier Proteinen zusammen, genannt Robo1-4. Drei Slit Gene wurden identifiziert. Die genaue Analyse ihrer Expressionsmuster in Hühnerembryonen zwischen dem Hamburger / Hamilton Stadium 14 und Stadium 42 weist darauf hin, dass Slits und Robos für die Wanderung der Neuralleistenzellen und die Enwicklung der sensorischen und motorischen neuronalen Netzwerke wichtige Funktionen ausüben. Robo1 und Robo2 sind in Neuralleistenzellen, in Spinalganglien, in Motoneuronen und Interneuronen des Rückenmarks exprimiert. Robo3 ist nur in Interneuronen des Rückenmarks exprimiert. Slit1-3 werden von Zellen entlang der Migrationswege von Neuralleistenzellen und entlang der Bahnen der auswachsenden sensorischen und motorischen Axone exprimiert. Zudem sind sie in der Region der Bodenplatte (Slit1-3), entlang des Zentralkanales (Slit1 und 3), in der Region der Dachplatte (Slit 1-3), im ventralen Horn (Slit 1-3) und in der Nähe des Motor axon exit point (MEP, Slit1 und 3) exprimiert.

Um die Funktionen der Robos und Slits in der Wanderung der Neuralleistenzellen und axonalen Wegfindung der sensorischen und Motoneuronen zu untersuchen, nutzten wir *in ovo* RNAi und Überexpressionsexperimente, gefolgt von Färbungen mit Neurofilament- und anderen Antikörpern an ganzen Embryonen und auf Quer- und Längsschnitten. Störung der Robo1, Robo2 und Slit1-3 Funktion mittels *in ovo* RNAi führte zu ektopischen Neuralleistenzellen im posterioren Teil der Somiten und im Dermamyotom und zur Aufhebung der metameren Segregation der Spinalganglien. Zentrale und periphere sensorische Fasern genauso wie die Axone von Motoneuronen machten Fehler in der Wegfindung in der Peripherie. Die Spinalganglien und Hinterwurzeln waren teilweise fusioniert und die peripheren Ausläufer defaszikuliert. Slit Überexpression führte zu verkleinerten Spinalganglien und zu starker Reduktion der Hinterwurzeln sowie der peripheren sensorischen und motorischen Nerven. *In vitro* Experimente, bei denen dissoziierte sensorische Neuronen oder ganze Spinalganglien auf einem Monolayer von Slit-exprimierenden COS-7 Zellen kultiviert wurden, zeigten, dass alle drei Slits das Neuritenwachstum stark hemmten.

Zudem analysierten wir die Wegfindung von nozizeptiven (Schmerz-leitenden) und propriozeptiven (Reflexbogen) Kollateralen im Zentralnervensystem mit dem Tracer Fast DiI. Nozizeptive Kollateralen zeigten Wegfindungsfehler in Embryonen mit gestörter Robo1, Robo2, Slit1 und Slit3 Funktion. Die Zielfindung der propriozeptiven Kollateralen war in Embryos mit gestörter Slit3 Funktion fehlerhaft. Zusammenfassend zeigen meine Resultate neue Funktionen der Robos und Slits in der Migration der Neuralleistenzellen und in der Wegfindung der sensorischen und motorischen Axone in der Entwicklung des peripheren und zentralen Nervensystems im Hühnerembryo.

3. Introduction

3.1 Neural crest cell migration

Neural crest cells emerge and delaminate in early vertebrate development from the dorsal neural tube shortly after its closure. They start their journey as multipotent stem cells and migrate along distinct pathways guided by receptors on their surface and using permissive substrates along their trajectory as well as inhibitory/repulsive molecules in adjacent tissues. Trunk neural crest cells choose between a ventro-medial and a dorso-lateral pathway and migrate in different waves. Neural crest cells that select the former pathway start their journey earlier (therefore called early neural crest cells), migrate only into the anterior part of the developing somite/sclerotome and form Schwann cells, satellite cells, boundary cap cells, sensory, sympathetic and parasympathetic neurons. Neural crest cells choosing the latter pathway migrate in a later wave (for this reason called late neural crest cells), choose a dorso-lateral route between the ectoderm and dermomyotome and become melanocytes in the skin.

3.2 Axon Guidance

The nervous system is the most complex organ, evolution has created. Billions of neurons have to be organised and connected to each other in a correct manner. As an extending axon navigates towards its target, the trajectory is determined by its responses to different environmental cues. Once the growth cone, the tip of the elongating axon, has reached its target, it converts into a synapse which then passes information to the neighbouring cell. Because neuronal regeneration after injury is to a certain extent a recapitulation of development, studying the mechanism of axon guidance will not only help to discover the causes of various neurological disorders due to erroneous axonal guidance, but also shed light on potential ways of clinical treatment of the injured nervous system. A growing number of guidance molecules including also morphogens have been identified, but our knowledge is still too limited to fully understand these complex processes. Together with their interacting partners, these pathfinding molecules serve as attractive or repulsive cues, acting locally or over some distance to obtain proper wiring of the nervous system.

3.3 The principle of neural crest and axonal pathfinding: Long-range and short-range forces, attraction versus repulsion

Neural crest cells and the growth cones of axons integrate multiple signals from the environment. As they migrate or elongate, respectively, they come in contact with many types of cells. Secretion of local cues by the surrounding tissue and intermediate targets or expression on the surface of adjacent cells provides information for the migrating neural crest cells and growing axons. This mechanism is called contact-mediated short-range guidance. Contact-mediated attraction and repulsion are distinguished. For long-range guidance, target cells secrete diffusible pathfinding molecules that travel over some distances in the extracellular matrix (ECM) and attract or repel the migrating neural crest cell or growth cone (Fig. 1).

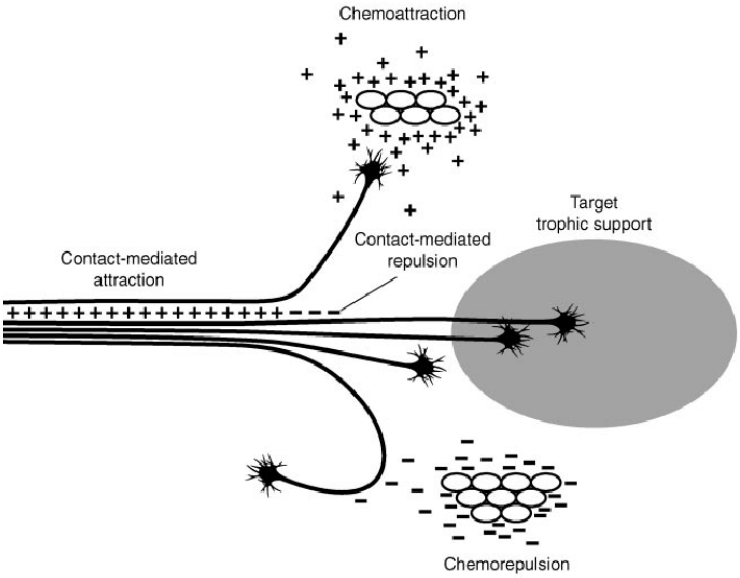

Figure 1 Schematic representation of the four different forces guiding axons: Short-range cues are divided up in contact repulsion and -attraction and long-range cues in chemorepulsion and -attraction (from Huber et al., 2003).

3.4 Growth cones

The growth cone is a highly motile structure at the tip of the axon that integrates the abundance of signals present in its environment (Fig. 2). It translates these signals into structural changes of the cytoskeleton that determine the rate and direction of axonal extension. The leading tip of a growth cone is composed of filopodia, finger-like structures containing bundled F-actin, which sense the extracellular environment, and of lamellipodia, web-like cytoplasmic structures composed of an actin filament network. When an axon guidance cue binds to its receptor located on filopodia or lamellipodia, an intracellular pathway is activated and the growth cone is guided towards or away from the source of the guidance molecules. The relative rate of Actin polymerisation in the proximal and actin depolymerisation in the distal part of the growth cone regulates the advancement or retraction, respectively. At the distal end of the growth cone microtubules are arranged to transport molecules from and towards the neuronal soma (Fig. 3; Huber et al., 2003).

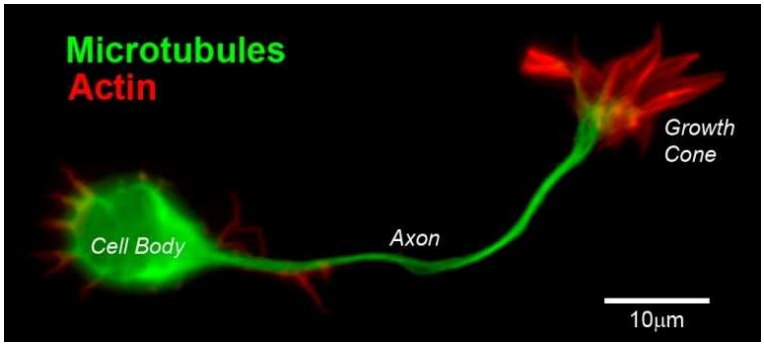

Figure 2 Organisation of a neuron: a neuron is composed of a cell body, the neuronal soma, an elongating branch, the axon with a highly specialised dynamic tip, the growth cone. Microtubules and actin filaments are responsible for shape and morphology (from http://sites.google.com/a/blueprint.org/sandbox).

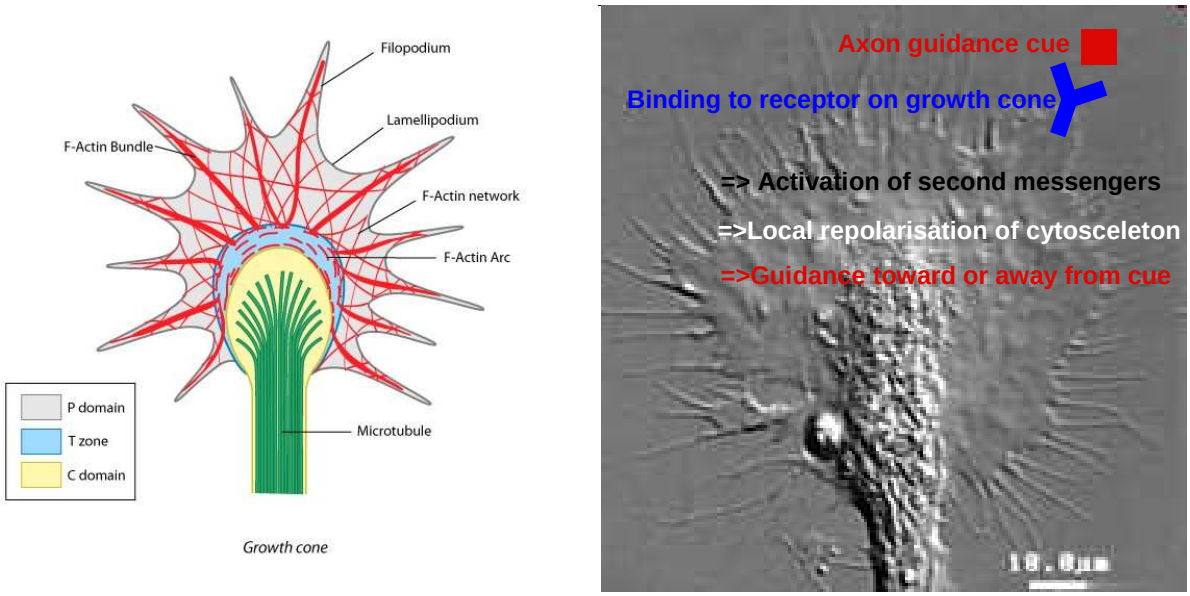

Figure 3 Growth cone structure and organisation. Finger-like filopodia and web-like cytoplasmic lamellipodia that sense the extracellular environment are the main structures in the peripheral domain of a migrating growth cone. The central domain is mainly composed of microtubules (Left: schematic representation from http://handbook.blueprint.org/Home/glossary-of-terms/mechano-glossary--g/mechano-glossary-growth-cone; Right: picture adapted from http://cellbio.emory.edu/lab/zheng/overview.htm).

3.5 Dorsal root ganglia

Dorsal root ganglia are metameric structures of the peripheral nervous system and provide the brain with sensory input. Early neural crest cells aggregate in chicken embryos at around HH17 on both sides of the spinal cord in the trunk in a segregated metameric manner and differentiate into bipolar sensory neurons, Schwann cells, and satellite cells. Together they form the dorsal root ganglion (DRG). The ventrally extending axon, called peripheral branch extends into the periphery and innervates skeletal and limb muscles and other target tissue. The central branch or so-called dorsal root extends towards the spinal cord, enters it at the dorsal root entry zone (DREZ) from where it bifurcates and elongates rostrally and caudally. At about HH29 central collaterals start to invade the grey matter. Sensory neurons of the DRG are divided into different classes depending on their modality. In humans and chicken, but not in rodents, the different subpopulations are more or less segregated in the DRG (Fig. 4; Snider, 1994). Nociceptive neurons with small-diameter axons have their somas concentrated in the dorsal part of the DRG. Mechanoreceptive neurons are located in the central part of the DRG. Proprioceptive neurons, the myelinated large-diameter muscle spindle afferents are positioned in the ventro-lateral part of the DRG. Due to their different modalities, these different neuronal types have to grow into subpopulation-specific target layers in the spinal cord. Nociceptive fibres extend to the dorsal-most layers (lamina I – II) (Ruit et al., 1992; Crowley et al., 1994; Smeyne et al., 1994; Snider, 1994), where they synapse with interneurons which ascend to the brain. Mechanoreceptive neurites grow to deeper layers (lamina III to VI) in the grey matter and proprioceptive fibres extend collaterals to the ventral horn, where they form synapses that connect to motoneurons (Davis et al., 1989; Ozaki and Snider, 1997).

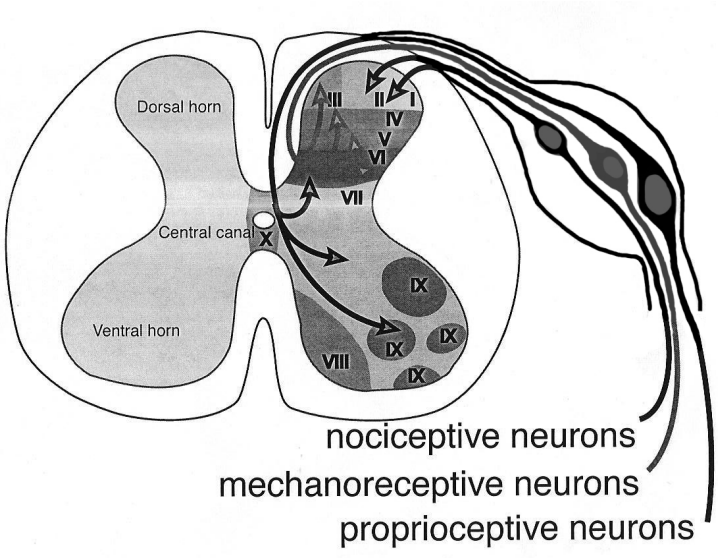

Figure 4 Schematic cross section through a chicken spinal cord. Nociceptive sensory neurons are located in the dorsal part of the DRG and their axons grow into the dorsal-most layers (Lamina I-II) of the grey matter. Mechanoreceptive neurons have their somas concentrated in the central part of the DRG and their axons migrate to deeper layers (lamina III to VI). Proprioceptive neurons are positioned in the ventral part of the DRG and extend collaterals to the ventral horn, where they synapse with motoneurons (adapted drawing from M. Philipp).

3.6 Spinal cord and nearby tissues (notochord, somite, sclerotome and dermomyotome): Their role in neural crest cell migration and DRG axon guidance

The notochord is a transient rod-like structure (Fig. 5). It arises from mesodermal cells, is evolved in earliest chordates as a structure for muscle attachment and is found in all embryos of vertebrates. However during embryonal development of most vertebrates it degenerates and its supporting function gets replaced by the vertebrae. Around the notochord the perinotochordal sclerotomal cells are located. There is *in vitro* and *in vivo* evidence that the notochord and the perinotochordal sclerotomal cells are sources of repulsive cues both for migrating neural crest cells and DRG axons. At least three different chemorepellents, Semaphorin3A, Chondroitin sulphate proteoglycans (CSPGs), and an unknown chemorepellent interacting with TAG-1/Axonin-1 may mediate the chemorepulsive effect (Masuda and Shiga, 2005).

The somites are segmental units that arise from paraxial mesoderm (Fig. 5 and 6). They were first described by Balfour 1881, followed by a more detailed description by Williams 1910. They are surrounded by a basement membrane that is connected with the nearby tissue by extracellular matrix (ECM) components. The somites are embedded between the neural tube and notochord medially, the surface ectoderm dorsally, and the endoderm and aorta ventrally. Laterally, the somite is connected with the lateral plate mesoderm by a continuous cell layer, the intermediate mesoderm, with the Wolffian duct on its dorsal side. Before segmentation, the rostral part of the presomitic mesoderm undergoes a mesenchymal-to-epithelial transition (MET), with the exception of the cells lying inside, which keep their mesenchymal organization to form the cells of the somitic core, the somitocoele cells. The other cells rearrange to surround these core cells. Somites emerge in a rostro-caudal direction by a closely timed mechanism, triggered by Notch and Delta signalling. The rostro-caudal gradient is set up by Fibroblast growth factor (FGF) and a pair of somites is generated in avian embryos every 90 minutes. The somites display a metameric pattern within the embryo that determines the segmental arrangement of the vertebrae, rib cage, muscles, ligaments and blood vessels (Christ et al., 1972, 1979, 1998). The metamerism of these structures is the precondition for the ability of the body to execute bending and rotating movements (Christ et al., 2004).

The sclerotome emerges from the ventral part of the somite (Fig. 5 and 6). It has been demonstrated that the initiation and maintenance of the sclerotome depends on both Sonic hedgehog (Shh) and Noggin, a Bmp4 antagonist, which are both expressed in the notochord when the sclerotome is developing (Fan and Tessier-Lavigne, 1994; Johnson et al., 1994; Fan et al., 1995; Marti et al., 1995; Müller et al., 1996; McMahon et al., 1998). The size of the sclerotome is the result of the balance between dorsal and ventral signals. Dorsal signals promote the development of the dorsally located dermomyotome and suppress sclerotome formation (Ikeya and Takada, 1998; Olivera-Martinez et al., 2001). These signals are produced by the dorsal neural tube and the surface ectoderm, and are mediated by the Wnt family of signalling molecules and their receptors (Hoang et al., 1998; Cauthen et al., 2001). The ventral signals including Shh and Noggin promote sclerotome formation. A detailed schematic representation of the development and formation of the avian sclerotome is shown in Figure 6.

The dermomyotome arises from the dorsal part of the somite (Fig. 5 and 6). It is a transient structure lying in between the sclerotome and the surface ectoderm. Most of the mesodermal tissues in the body emerge from the dermomyotome, including cell types as different as muscle, connective tissue, endothelium, dermis and cartilage. The dermomyotome is subdivided into the underlying myotome which gives rise to all skeletal muscles and the epithelial dermomyotome, source of the dorsal dermis.
The fate of the dermomyotome is determined by dorsalizing signals from adjacent structures. *In vivo* and *in vitro* experiments in the chicken embryo have established that the dorsalizing signals are Wnts, secreted by the dorsal neural tube and the dorsal surface ectoderm (reviewed in Brent and Tabin, 2002; Scaal and Christ, 2004).

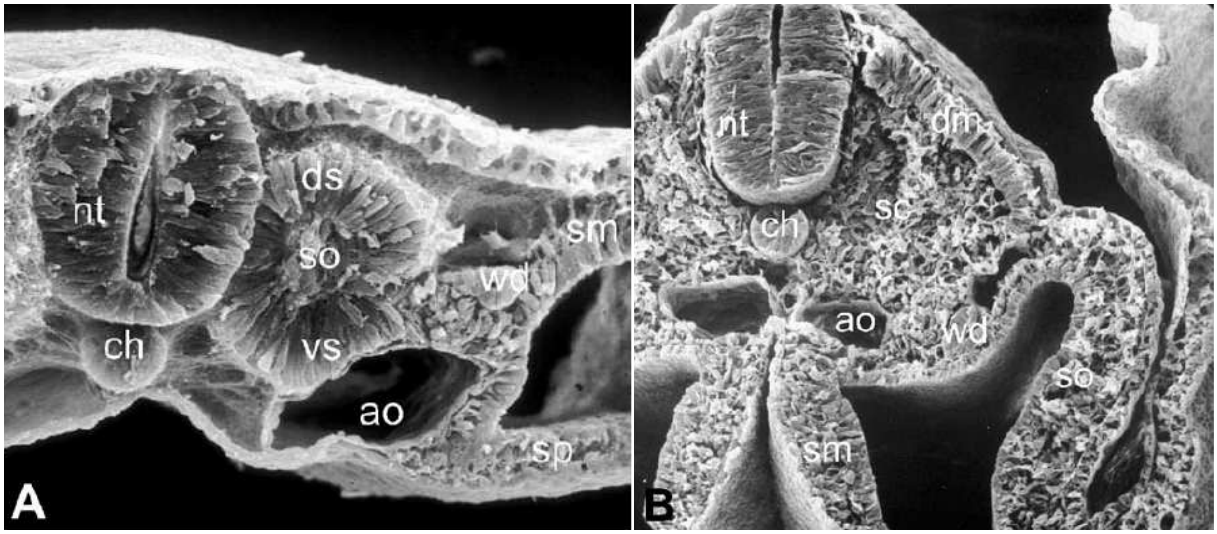

Figure 5 Scanning electron microscopic pictures of transverse fractures of a 2-day (A) and a 3-day (B) chicken embryo (ao aorta, ch notochord, dm dermomyotome, ds dorsal somite, nt neural tube, sc sclerotome, so somitocoele, sm somatopleure, sp splanchnopleure, vs ventral somite, wd Wolffian duct; from Christ et al., 2004).

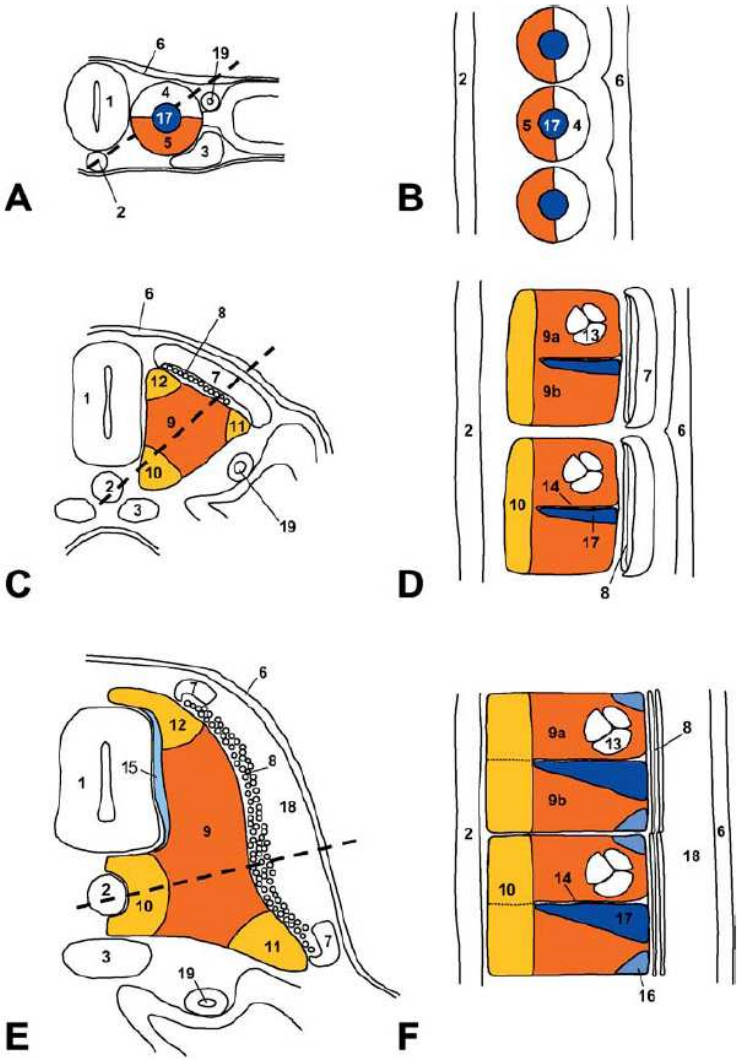

Figure 6 (A–F) Schematic drawing of transverse (A, C, D) and longitudinal (B, D, F) sections of chick embryos at different developmental stages. (A, B) Epithelial somites at HH14-15. (C, D) Somites after compartmentalization at HH17/18. (E, F) Mature somites at HH20/22. The broken line in A, C, E indicates the section plane of B, D, E. 1 neural tube, 2 notochord, 3 aorta, 4 dorsal half-somite, 5 ventral half-somite, 6 surface ectoderm, 7 dermomyotome, 8 myotome, 9 central sclerotome, 9a cranial half of central sclerotome, 9b caudal half of central sclerotome, 10 ventral sclerotome, 11 lateral sclerotome, 12 dorsal sclerotome, 13 spinal nerve, 14 von Ebner's fissure, 15 meningotome, 16 syndetome, 17 somitocoele cells/arthrotome, 18 dermis, 19 Wolffian duct (from Christ et al., 2004).

The expression of permissive substrata and attractive cues in the developing somite/sclerotome helps moving neural crest cells and extending sensory axons finding their way. Repulsive guidance systems, with receptors expressed on migrating neural crest cells and sensory neurites, and ligands, secreted or presented from posterior somitic, sclerotomal and dermomyotomal cells, are important for the guidance of neural crest cells into the ventro-medial pathway through the rostral part of the somite and for proper extension of sensory neurites. The following guidance systems which will be discussed later in more detail play important roles: EprinBs with the receptors EphBs (Krull et al., 1997; Wang and Anderson, 1997; Poliakov et al., 2004; Davy and Soriano, 2005), secreted class3 Semaphorins, namely Semaphorin3A and Semaphorin3F, together with Neuropilin1 and Neuropilin2, and Plexins receptor complexes (Gammill et al., 2006; Roffers-Agarwal and Gammill, 2009; Schwarz et al., 2009;

Eickholt et al., 1999), the chondroitin sulphate proteoglycans versican V0 and V1 (Dutt et al., 2006), F-spondin (Debby-Brafman et al., 1999), T-cadherin (Rantsch and Bronner-Fraser, 1991) and the Slit / Robo system (Yuan et al., 1999; Vargesson et al., 2001; De Bellard et al., 2003; Jia et al., 2005).

3.7 Pathfinding of central and peripheral branches of DRG neurites

Sensory axons navigate over long distances in the periphery of the growing embryo. They need a whole set of guidance cues to find and connect to the correct target. Attractive long-range guidance cues attract them and repulsive molecules shape sharp borders to form the path of migration. Neural crest cells first migrate to their destination along the neural tube, differentiate into a bipolar neuron that extends its processes towards and into the spinal cord via the dorsal root entry zone (DREZ) and towards the peripheral target tissue. When the central branch of the sensory axon reaches the DREZ, it bifurcates and extends two processes rostrally and caudally from where collaterals later sprout into the gray matter to connect to the correct target layer. Therefore, sensory neurons represent a linker between the CNS and the PNS. It is a multistep journey with several intermediate stops where the growth cone processes a multitude of guidance cues. For the extension of central branches towards the DREZ only few factors are known in vertebrates, namely F11/Contactin (Perrin et al., 2001) and Semaphorin3A together with Neuropilin1 (Gammill et al., 2006; Roffers-Agarwal and Gammill, 2009; Schwarz et al., 2009).

3.8 Molecules involved in neural crest cell migration and sensory axon pathfinding

An enormous number of guidance cues and receptors for neural crest cell migration and sensory axon guidance have been identified and characterized up to now. The large number is not surprising given the complexity of nervous system wiring. The guidance cues and their receptors can be classified into different families according to sequence similarity and conserved regions both on DNA and on protein level: Neurotrophins and Receptor Protein Tyrosine Kinases (Trk); Semaphorins, Plexins and Neuropilins (Nrp); Eph receptors and Ephrins; Chondroitin sulfate proteoglycans (CSPGs) and other extracellular matrix proteins (e.g. Collagen, Fibronectin, Tenascin); Immunoglobulin superfamily cell adhesion molecules (IgSF CAMs) like TAG1/Axonin-1, Deleted in colorectal cancer (Dcc), the receptor for Netrin; morphogens such as Sonic hedgehog (Shh), Bone morphogenic proteins (BMPs) and Wnts. In my dissertation I focussed on the Slit / Robo system. In the following chapter I introduce the guidance systems which are involved in neural crest cell migration and sensory axon guidance.

3.8.1 Neurotrophins and their receptors

The neurotrophins build a family of four proteins, all of which bind to the low affinity nerve growth factor receptor P75 (LNGFR) and to one of the family members of the high affinity receptors that are discussed later. They include Nerve Growth Factor (NGF), Brain Derived Neurotrophic Factor (BDNF), Neurotrophin-3 (NT-3), and Neurotrophin-4 (NT-4). These growth factors are critical for the survival and maintenance of sympathetic and sensory neurons. They are secreted from the target tissue, bind

to and activate their high affinity receptor tyrosine kinases (TrkA, TrkB or TrkC). Sensory neurons have also been characterized based on their dependence from these neurotrophins. Nociceptive neurons are NGF dependent and proprioceptive Ia muscle afferents are NT-3 dependent (Ernfors et al., 1994; Klein et al., 1994; Tessarollo et al., 1994; Snider, 1994). TrkA is expressed on nociceptive sensory afferents and binds NGF. TrkB is the receptor for BDNF (Brain-derived nerve growth factor) and with lower affinity for NT-3 and is expressed on mechanoreceptive neurons. TrkC binding the ligand NT-3 is located on proprioceptive neurons. Limb ablation experiments (when the neurotrophin secreting limbs are cut off) lead to a reduction of sensory and motoneurons innervating it and knockout mice lacking either a receptor or a ligand show similar phenotypes (Snider et al., 1994). Injections of either NGF or NT-3 into the flank of the embryo after limb ablation, selectively rescue nociceptive or proprioceptive neuron populations (Caldero et al., 1998; Bourikas, 2005, dissertation).

3.8.2 Migration-promoting ECM molecules: Collagen, Laminin, Fibronectin, Tenascin and Thrombospondin-1

The extracellular matrix molecules Laminin and Fibronectin promote enhanced neural crest cell migration but are expressed in the whole somite indicating that negative guidance cues might play more important roles in guiding neural crest cells (Rovasio et al., 1983, Rickmann et al., 1985). Only one Laminin subunit, namely Laminin α5, was shown to restrict neural crest cells moving along their migratory pathways and aggregating into sympathetic ganglia. Laminin α5 is needed for migration and timely differentiation of neural crest populations (Coles et al., 2006). Fibronectin is an extracellular matrix glycoprotein that binds to Integrins, collagens, fibrin and heparan sulfate proteoglycans. Two types of Fibronectin are present in vertebrates, a soluble form in the plasma and an insoluble form in the ECM. Fibronectin plays a role in cell adhesion, growth, migration and differentiation of different cell types. Furthermore Collagens (Perris et al., 1991), Tenascin (Stern et al., 1989; Tucker and McKay, 1991) and Thrombospondin-1 (Tucker et al., 1999) are molecules promoting neural crest cell migration. Collagens build a large group of proteins. They are located in the ECM and are the most abundant protein in mammals. Tenascins are large multimeric glycoproteins that are highly conserved among vertebrates (Chiquet-Ehrismann and Chiquet, 2003). In mammals, the family is composed of four members. They are built of an amino-terminal cysteine-rich oligomerization region composed of helical heptad repeats, EGF-like elements, fibronectin type III-repeats (FN III) and a carboxyl-terminal Fibrinogen-like globular domain (Zimmermann and Dours-Zimmermann, 2008). Thrombospondin-1 (TSP-1) is a large multifunctional glycoprotein. It was first found in platelets that had been stimulated with thrombin. Functions for TSP-1 have been found in multiple biological processes including angiogenesis, apoptosis, activation of TGF-beta, Immune regulation and in neural crest cell migration as a potent promoter of migration and adhesion. TSP-1 has multiple receptors, among which Integrins are of particular interest (Tucker et al., 1999).

3.8.3 Semaphorins, Plexins and Neuropilins

Semaphorins are a large family of secreted and cell membrane-bound molecules, which are implicated in many biological processes as divers as regulation of axon guidance, cell migration, immune function, angiogenesis or cancer. At least 20 Semaphorins, divided into seven subclasses and named according to structural similarities have been described (Fig. 7). An additional group comprises viral Semaphorins. Semaphorins can also be classified due to their structure as secreted, membrane glycosylphosphatidylinositol (GPI) -anchored or transmembrane molecules (Fig. 8). A subset of Semaphorins interacts with Neuropilins (Nrp1 and Nrp2), membrane bound co-receptors that lack an intracellular cytoplasmic domain and are exclusively found in mammals and avians (Fig. 7 and 8). Plexins, another family of transmembrane molecules, have been identified as high affinity Semaphorin receptors (Fig. 7 and 8). Nine different Plexins have been found in the mammalian genome. They are classified into four different subfamilies (A-D). Their large cytoplasmic domains include the conserved sex-plexin (SP) domain which is thought to activate intracellular signalling pathways. Besides Neuropilins and Plexins, Semaphorins interact and bind to additional molecules (Fig. 9).

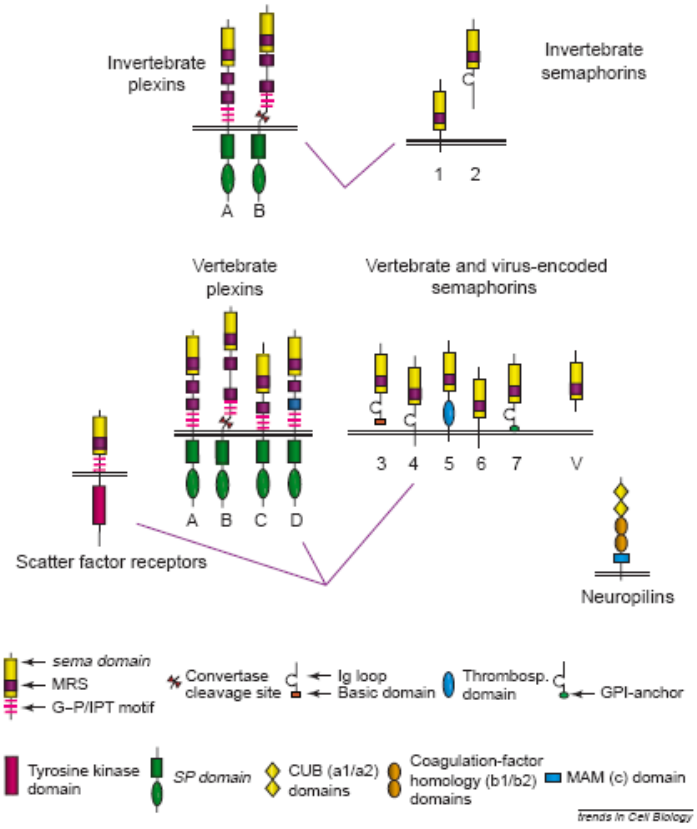

Figure 7 Semaphorins and their receptors, the Plexins and Neuropilins. Semaphorins and Plexins share *sema domains.* Semaphorins are classified into eight different subfamilies (Semaphorin 1- 7 and a virus encoded Semaphorin), Plexins are classified into four families (Plexins A to D). Abbreviations: G–P/IPT motif, glycine–proline repeat3/immunoglobulin-like fold66; GPI, glycosylphosphatidylinositol; *SP domain*, sex-plexin domain; CUB domain, complement-homology domain; MAM domain, meprin/A5/mu-phosphatase homology domain (from Tamagnone and Comoglio, 2000).

Semaphorins, Neuropilins and Plexins are expressed in embryonic and adult tissues and have a broad spectrum of functions. In vitro and in vivo experiments have unravelled that Semaphorins act in the pathfinding of elongating axons and dendrites, in axon branching, axon pruning (Bagri et al, 2003) and axon degeneration (He et al., 2002; Tamagnone and Comoglio, 2004). Furthermore, Semaphorins are implicated in guidance of a range of migrating cells. They direct oligodendrocyte migration (Spassky et al., 2002), function in the glial ensheathment of axons (Oster et al., 2003) and the migration of neural crest cells (Eickholt et al., 1999; Tamagnone and Comoglio, 2004). Defects in neural crest cell migration lead to mispositioning of cells in the sclerotome and in the developing cardiovascular system (Behar et al., 1996; Brown et al., 2001; Tamagnone and Comoglio, 2004). Recent studies on Neuropilin / Semaphorin signalling in vertebrates demonstrated that this family of guidance cues is involved in proper formation of both metameric neural crest cell patterning and segmented dorsal root gangliogenesis in vivo (Gammill et al., 2006; Roffers-Agarwal and Gammill, 2009; Schwarz et al., 2009). Whereas Neuropilin2 and Semaphorin3F is required for segmental neural crest cell migration, Neuropilin1 together with Semaphorin3A is necessary for metameric DRG segregation (Gammill et al., 2006; Roffers-Agarwal and Gammill, 2009; Schwarz et al., 2009). Semaphorin3A plays a role in controlling endothelial cell migration and angiogenesis (Miao et al., 1999; Serini et al., 2003; Shoji et al., 2003). A repulsive effect of Semaphorin3A on nociceptive sensory fibres has been shown in vitro and in vivo (Messersmith et al., 1995; Puschel et al., 1996; Shepherd et al., 1997). Semaphorin3A is expressed in the ventral horn of the spinal cord and was proposed to prevent NGF-dependent nociceptive fibres from migrating ventrally. NT-3-dependent proprioceptive axons do not express Neuropilin-1, a component of the Semaphorin3A receptor which is required to mediate the repulsive effect and which is expressed on nociceptive fibres (He and Tessier-Lavigne, 1997; Kolodkin et al., 1997; Fu et al., 2000). Additionally, Semaphorins control epithelial cell migration and morphogenesis (Fujii et al., 2002; Ginzburg et al., 2002; Giordano et al., 2002), as well as leukocyte migration (Delaire et al., 2001; Tamagnone and Comoglio, 2004). Semaphorins have been mainly described as inhibitory molecules because they repel migrating cells and axons and cause collapse of axonal growth cones (Tamagnone and Comoglio, 2004). However, it has been shown that Semaphorins can also administrate cell chemotaxis, axon/dendrite outgrowth and attraction (Polleux et al., 2000; Giordano et al., 2002; Moreno-Flores et al., 2003; Pasterkamp et al., 2003; Tamagnone and Comoglio, 2004). Different Semaphorin receptor complexes may mediate these opposite responses (Tamagnone and Comoglio, 2004). Additionally, it was shown that Semaphorin function can be modulated by the intracellular levels of cyclic nucleotides, that convert a repulsive into an attractive signal (Song et al., 1998; Castellani et al., 2002; Tamagnone and Comoglio, 2004).

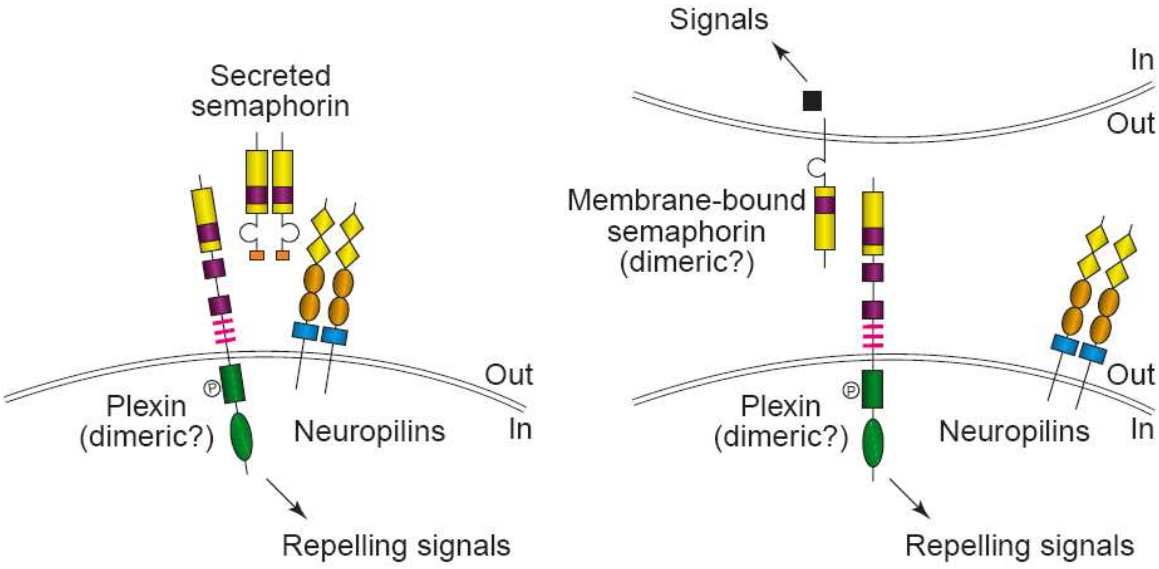

Figure 8 Schematic representation of receptor complexes of secreted (subclass 3) or membrane-bound Semaphorins, Plexins (probably dimeric) and Neuropilins (homo- or heterodimeric). Plexins are required for the Semaphorin-binding specificity and mediate the intracellular signalling; Neuropilins are needed for binding. Membrane-bound Semaphorins bind to Plexins and transmit intracellular signals through the sex-plexin (SP) domain. Transmembrane Semaphorins might produce bidirectional signals by associating with cytoplasmic transducers (black box; from Tamagnone and Comoglio, 2000).

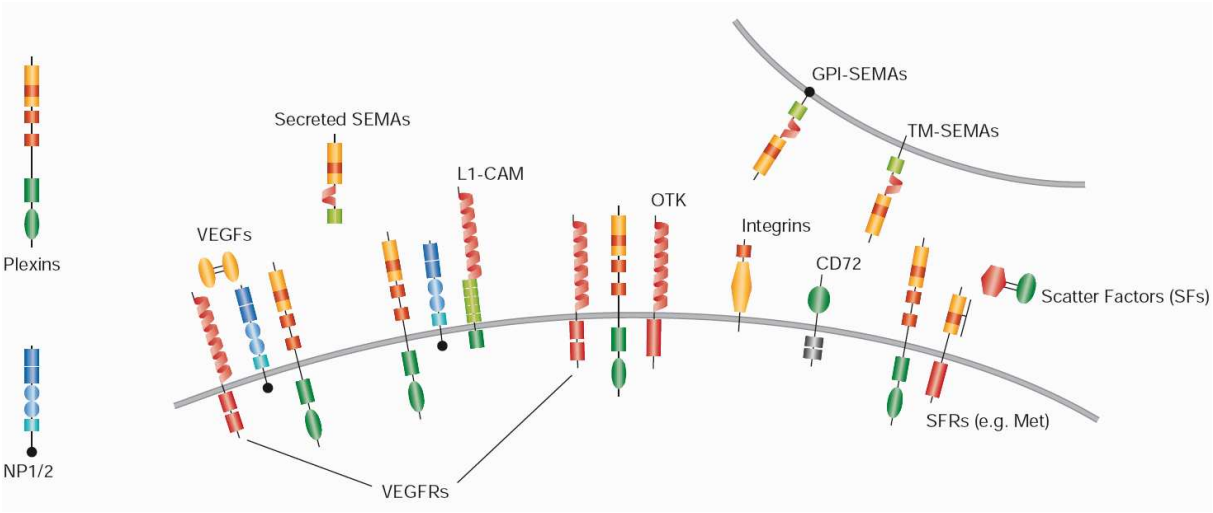

Figure 9 Semaphorin receptor complexes. Besides Plexins and Neuropilin 1 and 2, Semaphorin can interact and bind to additional molecules including: Cell adhesion molecule L1 (L1-CAM) and receptor tyrosine kinases, scatter-factor receptors (SFRs), Integrins and vascular endothelial growth factor receptors (VEGFRs). Neuropilins bind as co-receptors both secreted Semaphorins and VEGFs. GPI, glycosylphosphatidylinositol; TM, transmembrane (from Tamagnone and Comoglio, 2004).

3.8.4 Ephrins and Eph receptors

Eph receptors and Ephrins are both membrane associated proteins and build a receptor-ligand system. Whereas 13 Eph receptors and 8 Ephrins are known in mammals (Tuzi and Gullick, 1994; Orioli and Klein, 1997; Pasquale, 1997), one Eph receptor and 4 Ephrins are characterised in *Caenorhabditis elegans* (George et al., 1998; Scully et al., 1999; Wang et al., 1999; Bossing and Brand, 2002) and only one Eph receptor and one Ephrin are identified in *Drosophila melanogaster*. Eph receptors and Ephrins build two classes based on sequence homology and binding preferences (Fig. 10). EphA receptors bind to EphrinAs (with the exception of EphA4) and EphB receptors bind to EphrinBs. However, new experiments suggest that interactions across classes occur (Himanen et al., 2004). The two Ephrin groups show structural differences. EphrinAs are tied to the membrane by a glycosylphosphatidylinositol anchor, whereas EphrinBs are transmembrane proteins with a cytoplasmic domain. Eph receptors are members of the superfamily of receptor tyrosine kinases. They auto-phosphorylate upon binding to their Ephrin ligands and activate downstream signalling cascades (forward signalling). Both Ephrin classes have no catalytic activity, but they can activate signal transduction pathways after interaction with Eph receptors (reverse signalling; Davy and Soriano, 2005). Reverse signalling activated by Ephrins implies tyrosine phosphorylation of their cytoplasmic tail and interactions with different signalling molecules (Davy and Soriano, 2005). Oligomerization and clustering of Eph receptors and Ephrins is necessary for their signalling function (Cowan and Henkemeyer, 2002; Kullander and Klein, 2002; Davy and Soriano, 2005). Both forward and reverse signalling regulates cell motility. Depending on cell type and on the members of the Eph / Ephrin system involved, the result of the interaction can be either increased adhesion (attraction), or decreased adhesion (repulsion; Davy and Soriano, 2005). Both reverse signalling and forward signalling can be either attractive or repulsive (Davy and Soriano, 2005). The Eph / Ephrin system acts in interaction with adhesion proteins such as Integrins and different proteins implicated in cytoskeletal organization (Murai and Pasquale, 2003; Davy and Soriano, 2005).

The repulsive role of Eph receptors and Ephrins in axon guidance was first analysed (Davy and Soriano, 2005). Their expression patterns in navigating axons and their targets are in agreement with a role in topographic mapping of axonal projections (Davy and Soriano, 2005). It was elaborated that cells expressing Eph receptors avoided regions expressing Ephrins, thus providing repulsive cues to guide axons to their correct target (O'Leary and Wilkinson, 1999; Davy and Soriano, 2005). More recently it was shown that Eph receptors and Ephrins can also control axon guidance through attractive interactions (Knoll et al., 2001; Kullander et al., 2001b; Hindges et al., 2002; Mann et al., 2002; Eberhart et al., 2004) and that Ephrins can act as receptors on navigating axons (Davy and Soriano, 2005). In addition to their functions in axon guidance, Ephs and Ephrins were shown to be implicated in segmentation (Wilkinson, 2000; Davy and Soriano, 2005). Expression studies of these receptors and ligands exhibited that several members of both the Eph receptors and the Ephrins are expressed in a segmented pattern in somites and in the hindbrain, suggesting that Ephs and Ephrins play a role in segmentation during development (Gale et al., 1996; Davy and Soriano, 2005). Functional studies showed that Eph receptors and Ephrins participate in both cranial and trunk neural crest cell migration (Holder and Klein, 1999; Wilkinson, 2000). Ephrins expressed by the somites act

as ligands non-cell autonomously on neural crest cells expressing Eph receptors (Krull et al., 1997; Wang and Anderson, 1997). It has been shown that perturbation of the Eph receptor function led to abnormal migration of branchial neural crest cells (Smith et al., 1997). Important articles and reviews on Eph / Ephrin signalling are: Robinson et al., 1997; Nakamoto, 2000; Xu et al., 2000; Poliakov et al., 2004; Davy and Soriano, 2005.

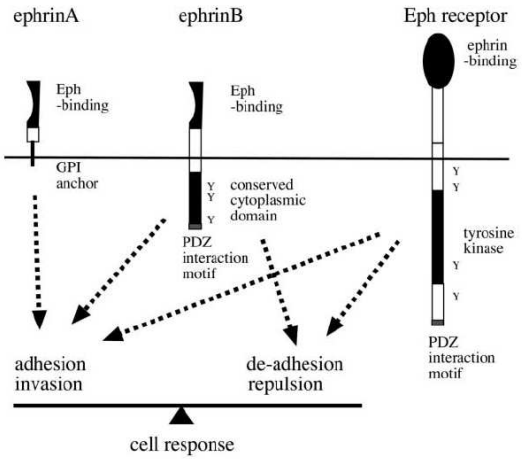

Figure 10 Schematic representation of Eph receptors and their ligands, the EphrinAs and EphrinBs and their possibilities in cellular responses (from Poliakov et al., 2004).

3.8.5 Chondroitin sulphate proteoglycans (CSPGs)

Lecticans are members of the Chondroitin sulphate proteoglycans. In mammals, four different lecticans are known: brevican, neurocan, aggrecan and versican (Fig. 11). Common structures among the chondroitin sulphate proteoglycans are the highly homologous G1 and G3 domains (Mörgelin et al., 1989; Retzler et al., 1996; Zimmermann and Dours-Zimmermann, 2008). The part between the G1 and G3 domains includes most of the O- and N-linked oligosaccharides and all glycosaminoglycan side chains (Zimmermann and Dours-Zimmermann, 2008). Besides the variations within the carbohydrate parts, alternative splicing also increases the structural diversity of lecticans (Zimmermann and Dours-Zimmermann, 2008). Four different versican isoforms (V0, V1, V2 and V3) are known as a result of alternative assembly of two giant exons (Dours-Zimmermann and Zimmermann, 1994; Zako et al., 1995; Zimmermann and Ruoslahti, 1989). Besides the large proteoglycans of the lectican family, phosphacan, a secreted CSPG-isoform of receptor-type protein-tyrosine phosphatase β (RPTP β), plays a role in the ECM of the brain (Barnea et al., 1994; Maurel et al., 1994; Shitara et al., 1994; Zimmermann and Dours-Zimmermann, 2008). Phosphacan and all lecticans of the CNS inhibit axonal growth *in vitro* (Bandtlow and Zimmermann, 2000; Yamaguchi, 2000; Zimmermann and Dours-Zimmermann, 2008). This function seems to be core protein-dependent in versican V0, V1 and V2 (Dutt, Stoeckli and Zimmermann, unpublished; Niederöst et al., 1999; Schmalfeldt et al. 2000; Zimmermann and Dours-Zimmermann, 2008), phosphacan (Maeda and Noda, 1996) and neurocan (Margolis et al., 1996; Zimmermann and Dours-Zimmermann, 2008) as

their functional properties persisted after chondroitinase ABC digestion. No axon inhibition has been found of aggrecan (Snow et al., 1990) and brevican (Yamada et al., 1997a) after chondroitinase ABC digestion (Zimmermann and Dours-Zimmermann, 2008). The axonal growth inhibition may be dependent on a pericellular hyaluronan coat that covers different cell types and often comprises lecticans, link proteins and tenascins (Evanko et al., 2007; Zimmermann and Dours-Zimmermann, 2008). Synthesis of hyaluronan alone promotes the development of membrane protrusions in different cell types (Kultti et al., 2006; Rilla et al., 2008; Zimmermann and Dours-Zimmermann, 2008). It is therefore imaginable that a coat containing only hyaluronan has a similar effect in generating growth cone filopodia (Zimmermann and Dours-Zimmermann, 2008). When these filopodia encounter regions expressing lecticans, they may incorporate the CSPGs into the pericellular hyaluronan structure and increase the thickness of their coat (Zimmermann and Dours-Zimmermann, 2008). The contacts to the surface of neighbouring cells or the extracellular matrix may then be compromised by sterical hindrance (Zimmermann and Dours-Zimmermann, 2008). Therefore, the advancing growth cone might decelerate, retract or turn away from the zones containing lectican (Zimmermann and Dours-Zimmermann, 2008). While high versican concentrations trigger retraction, low concentrations still allow a reduced growth (Yamagata and Sanes, 2005; Zimmermann and Dours-Zimmermann, 2008). This finding is confirmed by experiments *in vivo*, where knock down of versican causes a significant size reduction of the retinal arbors of the optic tectum indicating that low versican expression diminishes axonal growth (Zimmermann and Dours-Zimmermann, 2008). High expression of versican V0/V1 may account for the formation of barriers that block axon extension and restrict migration of neural crest cells in the developing peripheral nervous system (Dutt et al., 2006; Landolt et al., 1995; Oakley and Tosney, 1991). These supposed roles of the versicans cannot be verified in knock-out mice, as they die at around embryonic day 10.5 (Mjaatvedt et al., 1998; Zimmermann and Dours-Zimmermann, 2008) but could be analysed with knock-down experiments that bypass the early lethality of the knock-out mice.

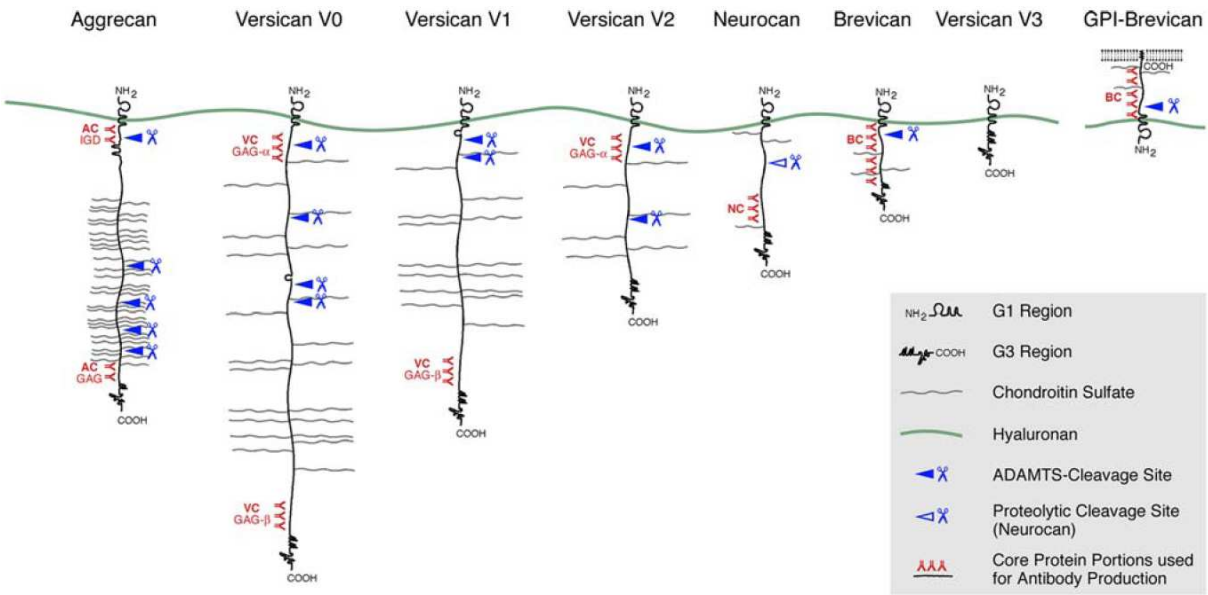

Figure 11 Schematic representations of the chondroitin sulfate proteoglycans of the lectican family (from Zimmermann and Dours-Zimmermann, 2008).

3.8.6 Immunoglobulin superfamily cell adhesion molecules (IgSF CAMs): TAG-1/Axonin-1 and NgCAM, F11/Contactin and NrCAM

Axonin-1/TAG-1 and F11/Contactin are two similar immunoglobulin superfamily cell adhesion molecules (IgSF CAMs). They are both linked to the cell membrane by a glycosylphosphatidylinositol anchor and share similar binding partners. Axonin-1/TAG-1 and F11/Contactin were shown to play roles in the subpopulation specific guidance of nociceptive and proprioceptive axons in the DREZ and towards their correct target layer in the spinal cord *in vivo* (Perrin et al., 2001). Proprioceptive neurons depend on F11/Contactin for proper extension to the ventral spinal cord and nociceptive fibres require Axonin-1/TAG-1 for the correct pathfinding to lamina I and II in the grey matter (Perrin et al., 2001). NgCAM (Kuhn et al., 1991; Brummendorf et al., 1993) and NrCAM (Morales et al., 1993; Suter et al., 1995; Fitzli et al., 2000) bind to both Axonin-1/TAG-1 and F11/Contactin *in vitro* and both show ubiquitous expression in the spinal cord. Whereas Axonin-1/TAG-1 interacts with NgCAM on nociceptive neurons, F11/Contactin and NrCAM interactions are required on proprioceptive axons. Function blocking antibodies against F11/Contactin lead to a split morphology of the dorsal roots in chicken embryos. Besides F11/Contactin no other attractive cue has been shown to guide central branches of sensory neurons towards the DREZ *in vivo*.

3.8.7 The Slit / Robo System

Robos are large transmembrane receptors from the immunoglobulin superfamily of cell adhesion molecules which bind to their large glycosylated secreted ligands, the Slits and were shown to act as an important repulsive guidance molecules in neuronal development of both invertebrates and vertebrates (Seeger et al., 1993; Kidd et al., 1998, 1999; Zallen et al., 1998; Brose et al., 1999; Erskine et al., 2000; Fricke et al., 2001; Challa et al., 2001; Long et al., 2004). Robos comprise five extracellular immunoglobulin-like and three fibronectin type III domains, a single transmembrane domain and intracellular C-terminal regions (Fig. 12). Slits are composed of four leucine-rich repeats, seven to nine epidermal growth factor-like domains, a laminin-G motive and C-terminal a cysteine knot (Fig. 12). It was shown that Slits bind to Robos through an interaction between the leucine rich repeats of the Slits and the immunoglobulin-like domain one and two of the Robos (Brose et al., 1999; Liu et al., 2004, Battye et al., 2001; Howitt et al., 2004). Furthermore it was demonstrated that Robo1 and Robo2 interact homo- and heterophilically (Simpson et al., 2000a; Hivert et al., 2002).

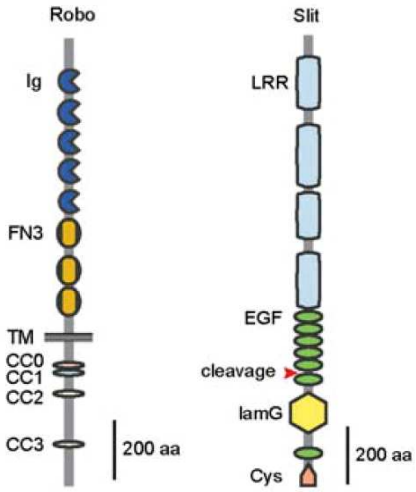

Figure 12 Schematic representation of the Robo and Slit axon guidance molecules. Robos comprise five immunoglobulin-like domains, which are binding sites for the Slits, three fibronectin-like domains, important for homo- and heterophilic interactions among the Robo members, a transmembrane domain and four C-terminal intracellular CC domains. The Slit members share four leucine-rich repeats, which interact with the Ig-like domains of the Robos, six EGF-like repeats, an ALPS domain and a C-terminal cysteine knot (from Dickson and Gilestro, 2006).

In Robo proteins, four intracellular motives, CC0, CC1, CC2 and CC3, are found and two of them, CC2 and CC3, are binding sites for Enabled (Ena) and Abl tyrosine kinase, respectively (Fig. 13; Kidd et al., 1998; Rajagopalan et al., 2000b; Simpson et al., 2000a). The three different Robo receptors contain different combinations of these four intracellular CC motives (reviewed in Dickson and Gilestro, 2006). The CC3 domain in rat Robo1 has also been shown to directly interact with GTPase activating proteins (GAPs), and Slit binding to this receptor results in changes in Cdc42 and Rac1 activity in isolated cells in culture (Wong et al., 2001).

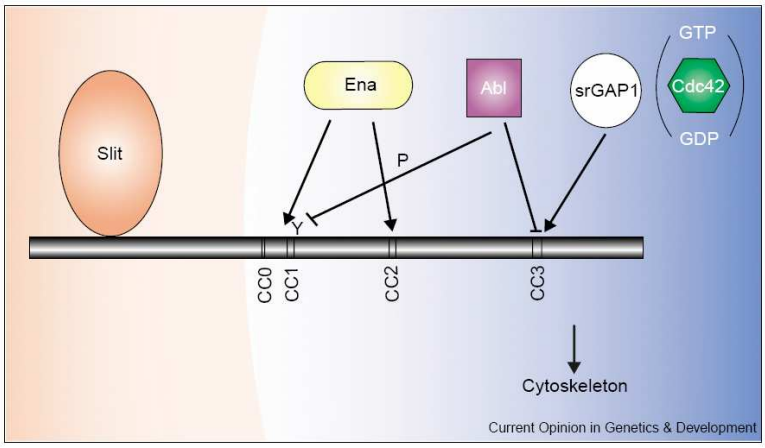

Figure 13 Intracellular Robo CC0-3 domains are binding sites for srGAPs (CC3), Ena (CC1 and CC2) and Abl (CC3 and inhibition of CC1). SrGAPs inactivate Cdc42 and therefore inhibit actin polymerisation which leads to growth cone repulsion (from Wong et al., 2002).

The intracellular signalling pathway triggered upon Slit binding to the Robo receptor was analysed in detail by Wong and colleagues (Wong et al., 2001 and 2002). Slit binding to Robo increases the srGAP activity on the side of the growth cone subjected to Slit. This leads to more inactivation of Cdc42. Thus, on the affected side of the growth cone, there will be less N-WASP activity, less Arp2/3 activity, and therefore less actin polymerization. The asymmetry in actin polymerization on different sides of the growth cone causes it to move away from the source of Slit or leads to retraction or branching (Fig. 14; Wong et al., 2001).

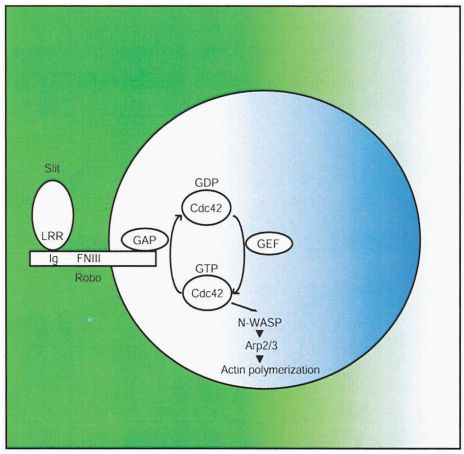

Figure 14 Schematic Robo/Slit intracellular signalling pathway. An intracellular gradient of active Cdc42 (blue) leads to actin cytoskeleton remodelling (actin depolymerisation on the left side of the cell and actin polymerisation on the right side of the cell) and therefore to growth cone retraction, turning or branching (from Wong et al., 2001).

The Slit / Robo system was first characterized in *Drosophila*, as regulator of midline crossing by commissural axons in the CNS (Seeger et al., 1993; Kidd et al., 1998, 1999; Murray and Whitington, 1999; Rajagopalan et al., 2000a; Simpson et al., 2000a; Plump et al., 2002). In invertebrates and vertebrates, the midline repellent that expels commissural axons and prevents them from recrossing is Slit. When commissural axons grow toward the midline in *Drosophila*, Robo1 receptors are kept in intracellular compartments away from the axon surface, by the Commissureless (Comm) protein (Fig. 15; Keleman et al., 2002). As the axons reach and cross the midline, the inhibition of Robo by Comm, is released, and Robo1 proteins are now presented at the surface of commissural growth cones, causing them to sense the Slit repellent and hence expelling the growth cone from the midline (Fig. 15; Kidd et al., 1998b). It is the tight temporal and spatial regulation of Robo expression that guarantees that Slit functions only after commissural axons have crossed the midline.

Furthermore, a combinatorial code of Robo receptors controls the lateral positions of commissural axons after they have crossed the midline and turned longitudinally to ascend to the brain. Axons which grow to most medially ascending longitudinal tracts express only Robo1, intermediate projecting axons express both Robo1 and Robo3, and lateral ascending axons express all three Robo receptors (Fig. 16; Rajagopalan et al., 2000b; Simpson et al., 2000a).

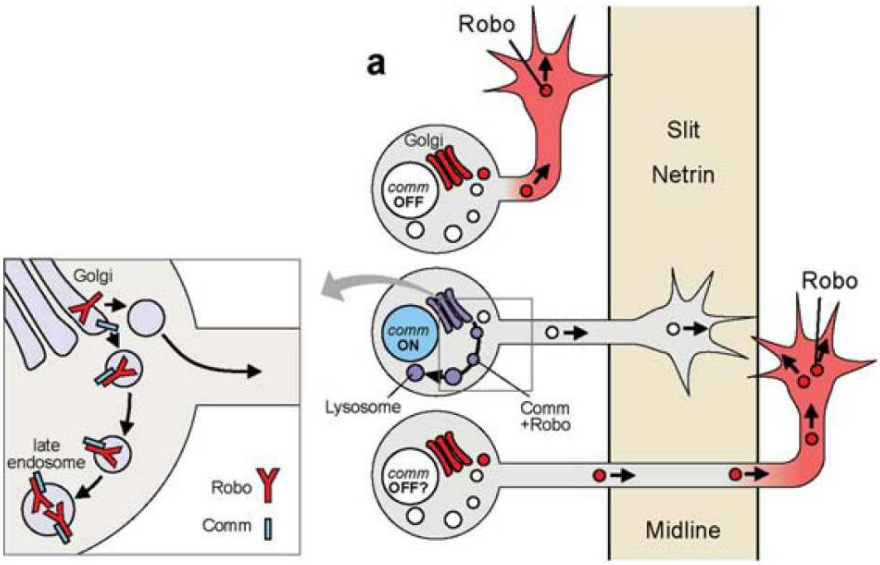

Figure 15 Model for midline crossing in *Drosophila*. On precrossing commissural axons Robo1 receptors are kept in intracellular compartments away from the growth cone surface by Commissureless (Comm). As the axons cross the midline, the inhibition of Robo1 by Comm is released, and Robo1 is now presented at the surface of commissural growth cones, causing them to sense the Slit repellent and hence expelling them from the midline (from Dickson and Gilestro, 2006).

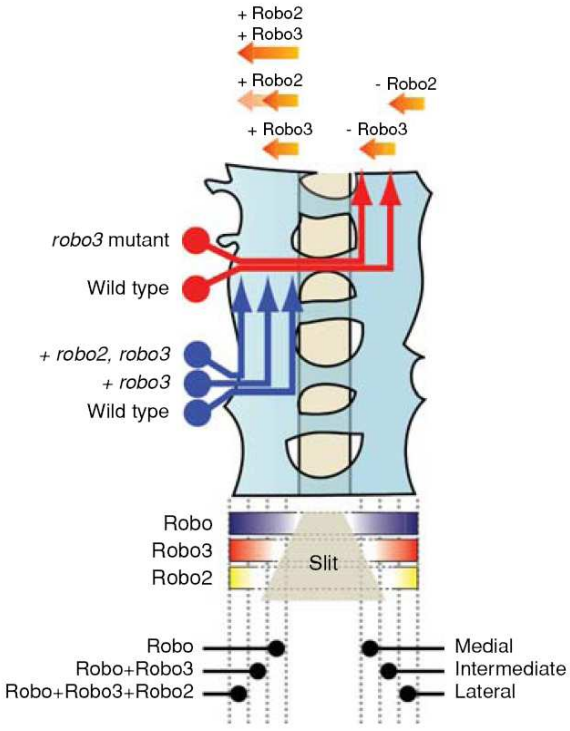

Figure 16 Robo receptors specify the lateral position of commissural and ipsilateral turning axons in the *Drosophila* CNS. Axons projecting most closely along the midline express Robo1, intermediate axons Robo1 and Robo3 and laterally extending axons express all three Robos (from Dickson and Gilestro, 2006).

In vertebrates, no Commissureless was found. Another mechanism leads to correct midline guidance. In mice the Slit-insensitivity of Robo1-positive precrossing commissural axons is attained by inhibition of Robo1 receptor through Rig1 / Robo3 protein on the axon surface (Fig. 17). Slit1-3, expressed by the floor plate and adjacent regions, are recognized by Robo1 on commissural axons as they extend towards the floor plate, but the presence of Rig1 on the growth cone membrane inhibits Robo1 from eliciting a repulsive response to these ligands. After crossing the floor plate, the inhibition of Slit responsiveness is cancelled due to the rapid downregulation of Rig1 and the strong upregulation of Robo1. This mechanism expels the axons out of the midline into the longitudinal tracts ascending to the brain (Fig. 17; Sabatier et al., 2004).

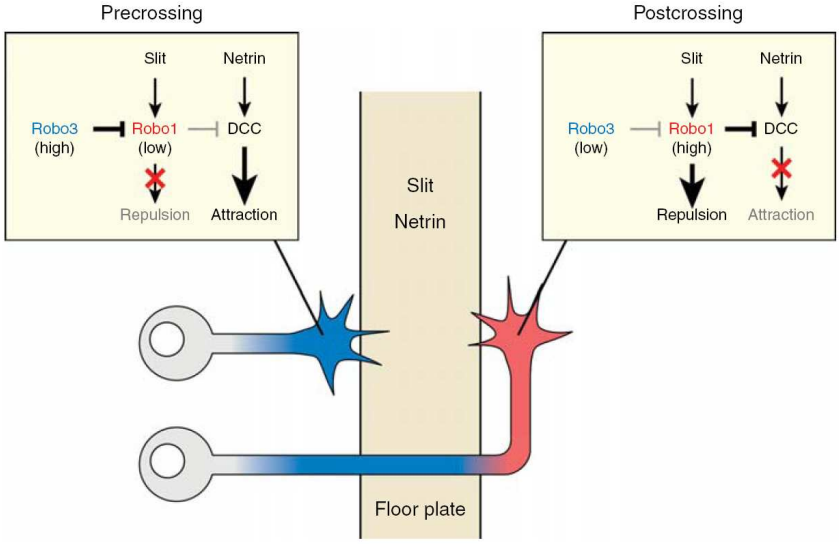

Figure 17 Schematic illustration of midline crossing in mice. Precrossing axons are attracted to the floor plate primarily through the effect of Netrin-1 and its receptor DCC. Slit1-3, expressed by the floor plate, are recognized by Robo1 on commissural axons, but the presence of Rig-1/Robo3 on the growth cone membrane inhibits Robo1 from triggering a repulsive response to these ligands. After crossing the floor plate, the inhibition of Slit responsiveness is relieved due to the absence of Rig1 on postcrossing commissural axons and the upregulation of Robo begins. This coincides with a loss of responsiveness to Netrin-1, presumably due to the interaction between Robo1 and DCC (Stein and Tessier-Lavigne, 2001). Upregulation of responsiveness to the repellent Slits expels the axons out of the midline (from Dickson and Gilestro, 2006).

In chicken embryos, Philipp and colleagues propose an additional mechanism. Robo1 regulation is not only realized by receptor inhibition on the growth cone membrane by Rig1 but by the inhibition of Robo1 insertion into the axon membrane. RabGDI (Rab guanine nucleotide dissociation inhibitor), a component of the vesicle fusion machinery (Pfeffer and Aivazian, 2004), is not expressed on precrossing commissural axons as they extend towards the floor plate (between HH18 and HH20). RabGDI is upregulated when commissural axons reach the floor plate area (HH21). RabGDI is required for the retrieval of RabGDP back from the growth cone membrane to new donor vesicles and, in case of midline crossing, for the membrane fusion of a subtype of vesicles containing Robo1 receptors which are important at the floor plate to change the balance between positive (e.g. Netrin1, Axonin-1/TAG-1 and NrCAM (Stoeckli and Landmesser, 1995)) and negative (Slits (Kidd et al., 1999))

guidance cues towards negative stimuli. RabGDP is reactivated through the exchange of GDP to GTP by a guanine nucleotide exchange factor (GEF). Thus RabGDI expression in axons at the floor plate allows the intracellularly stored vesicles, containing Robo1 receptors, to fuse to the growth cone membrane and therefore sense the repellent Slit2, which is expressed in the floor plate and Slit1 from cells flanking the floor plate. As Robo1-positive commissural axons sense Slit, they are pushed out of the floor plate to the contralateral side (Philipp et al., submitted).

There are other axon populations in the brain which are guided by Slit and Robo. The development of trigeminal ganglions (Shiao et al., 2008), corticofugal, callosal, thalamocortical tracts (Lopez-Bendito et al., 2007) and the optic chiasm (Bagri et al., 2002; Plump et al., 2002) is defective in absence of Slit / Robo signalling.

Generally Robo receptors mediate growth cone repulsion (Kidd et al., 1998), but in some cases, Robo function results in the opposite effect, axon attraction through homo- or heterophilic interactions of Robo1 and Robo2 by Slit-independent mechanisms. Some of the axon growth defects observed in Robo mutants in *C. elegans* (Zallen et al., 1998, 1999) and in zebrafish (Karlstrom et al., 1996; Fricke et al., 2001) cannot be explained based on Slit – Robo interactions. In addition, Hivert and coworker have shown that the *in vitro* growth of neurites from Robo-positive retinal and olfactory neurons is stimulated if the cells over which they are growing express human Robo1 or Robo2 (Hivert et al., 2002). Their findings raise the possibility that Robo proteins may function *in vivo* as homophilic or heterophilic cell adhesion molecules to promote axon growth. Furthermore, there are strong structural similarities between the extracellular region of Robo proteins and a number of cell adhesion molecules of the immunoglobulin superfamily (Kidd et al., 1998; Rajagopalan et al., 2000b; Simpson et al., 2000a). In the *Drosophila* embryo, Slit-dependent Robo2 but not Robo1 signalling is involved in long-range attraction of tracheal cells towards the target tissue (Englund et al., 2002) and both Robo1 and Robo2 mediate chemoattraction of muscle precursor cells to their epidermal insertion sites (Kramer et al., 2001). The PNS in *Drosophila* embryos offers some advantages over the CNS for the analysis of axon guidance. The cellular terrain encountered by sensory axons at early stages of growth is simpler than in the CNS, and the spatiotemporal pattern of axon growth from several individually identified sensory neurons has been described in detail (Giniger et al., 1993; Younossi-Hartenstein and Hartenstein, 1993; Harris and Whitington, 2001). Robo plays a familiar role in the PNS, inhibiting axon extension and exploration via the binding of Slit protein on the growth cones of chordotonal neurons. In contrast, Robo2 appears to play a novel axon guidance role, facilitating attraction of sensory axons to their early growth substrates, branches of the tracheal system. Robo2 activity is not required in the sensory axons themselves (cell autonomous), but within the trachea to attract the axons and this function does not involve an interaction with Slit.

Neural crest cell migration is another biological process that is regulated via Slit / Robo signalling. Slits most likely those that are expressed in the dermomyotome (Slit1 and Slit2) were shown to confine the Robo1- and Robo2- positive early NC cells to the ventro-medial pathway in chicken embryos (Jia et al., 2005). However they were not able to discriminate between Slit1 and Slit2 as major player in this situation. A study from Vargesson and colleagues showed that in developing limbs Slits are expressed in border zones to the trajectory of sensory and motor neurons (Vargesson et al., 2001). Ma and Tessier-Lavigne examined the role of the Slit / Robo system during the bifurcation of primary sensory

afferents in the DREZ and the invasion of the corresponding collaterals into the spinal cord. Double knock-out mice lacking Slit1 and Slit2 revealed failure of one daughter peripheral branch to bifurcate and turn into the longitudinal axis, resulting in an overshooting branch extending towards the dorsal midline. Slit1 or Slit2 are redundant in this process and only one copy of either gene can ensure the correct turning behaviour. It was demonstrated that Slits have a transient potential to induce collapse of E12 rat DRG growth cones (Ma and Tessier-Lavigne, 2007). Previously, it was shown that Slits can either act to enhance or restrict the migration of trunk neural crest cells and furthermore that Sli2 can act as branch promoter or branch repellent of sensory neurons (De Bellard et al., 2003; Ma and Tessier-Lavigne, 2007). How these different actions can be mediated by the same receptors remains elusive and further studies on the intracellular Slit / Robo signalling may shed light on this open question.

The role of the Slit / Robo system in innervation of the spinal cord by central sensory processes was reported for small diameter and for Ia large diameter sensory collaterals connecting to dorsal layers and to the ventral motor column, respectively (Ma and Tessier-Lavigne, 2007). Ma and Tessier-Lavigne demonstrated that the trajectory of the nociceptive and proprioceptive collaterals is altered in Slit1 / Slit2 or Robo 1/ Robo2 double-knockout mice.

Besides the involvement of the Slit /Robo system in neural crest cell migration and axon guidance, more and more studies show that Slit / Robo signalling controls other biological processes. Cancer, developmental and tumour angiogenesis (Wang et al., 2003), endothelial cell migration (Legg et al., 2008) and heart formation (Medioni et al., 2008; Santiago-Martinez et al., 2008; reviewed in Helenius and Beitel, 2008) are also regulated by Slit and Robo. Future studies may bring forward an even broader spectrum of biological processes regulated by Slit and Robo.

3.9 RNA interference (RNAi)

At present, RNA interference technology is one of the most powerful and fastest methods for functional gene analysis. It blocks gene expression and thus allows the induction of loss-of-function phenotypes to asses *in vivo* functions of the targeted genes. The characterisation of physiological functions of genes has become the rate-limiting step in biological research. Long double-stranded RNAs (typically >200bp), short hairpin RNA (shRNAs) vectors or short-interfering RNAs (siRNAs) can be used to silence genes with spatial and temporal control in a variety of organisms and cell types, e.g. in *C. elegans*, *Drosophila melanogaster*, chicken embryos, human cells and mammalian embryos (only siRNAs), and plants (Fire et al., 1998). The knock down happens posttranscriptionally because the DNA sequence of the target gene is not changed in animals treated with RNAi (Montgomery et al., 1998). The potency of RNAi was demonstrated by injection of dsRNA into the gut of *C. elegans* that caused gene silencing not only throughout the worm, but also in its first generation offspring. They also demonstrated that the initiation of transcription is not affected (Fire et al., 1998). After introduction of dsRNA (shRNA vectors or siRNAs) by feeding, soaking (*C. elegans*) or by injection into the embryo (*Drosophila, C. elegans*) or into the central canal of the spinal cord in chicken embryos, the dsRNAs enter a cellular pathway that is commonly referred to as the RNA interference (RNAi) pathway (Fig. 18). First, the dsRNAs gets processed into 21-23 bp long small interfering RNAs (siRNAs) by an

RNase III-like enzyme called Dicer. Then, the siRNAs assemble into endoribonuclease-containing complexes known as RNA-induced silencing complexes (RISCs). The siRNA strands subsequently guide the RISCs to complementary mRNA molecules by base pairing between the siRNA antisense strand and the mRNA. The bound mRNA is cleaved by RISC and the sequence-specific degradation of mRNA results in gene silencing. In mammalian cells, introduction of long dsRNA (>30 bp) initiates a potent antiviral response, effected by non-specific inhibition of protein synthesis and RNA degradation. The antiviral response can be bypassed by the introduction or expression of siRNAs.

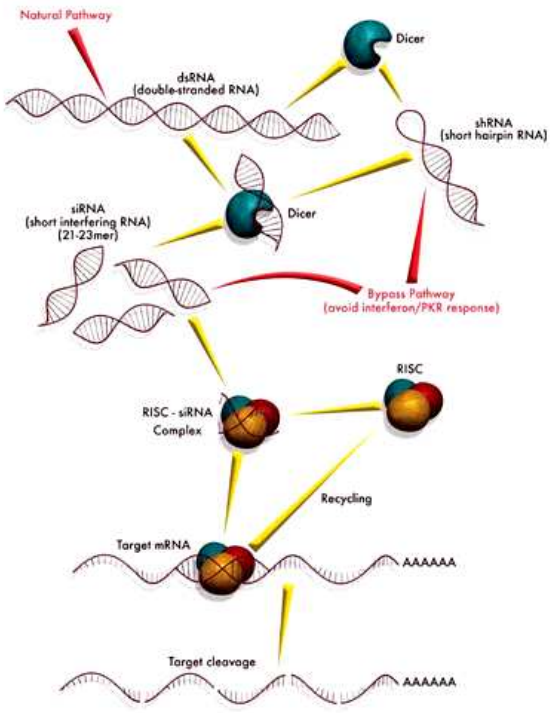

Figure 18 RNA interference pathway: dsRNAs get processed into 21-23 nucleotides small interfering RNAs by Dicer. The siRNAs assemble into endoribonuclease-containing complexes known as RNA-induced silencing complexes (RISCs). The siRNA strands subsequently guide the RISCs to complementary mRNA molecules. The cognate mRNA is cleaved by RISC and sequence specific degradation of mRNA results in gene silencing (from http://www.microbiologybytes.com/virology/3035Immunopath.html).

3.9.1 *In ovo* RNAi

In ovo RNAi is a technique, developed in our lab, to induce transient knock down in chicken embryos (Fig. 19; Pekarik et al., 2003). *In ovo* electroporation was established 1997 to increase the efficiency of gene transfer across cell membranes (Muramatsu et al., 1997). Combined with RNAi, we can analyse loss of function phenotypes in chicken embryos even at old developmental stages. Genes that would be lethal when silenced in early development due to an additional function that is indispensable for survival can be easily investigated due to the temporal control of gene silencing by *in ovo* RNAi. The time-consuming and expensive production of a knock-out mouse, that might not be viable, can be bypassed. Furthermore, the full-length sequence of a target gene is not required for *in ovo* RNAi. This is an additional advantage as candidate genes identified in a subtractive hybridization screen are only cDNA fragments. Full-length cloning of these fragments is not necessary for investigation of gene function with *in ovo* RNAi; the fragments can be directly cloned into a vector with flanking promoters on either side. By *in vitro* transcription *in situ* probes and dsRNAs can be rapidly produced, making *in ovo* RNAi a fast and powerful method. The time point of dsRNA injection into the central canal of the spinal cord, the applied voltage and the number of pulses are crucial parameters for targeting the cell populations of interest. In younger stages (HH10-14) all cell populations of the spinal cord, early and late neural crest cells can be targeted (18-20 Volt, 5-7 pulses). In this case, the phenotype can be found on both sides of the embryo, although stronger on one side, whereas in older stages (HH >18) only one half of spinal cord gets transfected and one side of the embryo can be used as a control. Targeting the posterior compartment of the developing somite/sclerotome and the dermomyotome needs more voltage and an increased number of applied pulses (HH10-14, 22 Volt, 10 - 12 pulses).

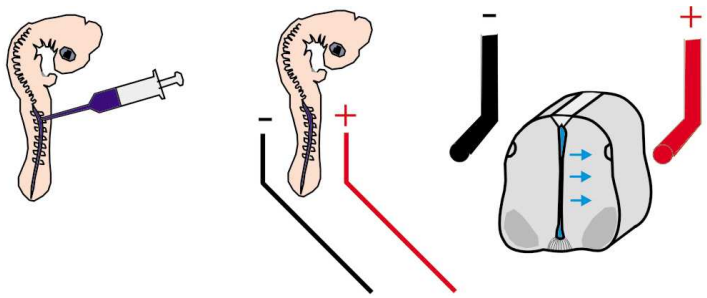

Figure 19 Schematic illustration of *in ovo* RNAi in chicken embryos. Injection of dsRNA into the central canal of the spinal cord, *in ovo* electroporation and direction of transfection in the spinal cord are depicted (from Pekarik et al., 2003).

3.10 Ectopic expression and overexpression *in ovo*

Gain-of-function studies leading to a hypermorph (overactivation of gene expression) or a neomorph mutation (resulting in a completely new phenotype) can be promising when a pathway gets over-activated. For my analysis it was useful to assess the consequences of Slit1-3 overexpression. Due to the fact that the complete full-length sequence of a gene of interest is needed to ectopically express it *in vivo* or *in vitro*, this technique is more time-consuming and more expensive than RNAi. The open reading frame is inserted in frame in an expression vector with appropriate ubiquitous or tissue specific promoters. If one lacks a specific antibody which recognises the produced protein one also need to attach a tag for which an antibody is available and with which one can prove expression of the constructs.

3.11 Aim of my dissertation and summary of used techniques

The aim of my dissertation was to study the expression pattern of the Slit and Robo family members in the developing chicken embryo and to characterize the functions of Robo1, Robo2, Robo3, Slit1, Slit2 and Slit3 in neural crest cell migration and sensory axon guidance in both the PNS and the CNS.
To this end I used the following techniques: *In situ* hybridization and immunohistochemistry to analyze the expression, *in ovo* RNAi (*in vivo* RNA interference and *in ovo* electroporation) to transiently silence genes of interest, ectopic expression and overexpression of full-length constructs and a variety of techniques for the analysis of the loss- and gain of-function phenotypes. Control and experimental embryos were either stained as whole-mounts with an anti-neurofilament antibody, or they were analysed after sectioning with immunohistochemical techniques on 25µm thick longitudinal and transverse cryosections. At late stages of development, axonal pathfinding was analysed using the lipophilic dye Fast DiI, injected in the lateral and in the medial part of the dorsal funiculus in 250µm thick transverse vibratome sections of the lumbosacral level of the spinal cord. This allowed for the analysis of the trajectories of nociceptive and proprioceptive sensory afferents in the grey matter of the spinal cord. Furthermore, I used Western blot analysis and *in vitro* assays with cultured dissociated sensory DRG neurons and cultures with DRG explants on cells expressing different constructs.

4. Results

4.1 Robo1 and Robo2 are dynamically expressed in migrating neural crest cells and DRG neurons

Several studies have investigated the expression pattern of Robos and Slits in the developing chicken embryo (Holmes and Niswander, 2001; Vargesson et al., 2001; Jia et al., 2005) and even more is known in rodents (Brose et al., 1999; Wang et al.,1999; Mambetisaeva et al., 2005; Ma and Tessier-Lavigne, 2007). However, in this study we focussed on the relatively short time slot of neural crest cell migration and sensory axon guidance between HH14 and HH26 and provide a detailed analysis of the expression pattern concerning structures which are involved in this process. Robo1 and Robo2 were already expressed at HH14/15 in migrating neural crest cells (Fig. 20A, E). HNK-1 immunostaining confirmed Robo1 and Robo2 expression in early neural crest cells (Fig. 20M-O). At HH19, Axonin-1 immunostaining marked first pioneer sensory neurons (Fig. 20P). At HH19-23, Robo1 and Robo2 were expressed throughout the DRG (Fig. 20B, C, F, G). At HH26 Robo1 and to a lesser degree Robo2 expression was restricted to the dorso-medial part of the DRG (Fig. 20D, H). In the dorso-medial part of the DRG, cells differentiate into nociceptive neurons around HH30 (when compared to TrkA expression). Robo3 expression was only detectable in interneurons within the spinal cord but neither detected in migrating neural crest cells nor in DRGs at any time point of our analysis by *in situ* hybridizations (HH14-28; Fig. 20I-L). Robo1 and Robo2 expression were also detected in the entire dermomyotome from HH14 on (Fig. 20A-H). Robo1 and Robo2 expressions persisted in DRGs up to HH42 although the expression got restricted from HH25 to several subpopulations of DRG neurons (Fig. 21). At HH28, Robo1 expression in DRGs was restricted to cells in the dorso-medial part. Furthermore, expression was detectable in lateral subpopulations of motoneurons and in different interneurons in the ventral grey matter (Fig. 21). At HH30 and HH32 Robo1 was expressed in lateral subpopulations of motoneurons, in different interneurons in the grey matter of the ventral spinal cord. Additionally, expression was detectable adjacent to the ventral motor axon exit point (MEP; Fig. 21). Robo1 expression at HH34 was comparable to the expression pattern observed at HH30 and HH32 with additional expression in a population of cells adjacent to the medial ventral funiculus (Fig. 21). At HH36 Robo1 was expressed in the ventral grey matter inclusive in the motor column, in lateral DRG neurons and adjacent to the MEP (Fig. 21). Between HH28 and HH36 Robo2 was strongly expressed in nociceptive neurons in the dorsal part of the DRG as well as in commissural and other interneurons in the grey matter and in the entire motor column (Fig. 21).

The *in situ* staining signals observed between HH38 to HH42 were stronger compared to the signals between HH32 to HH36 due to an additional proteinase K step during the hybridization procedure.

At HH38 Robo1 was strongly expressed in the entire grey matter, in the dorso-medial part of the DRG, in the entire motor column and adjacent to the MEP (Fig. 21). Robo1 expression did not change between HH38 and HH42: low expression in DRGs, strong expression adjacent to the MEP, in subpopulations of motoneurons and in the grey matter (Fig. 21). At HH38 Robo2 showed strong expression in the entire grey matter (only in lamina I and II the expression was weaker), in the entire DRG and in the entire motor column. Additionally the sympathetic ganglia and the developing

Hofmann nucleus expressed Robo2 (Fig. 21). At HH40 Robo2 expression was detectable in the medial part of the DRG, in the entire grey matter, in the sympathetic ganglia and in the developing Hofmann nucleus and at a lower expression levels than at HH38, in subpopulations of motoneurons (Fig. 21). At HH42 Robo2 expression showed strong expression in DRGs and low expression in the grey matter, but expression in the motor column disappeared. Additionally Robo2 expression was detectable in the developing Hofmann nucleus and in the sympathetic ganglia (Fig. 21).

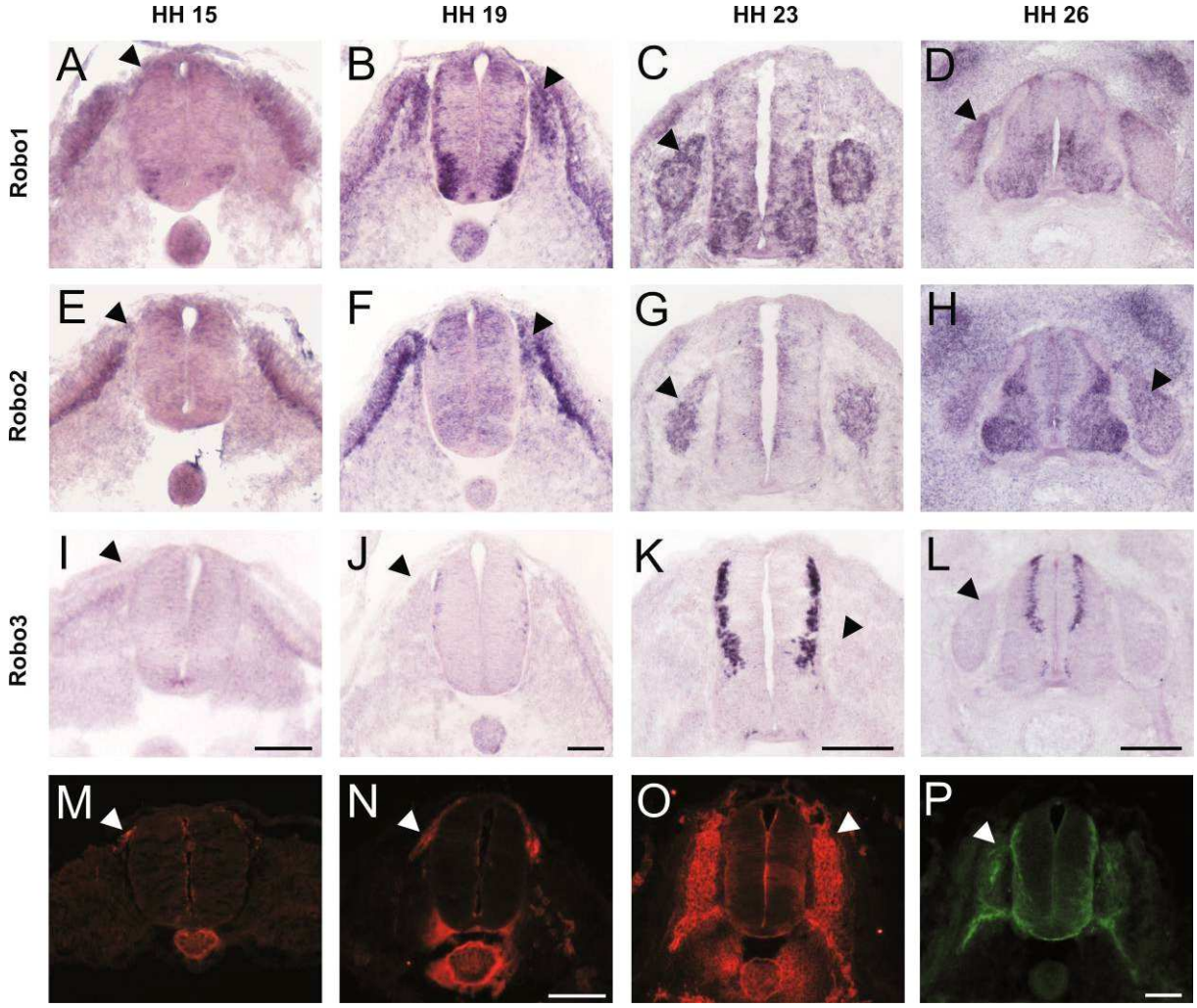

Figure 20 Expression pattern of the Robo family members during neural crest cell migration and early sensory axon guidance. (A - D) Robo1 was expressed in migrating early neural crest cells (arrowheads in A and B) and in all sensory neurons in the DRG at HH20-23 (arrowheads in B and C). (D) Robo1 expression in DRGs got restricted to the perimeter after HH23 (arrowhead in D). (E and F) Robo2 was expressed in early neural crest cells and throughout the DRG until HH23 (arrowheads in E and F). (H) The expression got restricted to putative nociceptive and proprioceptive neurons after HH23 (arrowhead in H). (I-L) Robo3/Rig1 was never expressed neither in migrating early neural crest cells nor in DRGs or other peripheral structures during the time slot of analysis (HH14-30, arrowheads in I-L). (M-O) HNK-1 immunostaining in HH15 (transversal section through trunk level (N) and putative lumbosacral level (M)) and in HH19 (O) embryos marked early neural crest cells (arrowheads). (P) Axonin-1 immunostaining revealed first pioneer central branches at HH19 (arrowhead). Scale bars: 50µm in A, B, E, F, I, J, M and N and 200µm in C, D, G, H, K, L, O and P.

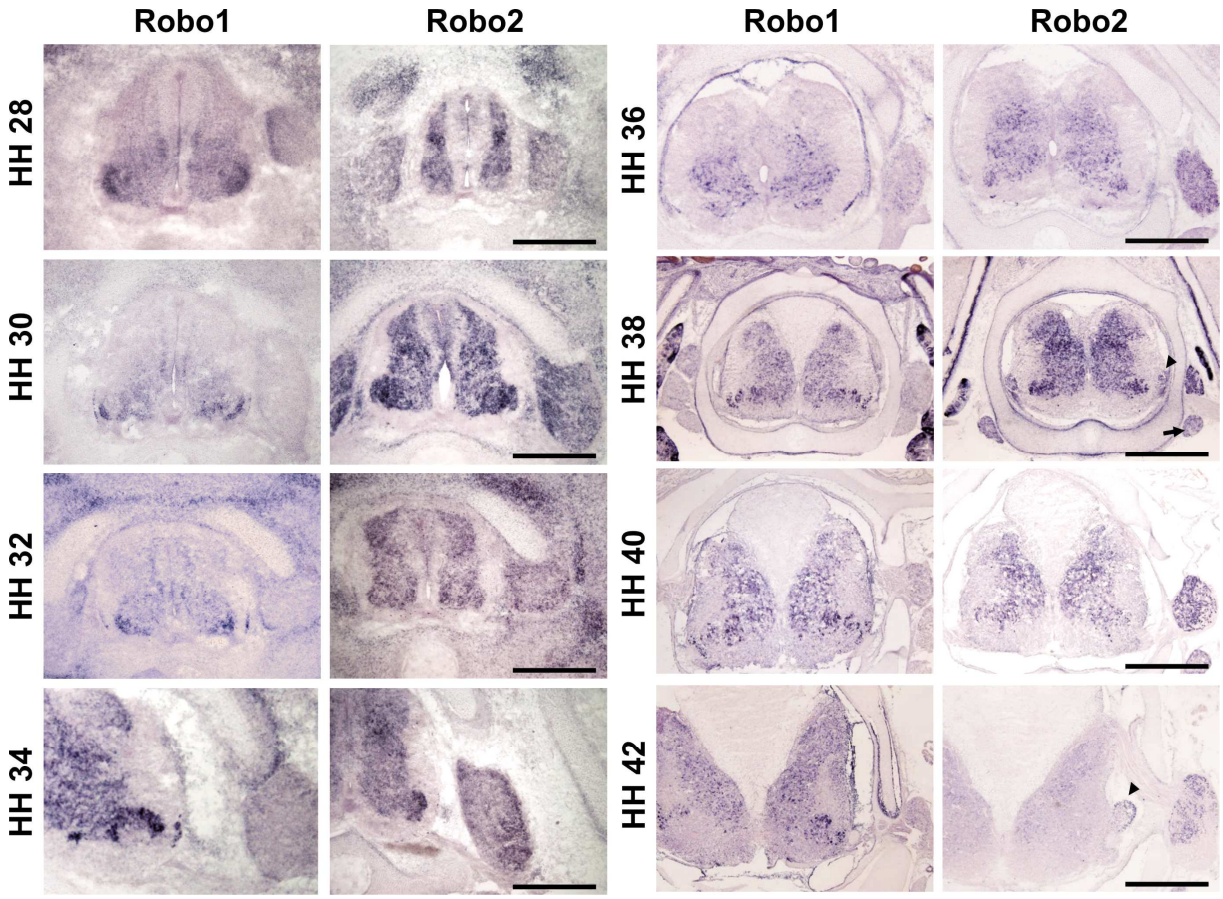

Figure 21 Expression patterns of Robo1 and Robo2 at older developmental stages, between HH28 and HH42, suggest roles in the formation of the sensory central collaterals. At HH28, Robo1 expression in DRGs was restricted to cells in the dorso-medial part. Furthermore, expression was detectable in lateral subpopulations of motoneurons and in different interneurons in the ventral grey matter. At HH30 and HH32 Robo1 was expressed in lateral subpopulations of motoneurons, in different interneurons in the grey matter of the ventral spinal cord and expression was detectable adjacent to the ventral motor axon exit point (MEP). Robo1 expression at HH34 was comparable to the expression pattern observed at HH30 and HH32 with additional expression in a population of cells adjacent to the medial ventral funiculus. At HH36 Robo1 was expressed in the ventral grey matter inclusive in the motor column, in lateral DRG neurons and adjacent to the MEP. Between HH28 and HH36 Robo2 was strongly expressed in nociceptive neurons in the dorsal part of the DRG as well as in commissural- and other interneurons in the grey matter and in the entire motor column. At HH38 Robo1 was strongly expressed in the entire grey matter, in the dorso-medial part of the DRG, in the entire motor column and adjacent to the MEP. Robo1 expression did not change between HH38 and HH42: low expression in DRGs, strong expression adjacent to the MEP, in subpopulations of motoneurons and in the grey matter. At HH38 Robo2 showed strong expression in the entire grey matter (the expression was weaker only in lamina I and II), in the entire DRG and in the entire motor column. Additionally the sympathetic ganglia (arrow) and the developing Hofmann nucleus (arrowhead) expressed Robo2. At HH40 Robo2 expression was detectable in the medial part of the DRG, in the entire grey matter, in the sympathetic ganglia and in the developing Hofmann nucleus and at a lower expression levels than at HH38, in subpopulations of motoneurons. At HH42 Robo2 expression showed strong expression in DRGs and low expression in the grey matter, but the expression in the motor column disappeared. Additionally Robo2 expression was detectable in the developing Hofmann nucleus (arrowhead) and in the sympathetic ganglia. Scale bars: 200 μm for HH28-36 and 500 μm for HH38-42.

4.2 The expression pattern of the Slit family members indicate navigation borders for both migrating neural crest cells and DRG neurons

Slits were expressed in dynamically changing populations of neurons and other cell types within the spinal cord and in regions adjacent to the trajectory of outgrowing peripheral neurons. We analysed the expression patterns between HH14 and HH42 and focussed on expression domains that may interact with neural crest cell migration and sensory axon guidance. Slit1 was already expressed at HH14 in the dorsal and ventral spinal cord and in cells dorsally to the spinal cord (Fig. 22A). At HH18-23 there was strong expression detected in the dorsal and ventral dermomyotome and dorsal part of the somite (Fig. 22B, C). When analysed in a longitudinal section it got clear that this expression domain was restricted to the caudal half of the developing somite and dermomyotome (Fig. 22E) indicating that Slit1 could not be the only repulsive force guiding neural crest cells towards the ventro-medial pathway. It rather suggested a border to ensure that early neural crest cells migrate into the anterior half of the somite and are prevented from entering the posterior part. More ventrally, it was also expressed in both the anterior and posterior part of the ventral dermomyotome (Fig. 45A, see chapter 4.9). Additionally, Slit1 was expressed from HH18 in lateral interneurons of the spinal cord, in the roof plate, the dorsal spinal cord and in cells adjacent to the floor plate (Fig. 22B-D).

In contrast, Slit2 was expressed at low levels in the entire dermomyotome at HH18-23 (Fig. 22G, H, J) and therefore the stronger candidate for confining the early neural crest cells to the ventro-medial pathway. Moreover, very weak Slit2 expression was also detected in the posterior somite indicating a complementary pattern (arrow in Fig. 22J; note also Fig. 2E of Vargesson et al., 2001). Slit2 expression was detected between HH14 and HH42 in the floor plate (Fig. 22F-J; Fig. 23). Slit2 expression in the dorsal spinal cord faded away at HH21 and was not detectable at HH23 (Fig. 22H). Slit2 expression in the motor column, that was coming up at HH18 (Fig. 22G), got restricted to subpopulations between HH25 and HH28 and persisted at very low levels until HH42 (Fig. 22I; Fig. 23). In addition there was strong Slit2 expression detected in the notochord between HH14 and HH22 (Fig. 22F, G) that was absent after HH23 (Fig. 22H).

Slit3 expression was detected after HH14 in the notochord, the ventral spinal cord and in the ectoderm overlaying the entire dermomyotome (Fig. 22K-N). Furthermore, expression was detected in the dermomyotome between HH18 and HH21 and weak expression detectable in the posterior somite (arrow in Fig. 22L, O; compare also Fig. 2I of Vargesson et al., 2001). The expression in the ventral spinal cord became more restricted after HH23 (Fig. 22M, N) and persisted in motoneurons until HH42 (Fig. 23).

At HH28 and HH30 Slit1 was expressed in the roof plate, in cells flanking the floor plate and in cells adjacent to the ventricular zone (Fig. 23). At HH32 Slit1 was expressed as at HH30 with additional expression adjacent to the MEP and weak expression in the DRGs (Fig. 23). At HH34 Slit1 was expressed in the floor plate, in the roof plate, adjacent to the MEP, in DRGs and in the entire ventral part of the grey matter and cells around the dorsal midline expressed Slit1 as well (Fig. 23). Slit1 expression at HH36 was comparable to the pattern at HH34 except that the expression in the ventral grey matter expanded and formed a ventro-dorsal mRNA-gradient (Fig. 23). At HH38, strong Slit1 expression was detectable at the ventral midline, adjacent to the MEP, in the lateral motor column, in

the developing Hofmann nucleus, in the sympathetic ganglia and in the entire DRGs (Fig. 23). Both, a dorso-ventral and a ventro-dorsal mRNA-gradient were found with strong expression in the dorsal- and in the ventral horn, forming an area of lower expression in the medial part of the grey matter. The dorsal and ventral roots showed Slit1 expression as well (Fig. 23). At HH40, Slit1 showed the same gradient and expression at the ventral midline, adjacent to the MEP, in the lateral motor column, in the developing Hofmann nucleus, in the sympathetic ganglia, in the DRGs and in cells ensheathing the ventral and dorsal roots (Fig.23).

Slit2 expression was detectable between HH28 and HH42 in the floor plate and at low levels in dynamic changing populations of motoneurons (Fig. 23).

At HH28 Slit3 was strongly expressed in the floor plate, in the roof plate and in the entire motor column (Fig. 23). Strong expression was detected in cells that extended from the ventral horn to the medial part of the central canal (Fig. 23). At HH30 Slit3 was expressed in the floor plate, the roof plate, in the motor column and in cells extending from the ventral horn to the medial part of the central canal (Fig. 23). At HH32 Slit3 was expressed in the floor plate, in the roof plate and in the entire motor column (Fig. 23). At HH34 Slit3 was expressed in the motor column (Fig. 23). At HH36 Slit3 expression was detected in subpopulations of motoneurons and in cells around the dorsal edge of the central canal and the dorsal midline (Fig. 23). Between HH38 and HH42 Slit3 was expressed in the motor column, at the ventral midline, dorsal to the MEP, in DRGs and in the sympathetic ganglia (Fig. 23).

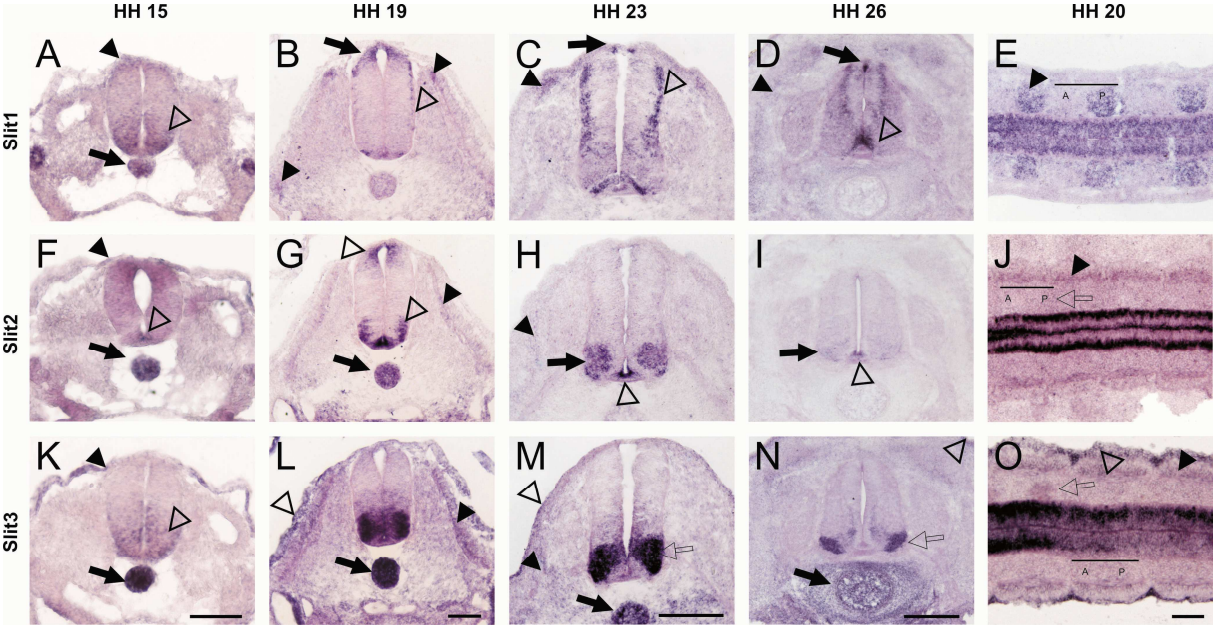

Figure 22 Expression pattern of the Slit family members during neural crest cell migration and early sensory axon guidance on transversal and longitudinal (E, J and O) sections. (A) The expression of Slit1 was already present at HH15 around the dorsal spinal cord (arrowhead), in the ventral spinal cord (open arrowhead) and in the notochord (arrow). (B and E) At HH18-20 it was expressed in the dorsal posterior part of the somite and in the dorsal and ventral rims of the dermomyotome (arrowheads), in the dorsal spinal cord (arrow) and in cells flanking the dorso-ventral border of the spinal cord (open arrowhead). (C) At HH23, expression was detected in the dorsal posterior part of the somite (arrowhead) and in cells flanking the dorso-ventral border of the spinal cord (open arrowhead). The expression pattern in the dorsal spinal cord got restricted to the roof plate (arrow). (D) After HH23 expression was found in the dermomyotome (arrowhead), in the roof plate (arrow), in interneurons in the lateral spinal cord and in cells adjacent to the floor plate (open arrowhead). (F) Slit2 was expressed at HH15 in the dorsal spinal cord (arrowhead), in the notochord (arrow) and in the floor plate (open arrowhead). (G and J) At HH18-20 Slit2 expression was detected in the dorsal and ventral spinal cord (open arrowheads), in the whole dermomyotome (arrowheads), weakly in the posterior part of the somite (open arrow in J; compare Vargesson et al., 2001; Fig. 2E) and in the notochord (arrow). (H) At HH23, Slit2 expression started to fade away from the dermomyotome (arrowhead) and was only prominent in the motor columns (arrow) and in the floor plate (open arrowhead). (I) At HH26 Slit2 was only prominent in the floor plate (open arrow) and in subpopulations of motoneurons (arrow). (K) Slit3 expression at HH15 was found in the surface ectoderm (arrowhead), in the ventral spinal cord (open arrowhead) and strongly in the notochord (arrow). (L and O) At HH18-20 Slit3 expression was detected in the surface ectoderm (open arrowhead), the dermomyotome (arrowhead), in the posterior part of the somite (open arrow in O; compare Vargesson et al., 2001; Fig. 2I), the ventral spinal cord and in the notochord (arrow). (M) At HH23, expression was found in the ventral spinal cord (open arrow), the notochord (arrow), weakly in the dermomyotome (arrowhead) and in the epidermis (open arrowhead). (N) At HH26 Slit3 was detected in the ventral spinal cord (open arrow), the epidermis (open arrowhead), in the notochord and perinotochordal cells (arrow). A= anterior somitic compartment, P= posterior somitic compartment. Scale bars: 50 μm in pictures of HH15, HH19 and HH20, 200 μm in HH23 and HH26.

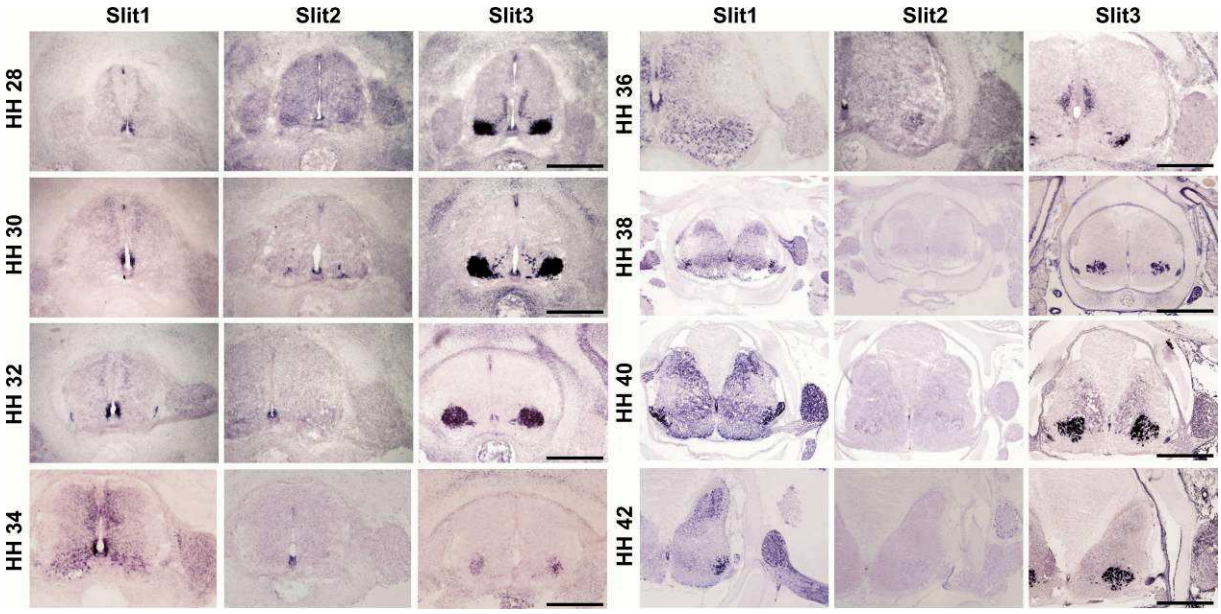

Figure 23 Expression patterns of Slit1-3 at older developmental stages, between HH28 and HH42, suggest roles in the formation of the sensory central collaterals. Slit1 was expressed in the roof plate, in cells flanking the floor plate and in cells adjacent to the ventricular zone at HH28 and HH30. At HH32 Slit1 was expressed as at HH30 with additional expression adjacent to the MEP and weak expression in the DRGs. At HH34 Slit1 was expressed in the floor plate, in the roof plate, adjacent to the MEP, in DRGs and in the entire ventral part of the grey matter and cells around the dorsal midline expressed Slit1 as well. Slit1 expression at HH36 was comparable to the pattern at HH34 except that the expression in the ventral grey matter expanded and formed a ventro-dorsal mRNA-gradient. At HH38, strong Slit1 expression was detectable at the ventral midline, adjacent to the MEP, in the lateral motor column, in the developing Hofmann nucleus, in the sympathetic ganglia and in the entire DRGs. Both, a dorso-ventral and a ventro-dorsal mRNA-gradient were found with strong expression in the dorsal- and in the ventral horn, forming an area of lower expression in the medial part of the grey matter. The dorsal and ventral roots showed Slit1 expression as well. At HH40, Slit1 showed the same gradient and expression at the ventral midline, adjacent to the MEP, in the lateral motor column, in the developing Hofmann nucleus, in the sympathetic ganglia, in the DRGs and in cells ensheathing the ventral and dorsal roots. Slit2 expression was detectable between HH28 and HH42 in the floor plate and at low levels in dynamic changing populations of motoneurons. At HH28 Slit3 was strongly expressed in the floor plate, in the roof plate and in the entire motor column. Strong expression was detectable in cells that extended from the ventral horn to the medial part of the central canal. At HH30 Slit3 was expressed in the floor plate, the roof plate, in the motor column and in cells extending from the ventral horn to the medial part of the central canal. At HH32 Slit3 was expressed in the floor plate, in the roof plate and in the entire motor column. At HH34 Slit3 was expressed in the motor column. At HH36 Slit3 expression was detected in subpopulations of motoneurons and in cells around the dorsal edge of the central canal and the dorsal midline. Between HH38 and HH42 Slit3 was expressed in the motor column, at the ventral midline, dorsal to the MEP, in DRGs and in the sympathetic ganglia. Scale bars: 200 μm for HH28-36 and 500 μm for HH38-42.

4.3 Targeting different tissues using *in ovo* RNAi in chicken embryos

The time point of dsRNA injection into the central canal of the spinal cord, the applied voltage and the number of pulses are crucial parameters for targeting the cell populations of interest. In younger stages (HH10-15) all cell populations of the spinal cord, early and late neural crest cells can be targeted (18 - 20 Volt, +5 - 7 pulses). In this case, the phenotype is found on both sides of the embryo, although stronger on one side, whereas in older stages (HH > 18) only one half of spinal cord gets transfected and one side of the embryo can be used as a control. Targeting the posterior compartment of the developing somite / sclerotome and the dermomyotome needs more voltage and an increased number of applied pulses (HH10-14, 22 Volt, 10 - 12 pulses; Fig. 24).

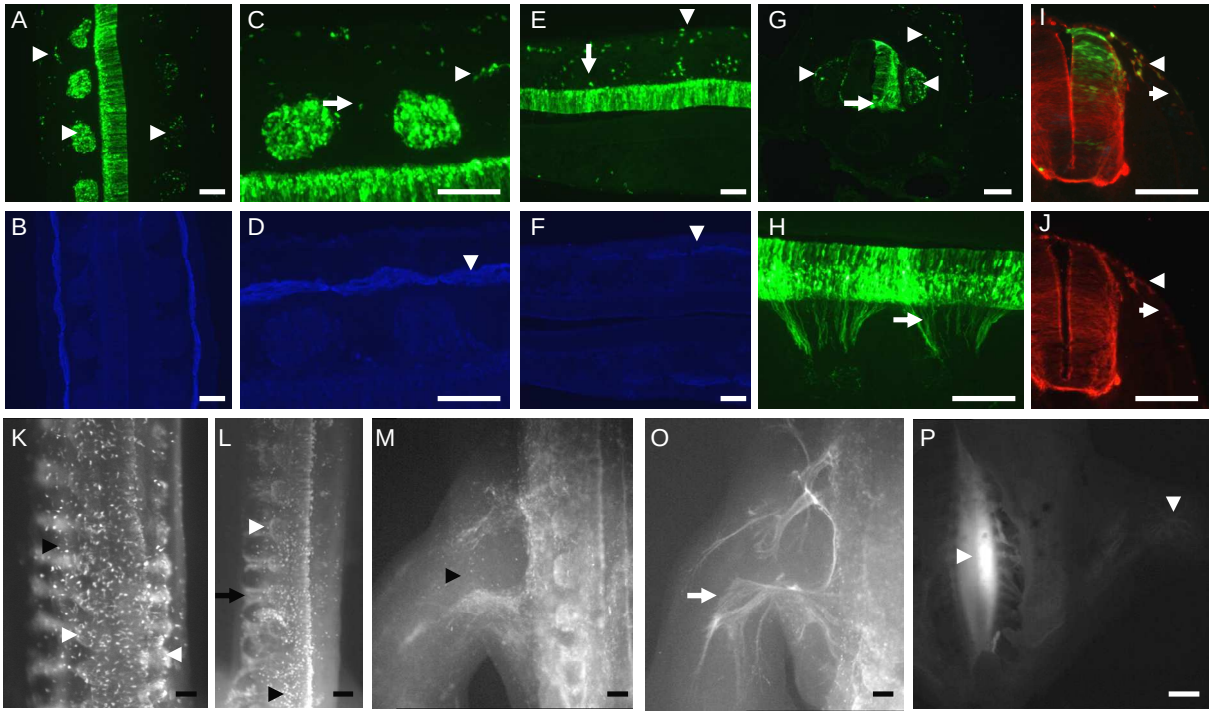

Figure 24 Targeting different areas within the chicken embryo. A pIRES-EYFP expression construct was injected into the central canal of the spinal cord and electroporated between HH10 and HH15 to target different tissues in the developing chicken embryo. All representations except P were stained with a FITC-labelled goat anti GFP antibody. DRGs can be targeted on both sides of the embryo with unilateral electroporation (22 Volt, 7 -10 pulses) up to HH16 (white arrowheads in A, G, K), on one side of the embryo up to HH17/18 (white arrowhead in L). Motoneurons (white arrows in G, H, O) and one side of the spinal cord are accessible up to HH20 (18-25 Volt, 5 - 7 pulses)). Early migrating neural crest cells are accessible between HH10-14 (white arrowhead in I, J; HNK-1 staining in red (22 Volt, 7 - 10 pulses)) and late migrating neural crest cells between HH10 and HH16 (white arrows in I and J; black arrowheads in K, L, M (22 Volt, 7 - 10 pulses)). The posterior part of the developing somite / sclerotome (white arrows in C, E) and the dermomyotome (white arrowheads in C, E; B, D, F are stained with an rabbit anti-Tropomyosin antibody to visualise the dermomyotome) can be targeted up to HH14 (22 Volt, 10 - 12 pulses). YFP expression persists throughout the development and is easily visible in a HH35 dissected embryo under a stereo microscope equipped with fluorescence optics (P). Scale bars: 200µm in A-O, 1000µm in P.

4.4 Downregulation by *in ovo* RNAi is effective and specific

The specificity and efficacy of *in ovo* RNAi was demonstrated previously (Pekarik et al., 2003; Bourikas et al., 2005; Mauti et al., 2007; Philipp et al., submitted). Nevertheless, we used for every analysed gene for the production of dsRNA and *in situ* probes two independent and non-overlapping fragments of cDNA. We approved downregulation quantitatively for Robo1 by qRT-PCR (Fig. 25; Downregulation of 31.35 % +/- 8.34 % in spinal cords (n = 6 wt embryos; n = 14 dsRobo1 embryos; Transfection efficiency around 40%) and 34.5 % +/- 14.88% in DRGs (n = 6 wt embryos; n = 5 dsRobo1 embryos; Tranfection efficiency around 40%)) and qualitatively by *in situ* hybridization. For Robo1, Robo2, Robo3, Slit1, Slit2 and Slit3 we revealed specificity and efficiency of downregulation qualitatively by *in situ* hybridization (Fig. 26-28). The fact that downregulation of Robo3 which is not expressed in sensory neurons never led to a phenotype in our experiments emphasises the specificity of our approach.

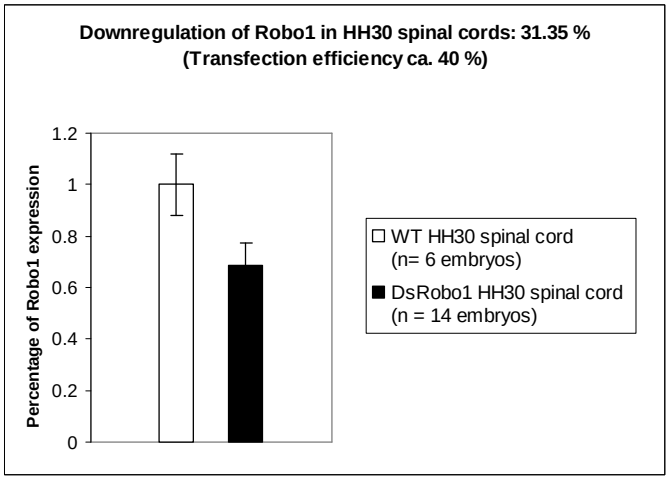

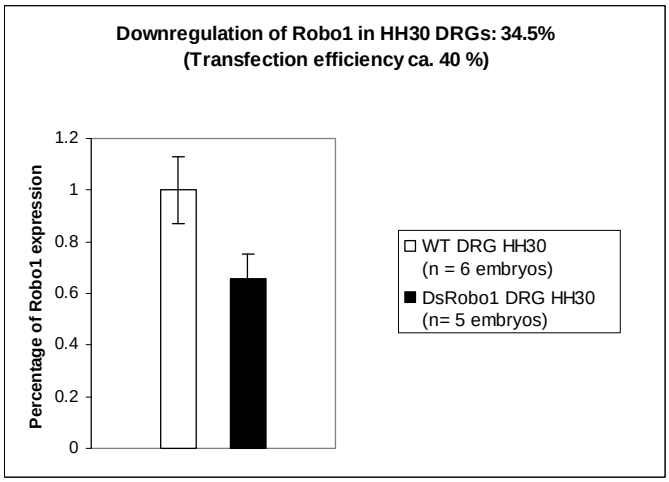

Figure 25 Quantitative real-time PCR analysis of the downregulation of Robo1 in chicken HH30 spinal cords (top panel) and DRGs (lower panel). Downregulation of Robo1 was 31.35 % +/- 8.34 % in spinal cords (n = 6 wt embryos; n = 14 DsRobo1 embryos; Transfection efficiency around 40%) and 34.5 % +/- 14.88% in DRGs (n = 6 embryos; n = 5 DsRobo1 embryos; Transfection efficiency around 40%). Error bars represent standard deviation.

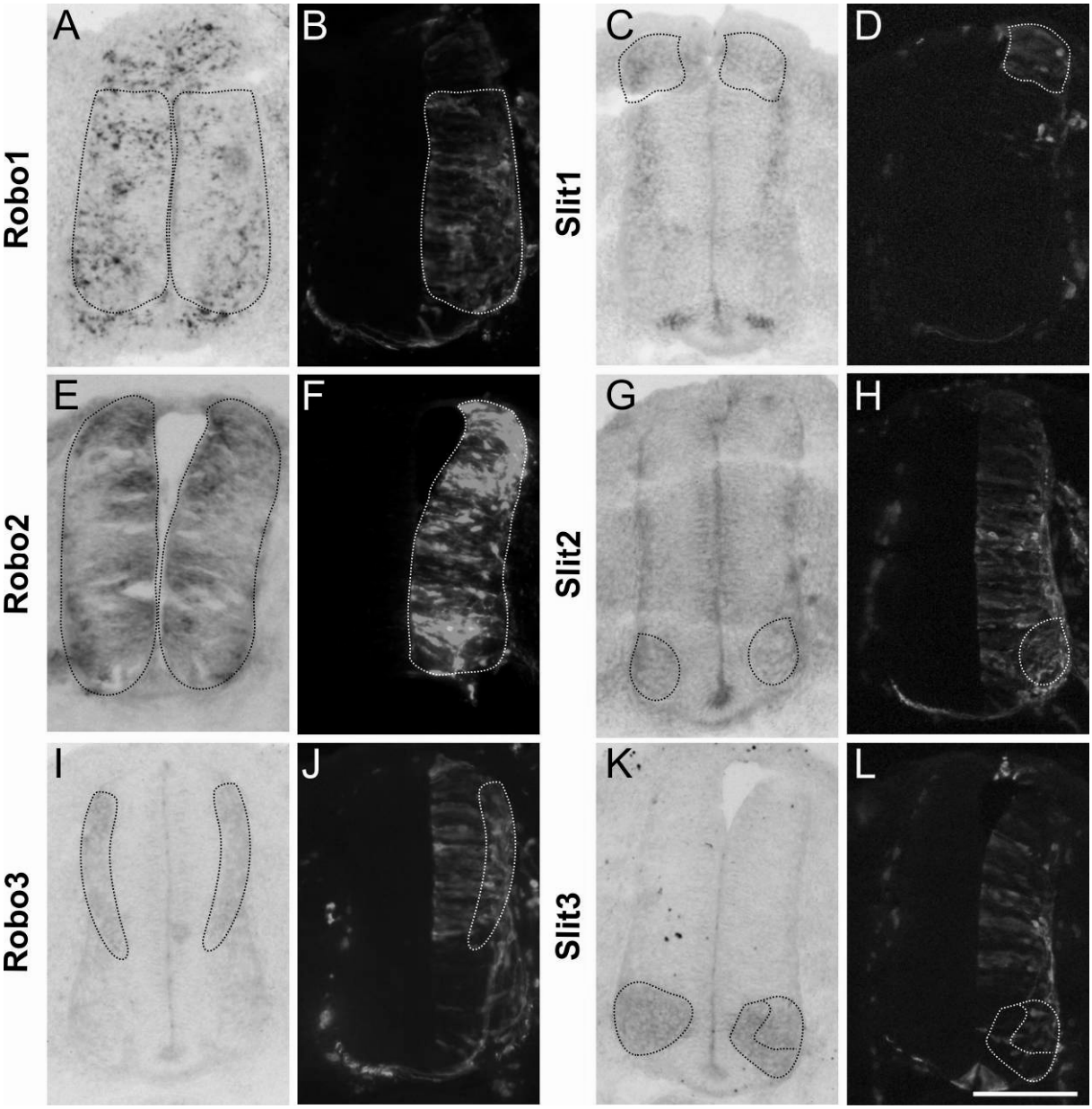

Figure 26 Qualitative analysis of the efficacy of downregulation by *in situ* hybridization. A different fragment was used for downregulation and detection respectively. The experimental side is the right half of the spinal cord. Dotted lines indicate where expression was compared. A and B: DsRobo1; C and D: DsSlit1; E and F: DsRobo2; G and H: DsSlit2; I and J: DsRobo3; K and L: DsSlit3. B, D, F, H, J and L represent pIRES-EYFP expression as transfection control. N embryos ≥ 3. Scale bars equal 200μm.

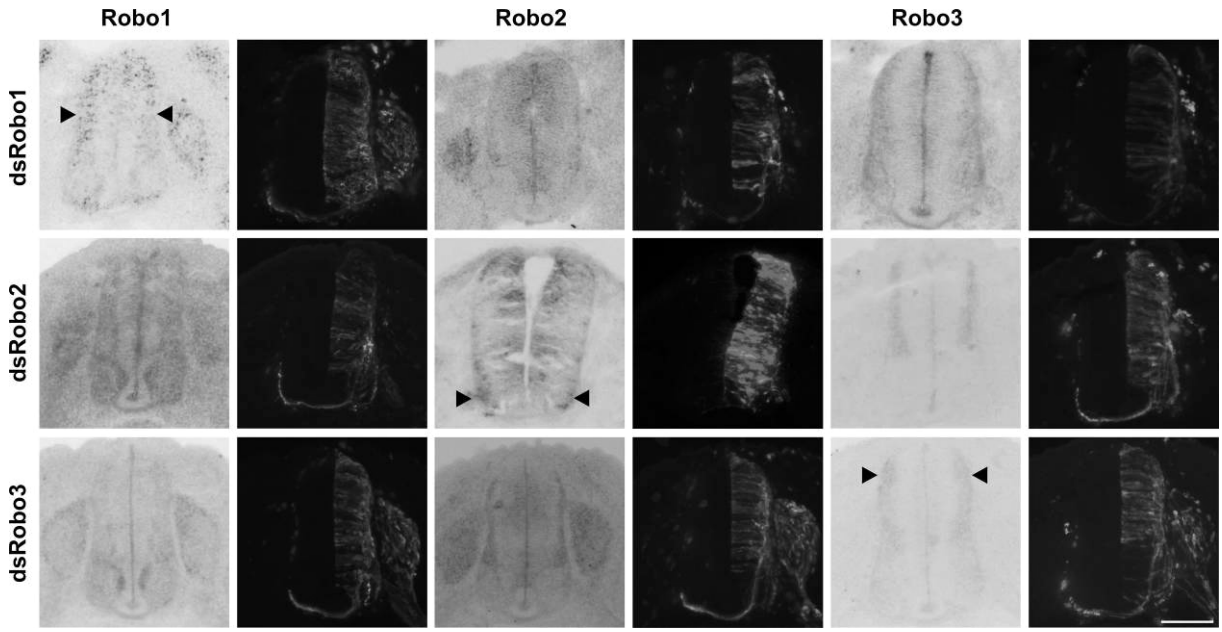

Figure 27 Qualitative analysis of the specificity of downregulation of Robos by *in situ* hybridization. A different fragment was used for downregulation and detection respectively. The experimental side of the spinal cord is right. YFP immunostainings represent pIRES-EYFP expression as transfection control to monitor the electroporated area. Arrowheads indicate sites of differential expression. N embryos ≥ 3. Scale bars equal 200µm.

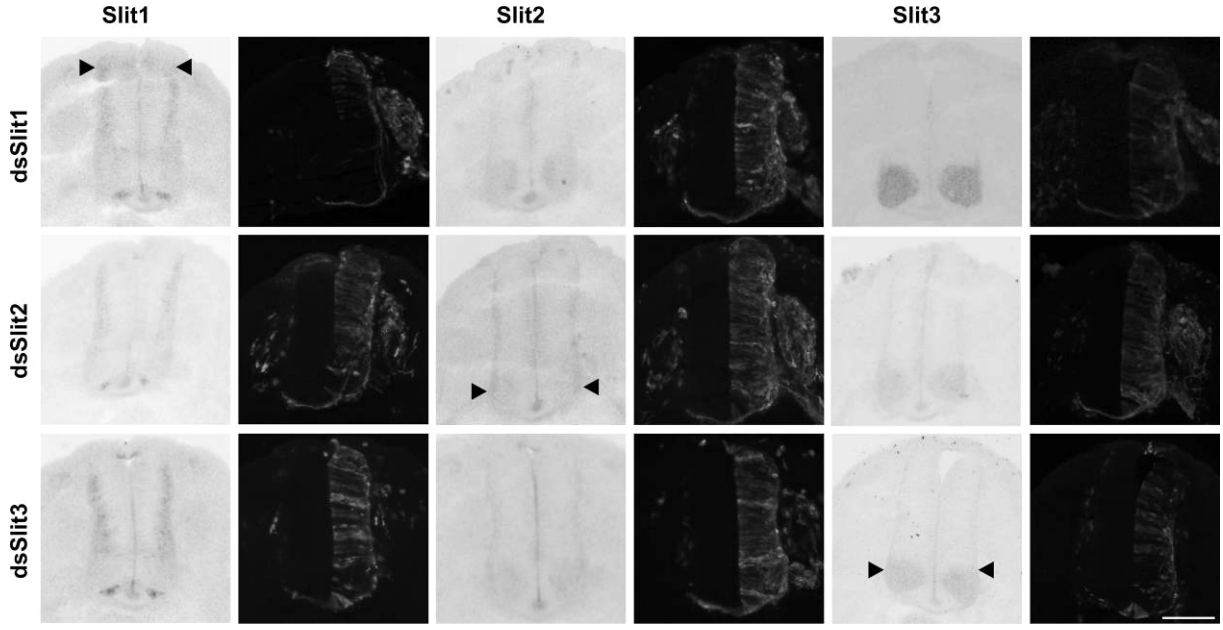

Figure 28 Qualitative analysis of the specificity of downregulation of Slits by *in situ* hybridization. A different fragment was used for downregulation and detection respectively. The experimental side of the spinal cord is right. YFP immunostainings represent pIRES-EYFP expression as transfection control to monitor the electroporated area. Arrowheads indicate sites of differential expression. N embryos ≥ 3. Scale bar: 200µm.

4.5 Lack of Robo1, Robo2, Slit1 and Slit2 leads to impaired early neural crest cell migration

To analyse the behaviour of early neural crest cells and sensory axons in absence of Slit / Robo signalling we generated double stranded RNA derived from plasmids encoding Robo1-3 and Slit1-3. An advantage of *in ovo* RNAi over knock out strategies is that one can manipulate the expression of genes shortly before the analysis of the desired process without running of risk that either the knock out is lethal or other genetic systems compensate for the lack of the missing gene. We injected the dsRNA at HH11-13 to dissect the process of early neural crest cell migration and at HH11-16 to analyse sensory axon guidance. By varying the position of electrodes and the number of pulses we are able to target neural crest cells, DRGs, the dorsal spinal cord (Pekarik et al., 2003) and cells lying in the posterior somite and in the dermomyotome (Fig. 24; Scaal et al., 2004). Due to the developmental delay along the rostro-caudal axis, it is impossible to target early neural crest cells at the same migration point along the embryonal axis. Transfection will always hit neural crest cells that have migrated for different distances within one single embryo. Therefore, we analysed every embryo very carefully with respect to the rostro-caudal gradient of transfection. As marker for early neural crest cells, we used HNK-1 (Fig. 29A-G). Sensory neurons were visualised with Islet-1 (Fig. 29H–N). In wild-type and control embryos neural crest cells always migrated into the anterior compartment of the somite / sclerotome (Fig. 29H) and aggregated into segregated DRGs in the anterior compartment of the sclerotome (Fig. 29A). Silencing of Robo1 (Fig. 29C, J) and Robo2 (Fig. 29D, K), but not Robo3 (Fig. 29B, I), resulted in neural crest cells migrating ectopically into the posterior part of the somite and into the dermomyotome. Consequently, DRGs were connected and elongated when analysed in whole-mount embryos stained with an anti neurofilament antibody at HH21-23 (Fig. 35-37). Downregulation of Slit1 (Fig. 29E, L) and Slit2 (Fig. 29F, M) resulted in the same phenotypes. These findings were also observed in whole-mount preparations stained with an anti neurofilament antibody at HH21-23 (Fig. 39-42). Although downregulation of Slit3 resulted in HNK-1 positive cells along the connected dorsal roots, (Fig. 29N) there were no Islet-1 positive cells found in the posterior part of the somite or the dermomyotome (Fig. 29G). Furthermore, we dissected DRGs from HH24/25 embryos and counted cells in the DRGs (Fig. 30). After downregulation of Robo1 (n = 9 embryos), Robo2 (n = 8 embryos), Robo1+2 (n = 4 embryos), Slit1 (n = 5 embryos), Slit2 (n = 5 embryos) or Slit1+2+3 (n = 5 embryos) the number of DRG cells was significantly reduced (Fig. 30; Table 1; n DRGs for each condition ≥ 15; see also Jia et al., 2005). The polarity of the somites was not affected when Robos or Slits were silenced as shown by Peanut-Agglutinin Lectin staining (Fig. 31; n embryos ≥ 3).

4.6 Boundary cap cell clustering is disrupted in Robo1, Robo2 and in Slit1-3 deficient embryos

A subpopulation of late migrating early neural crest cells turn into boundary cap cells which enclose dorsal roots entering the DREZ transiently. Boundary cap cells migrate to the DREZ some hours before the first primary afferents reach it (Golding and Cohen, 1997) and may have a role in preparing the spinal cord to be permissive for in-growth of sensory axons (Golding and Cohen, 1997). We analysed this subpopulation of cells on longitudinal sections with the specific marker IE8 at HH21-23 (Fig. 29O-U). In wild type (Fig. 29O) and control (Fig. 29P) embryos boundary cap cells always form a

regular set of five to six clusters at the DREZ in the anterior sclerotome. In Robo1 (Fig. 29Q), Robo2 (Fig. 29R), Slit1-3 (Fig. 29S-U) deficient embryos the clustering of boundary cap cells was disrupted. The clusters were smaller and positioned at the DREZ over the length of the entire sclerotome.

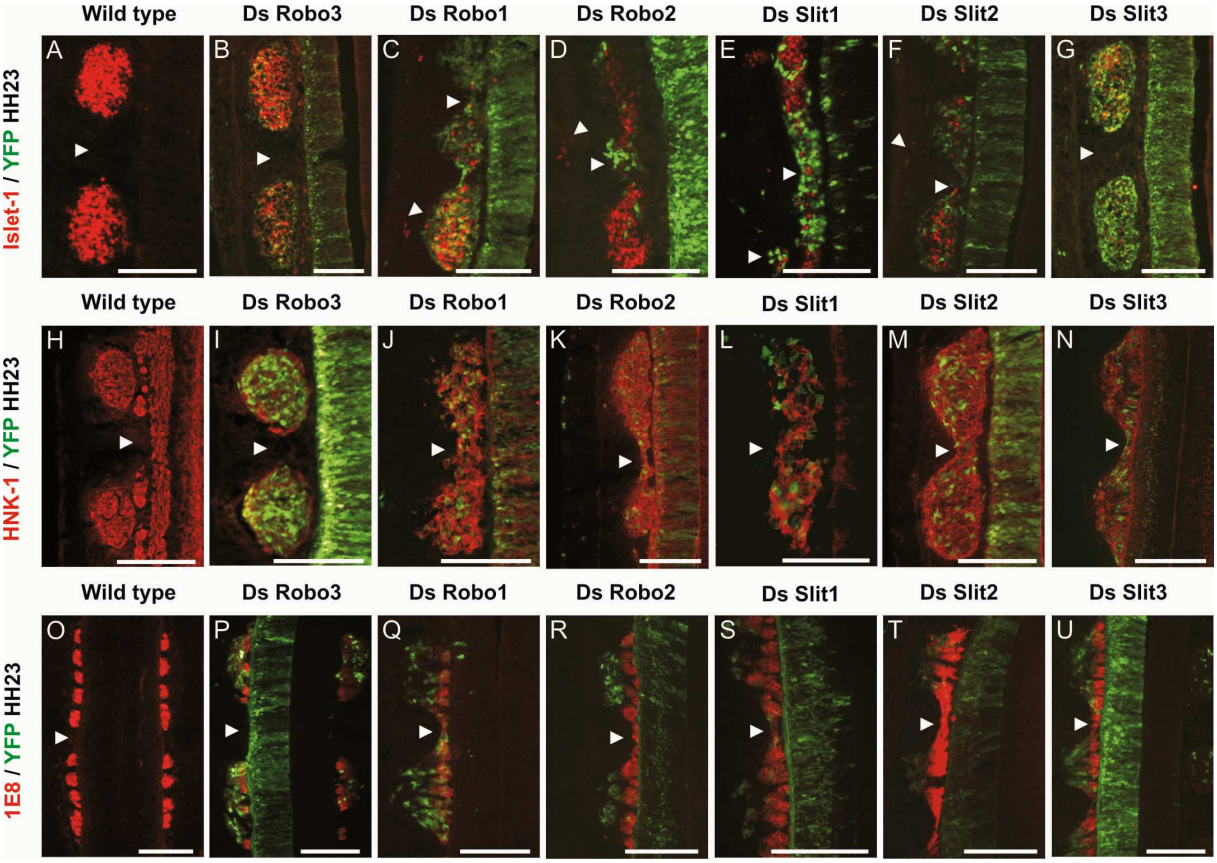

Figure 29 Lack of Robo1 and Robo2 or Slit1 and Slit2 leads to impaired early neural crest cell migration. Immunohistochemistry was done on longitudinal cryosections with different markers for early neural crest cells (HNK-1; A-G), sensory neurons (Islet-1; H-N) and boundary cap cells (1E8; O-U). In wild-type and control embryos neural crest cells always migrated into the anterior compartment of the somite / sclerotome (H) and aggregated into segregated DRGs in the anterior compartment of the sclerotome (A). Lack of Robo1 (C and J) and Robo2 (D and K), but not Robo3 (B and I) resulted in wrong migration of early neural crest cells into the caudal half of the somite and the dermomyotome (arrowheads). These findings were also attained when Slit1 (E and L) and Slit2 (F and M), but not Slit3 (G and N) were downregulated (arrowheads). Although downregulation of Slit3 resulted in HNK-1 positive cells along the connected dorsal roots (arrowhead in N), there were no HNK-1 or Islet-1 positive cells found in the posterior part of the somite or the dermomyotome (G). Counting cells in DRGs indicated that DRGs of Robo1, Robo2, Slit1 or Slit2 deficient embryos contained a significantly smaller number of cells (Fig. 30). (O-U) Boundary cap cell clustering. In wild-type or control embryos boundary cap cells always formed 4 to 5 clusters ensheathing the dorsal roots of one DRG (O,P). Boundary cap cell clustering was disrupted in Robo1 (Q) and Robo2 (R) and in Slit1 (S), Slit2 (T) and Slit3 (U) deficient embryos. The clusters were smaller and positioned at the DREZ over the length of the entire sclerotome. N embryos ≥ 3. Scale bars: 200µm.

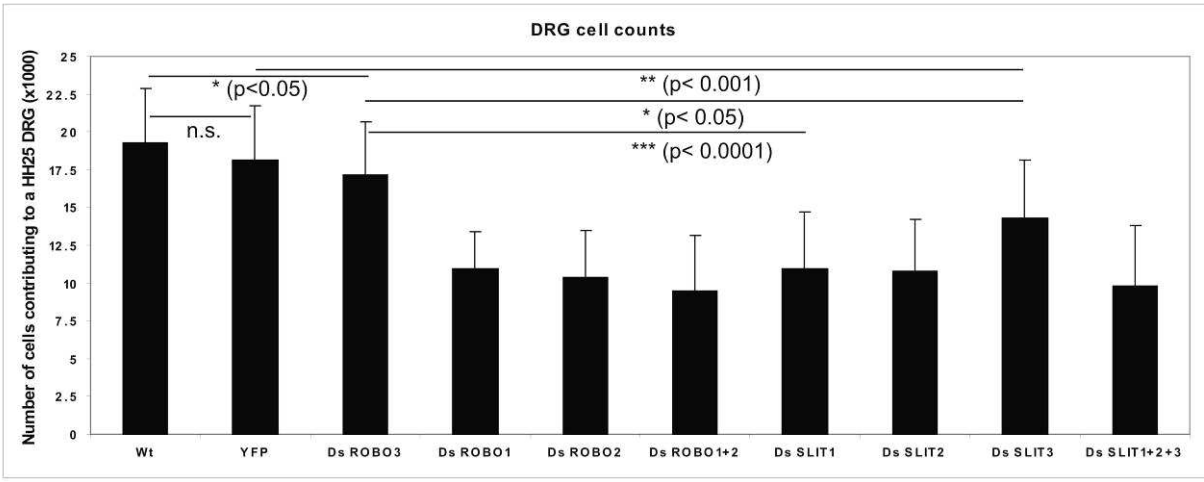

Figure 30 Counting cells in DRGs indicated that DRGs after silencing of Robo1, Robo2, Slit1 and Slit2 contained a significantly smaller number of cells. The most likely explanation is the additional migration into the caudal somite, the dermomyotome and the dorso-lateral pathway. N embryos for each condition ≥ 3, n DRGs for each condition ≥ 15. Error bars represent standard deviation.

	Average number of cells	standard deviation	n embryos	p values compared to wildtype	compared to dsRobo3	compared to YFP
Wildtype	19.26563	3.595549	4	0.5	0.045235697	0.137830382
YFP	18.125	3.597073	3	0.137830382	0.210959735	0.5
DsRobo3	17.125	3.573792	3	0.045235697	0.5	0.210959735
DsRobo1	10.91667	2.50376	9	9.8556E-17	1.16111E-06	7.64375E-11
DsRobo2	10.35938	3.146692	8	7.65877E-17	3.38152E-07	1.23702E-11
DsRobo1+2	9.4375	3.699003	4	1.42346E-16	4.46759E-08	3.01157E-12
DsSlit1	10.975	3.727374	5	1.60816E-13	3.0584E-06	6.5583E-10
DsSlit2	10.75	3.439648	5	8.9411E-14	1.79667E-06	3.52635E-10
DsSlit3	14.29167	3.850438	3	7.86273E-06	0.014633172	0.000361854
DsSlit1+2+3	9.8	3.983147	5	3.39015E-15	1.60209E-07	1.81943E-11

Table 1 DRG cell count. Average of counted DRG cells, standard deviation, number of embryos and probabilities of the Student`s t-test are shown.

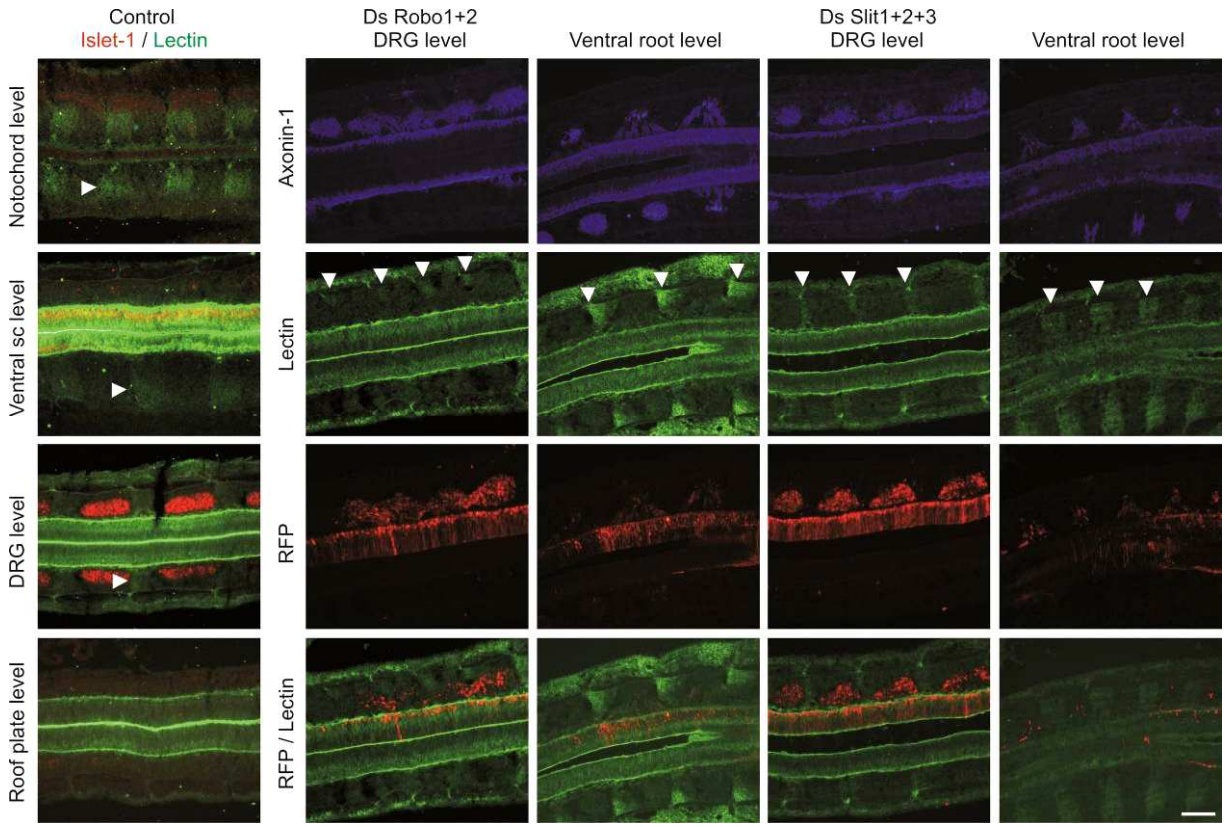

Figure 31 Peanut-Agglutinin Lectin staining (arrowheads, Marker for posterior somitic compartment) reveals no change of the somitic polarity in embryos deficient for Robo1+2 and Slit1+2+3 compared to control embryos. N embryos ≥ 2. Scale bar: 200μm.

4.7 The pathfinding of DRG neurons towards the dorsal root entry zone is severely affected in the absence of Robo1 and Robo2

After the differentiation of an early neural crest cell into a DRG neuron, two axons are extending, one towards the periphery and one in direction of the spinal cord. The former are called peripheral and the latter central branches. The dorsal roots formed by the central branches are segregated into four to six bundles that extend in the anterior sclerotome towards the dorsal root entry zone (DREZ; Fig. 32-34). Almost nothing is known about how these central branches grow towards the DREZ to invade the spinal cord. Therefore, we were interested in finding mechanisms giving more insight into this topic. An attractive cue that pulls central branches towards the DREZ is not known in vertebrates (Masuda and Shiga, 2005). In Drosophila, Robo2 can serve as an attractant in a Slit-independent non-cell-autonomous manner (Parsons et al., 2003). However, we silenced all Robos and Slits between HH11 and HH16 and checked in whole-mount preparations whether the formation of dorsal roots is perturbed (Fig. 34-37 and 39-42). Indeed a strong phenotype was prominent in Robo1 (Fig. 35; Table 2), Robo2 (Fig. 36; Table 2), Robo1+2 (Fig. 37; Table 2) but not in Robo3 (Fig. 34; Table 2) deficient embryos. The normal appearance of properly segregated dorsal roots was disrupted. DRGs and dorsal roots were fused and connected, DRGs elongated and smaller, dorsal roots were entering the DREZ along the anterior and posterior part of the sclerotome (arrowheads in Fig. 35A, 36A and 37A). A fraction of central branches was growing towards the dermomyotome and dorso-lateral sclerotome (arrows in Fig. 35A, 36A and 37A). Compared to control embryos (wild-type, YFP-injected or embryos lacking Robo3/Rig1), Robo1, Robo2 or Robo1+2 deficient embryos showed a significantly increased number of DRGs with phenotype (Fig. 38A). A schematic model with wild-type and experimental situation is depicted in Fig. 38B. A DRG was counted as phenotypic if the ratio of DRG length / segment length differed more than one standard deviation from the value obtained for YFP-injected control embryos. Robo1 and Robo2 showed similar defects and embryos with deficient Robo1+2 exhibited an increase in strength of the phenotype (Fig. 38). This implies an at least partial redundant function of Robo1 and Robo2 in this process.

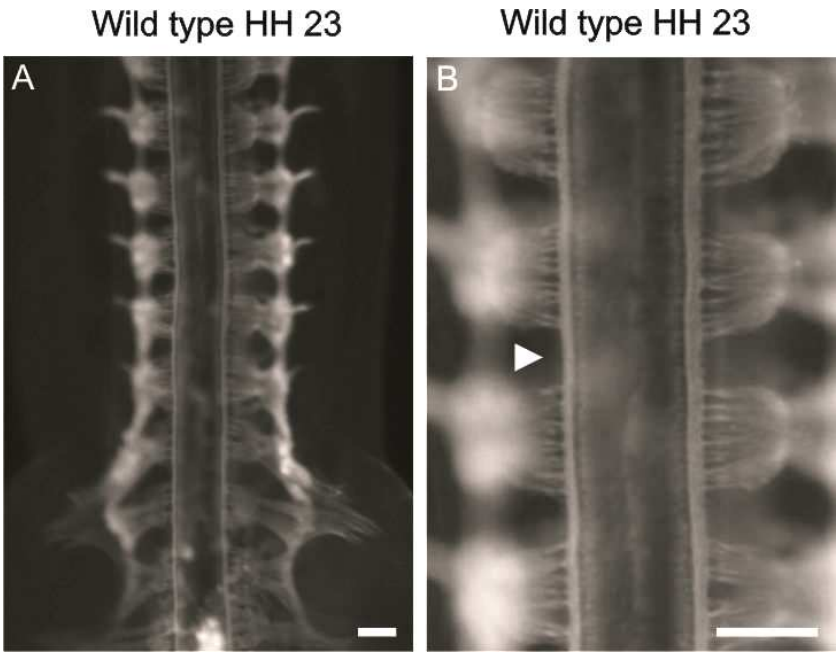

Figure 32 Wild-type whole-mount prepared HH23 chicken embryo. (A and B) Neurofilament immunostaining with RMO270 visualizes all of the peripheral axonal projections including central and peripheral branches of sensory neurons. DRGs were regularly spaced (arrowhead). Dorsal roots were arranged in parallel and form four to six bundles. Single neurites crossing from one DRG to another one were never seen. Quantification and a schematic model are depicted in Fig. 38. Nine DRGs (6 trunk and LS1-LS3) were measured per embryo. Scale bars equal 200 μm.

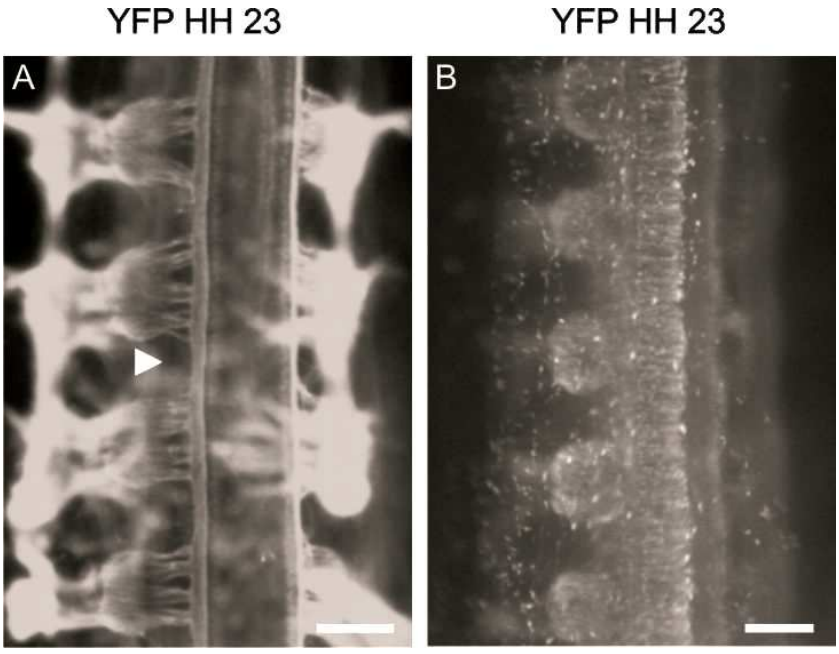

Figure 33 YFP-plasmid injected control embryo. (A) Neurofilament immunostaining with RMO270 visualizes all of the peripheral axonal projections including central and peripheral branches of sensory neurons. (B) YFP immunostaining reveals area of transfection within the embryo. DRGs were regularly spaced (arrowhead). Dorsal roots were arranged in parallel and form four to six bundles. Single neurites crossing from one DRG to another one were rarely seen. Quantification and a schematic model are depicted in Fig. 38. Nine DRGs (6 trunk and LS1-LS3) were measured per embryo. Scale bars equal 200 μm.

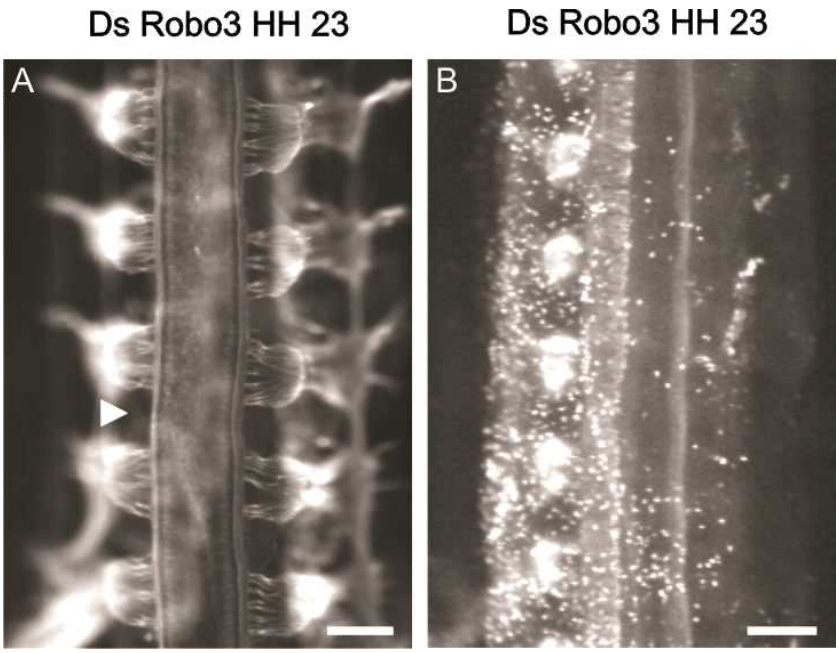

Figure 34 Representative Robo3/Rig1 deficient embryo. (A) Neurofilament immunostaining with RMO270 visualizes axonal projections including central and peripheral branches of sensory neurons. (B) YFP immunostaining reveals area of transfection within the embryo. DRGs were regularly spaced (arrowhead). Dorsal roots were arranged in parallel and formed four to six bundles. Single neurites crossing from one DRG to another one were rarely seen. Quantification and schematic model are depicted in Fig. 38. Nine DRGs (6 trunk and LS1-LS3) were measured per embryo. For every target gene two non-overlapping fragments were used to generate dsRNA. Values for aberrant DRGs did not differ significantly in any case. Therefore, the results for the two different fragments are pooled. Scale bars equal 200 μm.

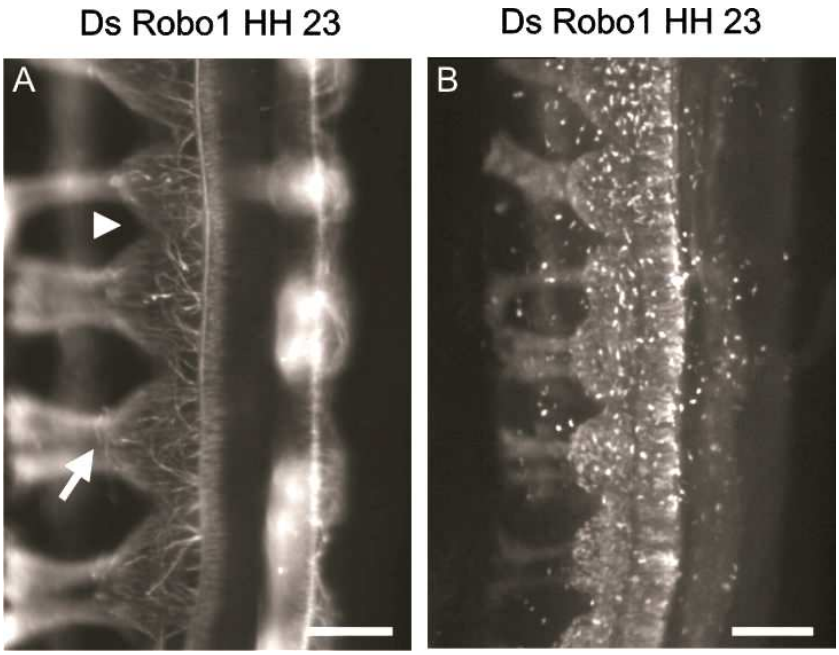

Figure 35 Representative Robo1 deficient embryo. (A) Neurofilament immunostaining with RMO270 visualizes peripheral axonal projections including central and peripheral branches of sensory neurons. (B) YFP immunostaining reveals area of transfection within the embryo. DRGs were no longer metameric segregated but fused, elongated and miss-formed (arrowhead). Dorsal roots were connecting between DRGs and crisscrossing within the DRG. Single central branches invaded the sclerotome and dermomyotome (arrow). Quantification and a schematic model are depicted in Fig. 38. Nine DRGs (6 trunk and LS1-LS3) were measured per embryo. Scale bars equal 200 μm.

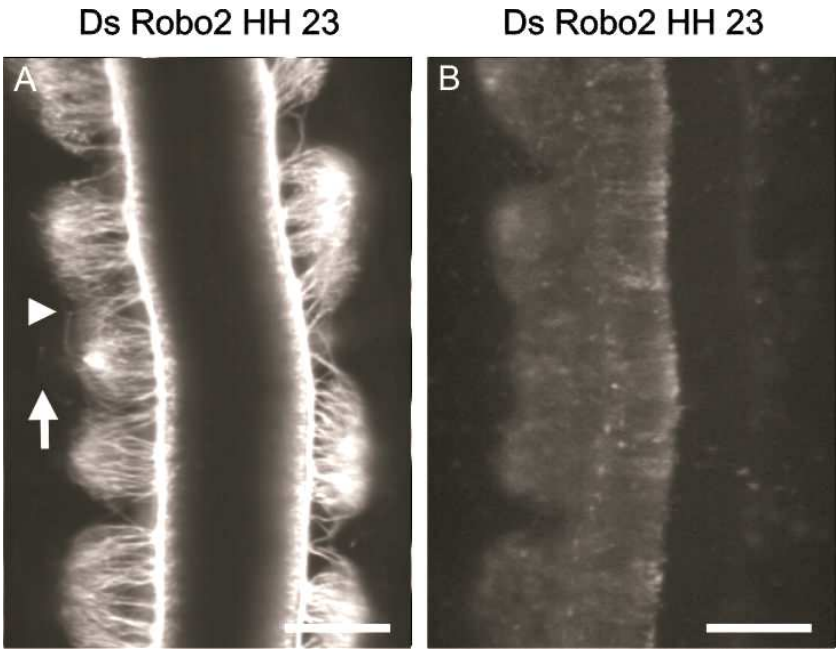

Figure 36 Representative Robo2 deficient embryo. (A) Neurofilament immunostaining with RMO270 visualizes peripheral axonal projections including central and peripheral branches of sensory neurons. (B) YFP immunostaining reveals area of transfection within the embryo. DRGs were no longer metameric segregated but fused, elongated and miss-formed (arrowhead). Dorsal roots were connecting between DRGs and crisscrossing within the DRG. Single central branches invaded the sclerotome and dermomyotome (arrow). Quantification and a schematic model are depicted in Fig. 38. Nine DRGs (6 trunk and LS1-LS3) were measured per embryo. Scale bars equal 200 μm.

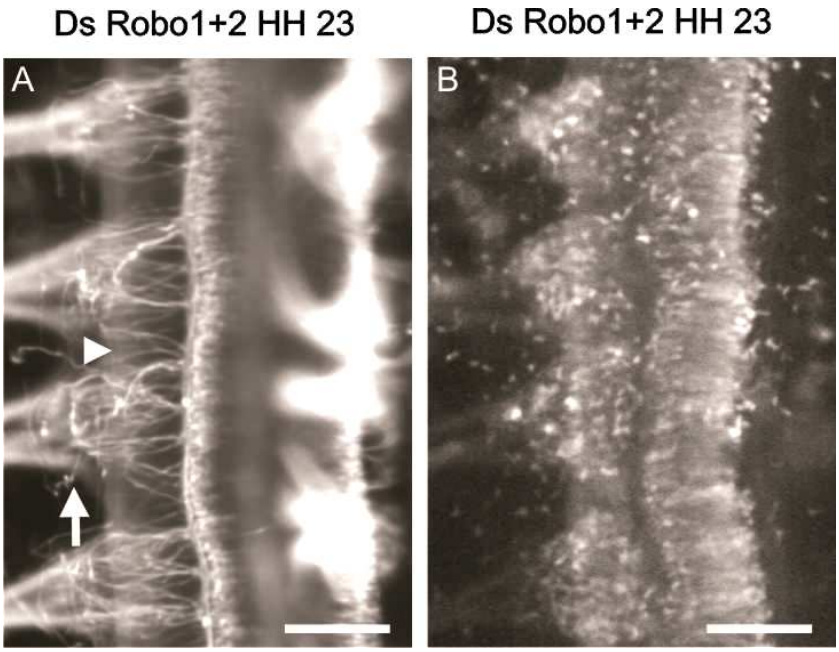

Figure 37 Representative Robo1+2 deficient embryo. (A) Neurofilament immunostaining with RMO270 visualizes peripheral axonal projections including central and peripheral branches of sensory neurons. (B) YFP immunostaining reveals area of transfection within the embryo. DRGs were no longer metameric segregated but elongated, fused, smaller and miss-formed (arrowhead). Dorsal roots were connecting between DRGs and crisscrossing within the DRG. A significant portion of central branches invaded the sclerotome and dermomyotome (arrow). Quantification and a schematic model are depicted in Fig. 38. Nine DRGs (6 trunk and LS1-LS3) were measured per embryo. Scale bars equal 200 μm.

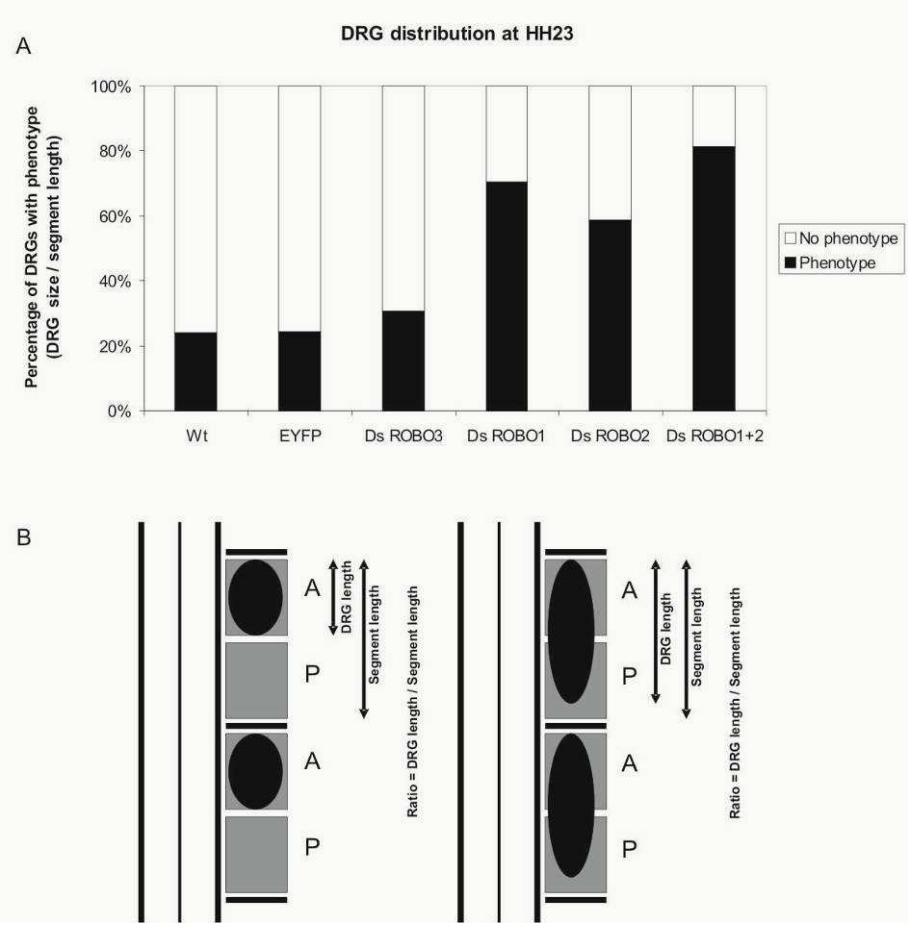

Figure 38 Quantification of the phenotypes observed in embryos where Robos were downregulated. (A) Compared to control embryos (wild-type, YFP-injected or embryos lacking Robo3/Rig1), Robo1, Robo2 or Robo1+2 deficient embryos showed a significantly increased number of DRGs with phenotype. (B) Schematic model with wild-type situation on the left side and experimental situation on the right side. A DRG was counted as phenotypic if the ratio of DRG length / segment length differed more than one standard deviation from the value obtained for YFP-injected control embryos. Nine DRGs (6 trunk and LS1-LS3) were measured per embryo. For each target gene two non-overlapping fragments were used to generate dsRNA. Values for aberrant DRGs did not differ significantly in any case. Therefore, the results for the two different fragments are pooled.

	Percentage of DRGs with phenotype	n embryos	n DRGs	p values compared to wildtype:	compared to YFP:	compared to dsRobo3:
Wildtype	24.10%	15	195		0.386416014	0.137839756
YFP	24.44%	16	135	0.386416014		0.103306611
DsRobo3	30.77%	10	78	0.137839756	0.103306611	
DsRobo1	70.39%	18	331	8.52026E-28	2.29E-24	2.52E-10
DsRobo2	58.73%	19	252	1.32012E-14	1.06E-13	6.16E-06
DsRobo1+2	81.46%	18	151	7.9634E-32	4.76E-29	4.25E-21

Table 2 Analysis of DRG segregation in whole-mount embryos. Percentage of embryos with phenotype, number of analysed embryos and DRGs and Student`s t-test data are shown.

4.8 Silencing of Slits in the dorsal spinal cord, the somites / sclerotome and in the dermomyotome phenocopies the impairments seen after silencing Robo1 or Robo2

We were interested whether we can reproduce the phenotypes obtained after silencing of Robo1 and Robo2 by interfering with their ligands, the Slits. To target all tissues where Slits are expressed, namely the dorsal and ventral spinal cord, the dermomyotome and the posterior sclerotome, a different electroporation procedure is required. Injection of dsRNA can still be done into the central canal of the spinal cord but the application of more pulses (twelve instead of five to seven) during electroporation is required to penetrate the somite and the dermomyotome (Fig. 24). Between HH10 and HH15, the basal lamina around the spinal cord is not yet tight and a penetration of nearby tissue by molecules injected into the central canal is possible (Fig. 24). The downregulation of Slit1, Slit2 and Slit3 between HH11 and HH14 resulted in similar phenotypes to the ones seen in Robo1 and Robo2 deficient embryos. The formation of dorsal roots and DRGs was perturbed, dorsal roots entered the spinal cord all along the spinal cord, both in the anterior and in the posterior part of the sclerotome (Fig. 39-42; arrowheads in Fig. 39A, 40A, 41A, 42A). Furthermore, central branches grew towards the dermomyotome and sclerotome (arrows in Fig. 39A, 40A, 41A, 42A). Compared to control embryos (wild-type, YFP-injected or embryos lacking Robo3/Rig1), Slit1, Slit2 and Slit3 deficient embryos showed a significantly increased number of DRGs with phenotype (Fig. 43A). A schematic model with wild-type and experimental situation is depicted in Fig. 43B. A DRG was counted as phenotypic if the ratio of DRG length / segment length differed more than one standard deviation from the value obtained for YFP-injected control embryos. Nine DRGs (6 trunk and LS1-LS3) were measured per embryo. For each target gene two non-overlapping fragments were used to generate dsRNA. Values for aberrant DRGs did not differ significantly in any case. Therefore, the results for the two different fragments are pooled. Embryos lacking Slit1 (Fig. 39A, B; Table 3), Slit2 (Fig. 40A, B; Table 3) or Slit3 (Fig. 41A, B; Table 3) showed similar phenotypes and triple downregulation of the Slits (Fig. 42A; Table 3) increased the severity of the phenotype (Fig. 43). This indicates that Slits act at least partially in a redundant manner but in slightly different areas within the chicken embryo depending on their different expression patterns.

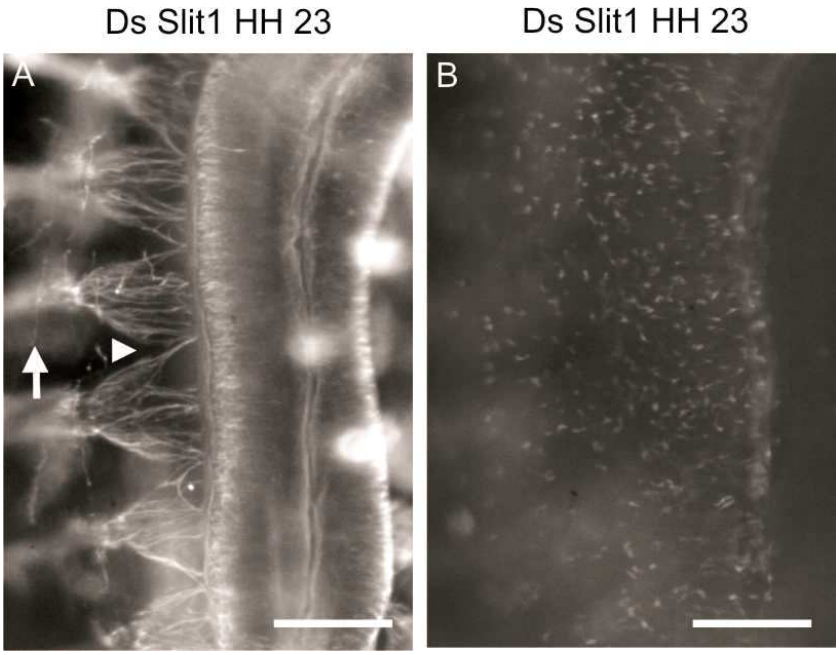

Figure 39 Representative Slit1 deficient embryo. (A) Neurofilament immunostaining with RMO270 visualizes peripheral axonal projections including central and peripheral branches of sensory neurons. (B) YFP immunostaining reveals area of transfection within the embryo. The formation of DRGs and dorsal roots was perturbed. DRGs were fused, elongated and smaller in Slit1 deficient embryos (arrowhead), the dorsal roots innervated the DREZ in the anterior and posterior somitic compartment / sclerotome (arrowheads). Furthermore, central branches grew towards the dermomyotome and sclerotome (arrow). Quantification and a schematic model are depicted in Fig. 43. Nine DRGs (6 trunk and LS1-LS3) were measured per embryo. Scale bars equal 200 µm.

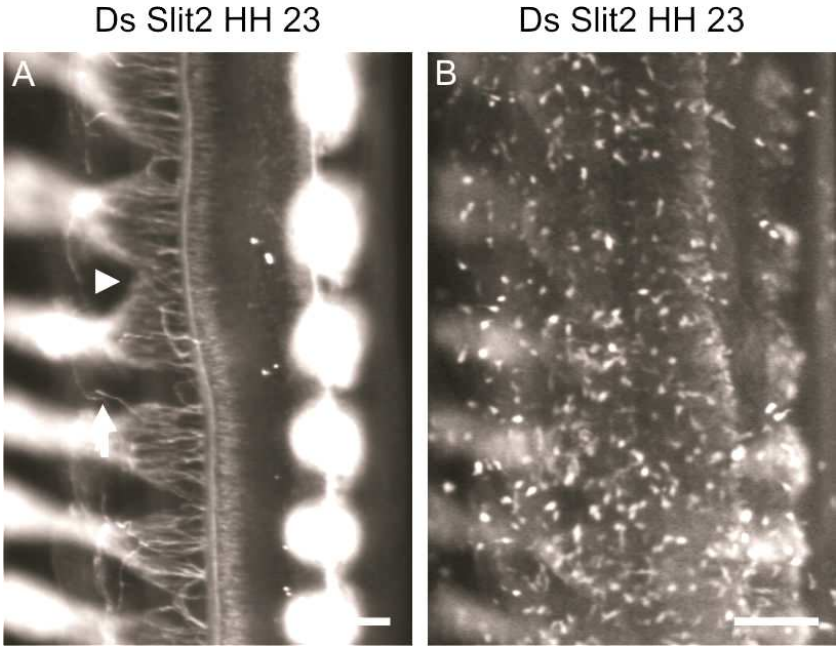

Figure 40 Representative Slit2 deficient embryo. (A) Neurofilament immunostaining with RMO270 visualizes peripheral axonal projections including central and peripheral branches of sensory neurons. (B) YFP immunostaining reveals area of transfection within the embryo. The formation of DRGs and dorsal roots was perturbed. DRGs were connected, elongated and smaller in Slit2 deficient embryos (arrowhead), the dorsal roots innervated the DREZ in the anterior and posterior somitic compartment / sclerotome (arrowheads). Additionally central branches grew towards the dermomyotome and sclerotome (arrow). Quantification and a schematic model are depicted in Fig. 43. Nine DRGs (6 trunk and LS1-LS3) were measured per embryo. Scale bars equal 200 µm.

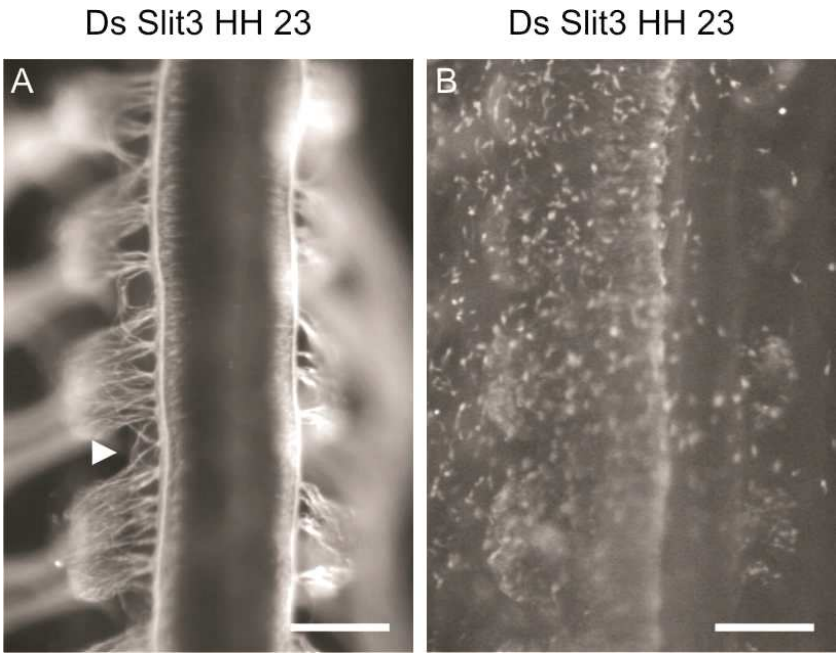

Figure 41 Representative Slit3 deficient embryo. (A) Neurofilament immunostaining with RMO270 visualizes peripheral axonal projections including central and peripheral branches of sensory neurons. (B) YFP immunostaining reveals area of transfection within the embryo. The formation of DRGs and dorsal roots was perturbed. DRGs were elongated and dorsal roots were fused in Slit3 deficient embryos (arrowhead). The dorsal roots innervated the DREZ in the anterior and posterior somitic compartment / sclerotome (arrowhead), the appearance of DRGs was slightly affected. Quantification and a schematic model are depicted in Fig. 43. Nine DRGs (6 trunk and LS1-LS3) were measured per embryo. Scale bars equal 200 μm.

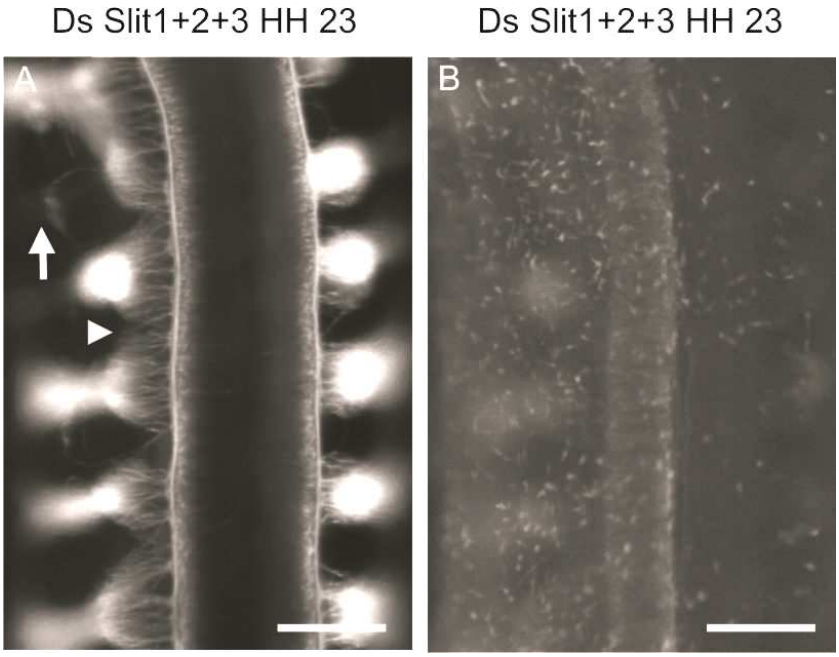

Figure 42 Representative embryo lacking Slit1, Slit2 and Slit3. (A) Neurofilament immunostaining with RMO270 visualizes peripheral axonal projections including central and peripheral branches of sensory neurons. (B) YFP immunostaining reveals area of transfection within the embryo. These embryos showed similar phenotypes compared to single Slit1 or Slit2 deficient embryos. The formation of DRGs and dorsal roots was perturbed. DRGs and dorsal roots were connected, elongated and smaller (arrowhead). Additionally central branches grew towards the dermomyotome and sclerotome (arrow). Triple downregulation of the Slits increased the severity of the phenotype. Quantification and a schematic model are depicted in Fig. 43. Nine DRGs (6 trunk and LS1-LS3) were measured per embryo. Scale bars equal 200 μm.

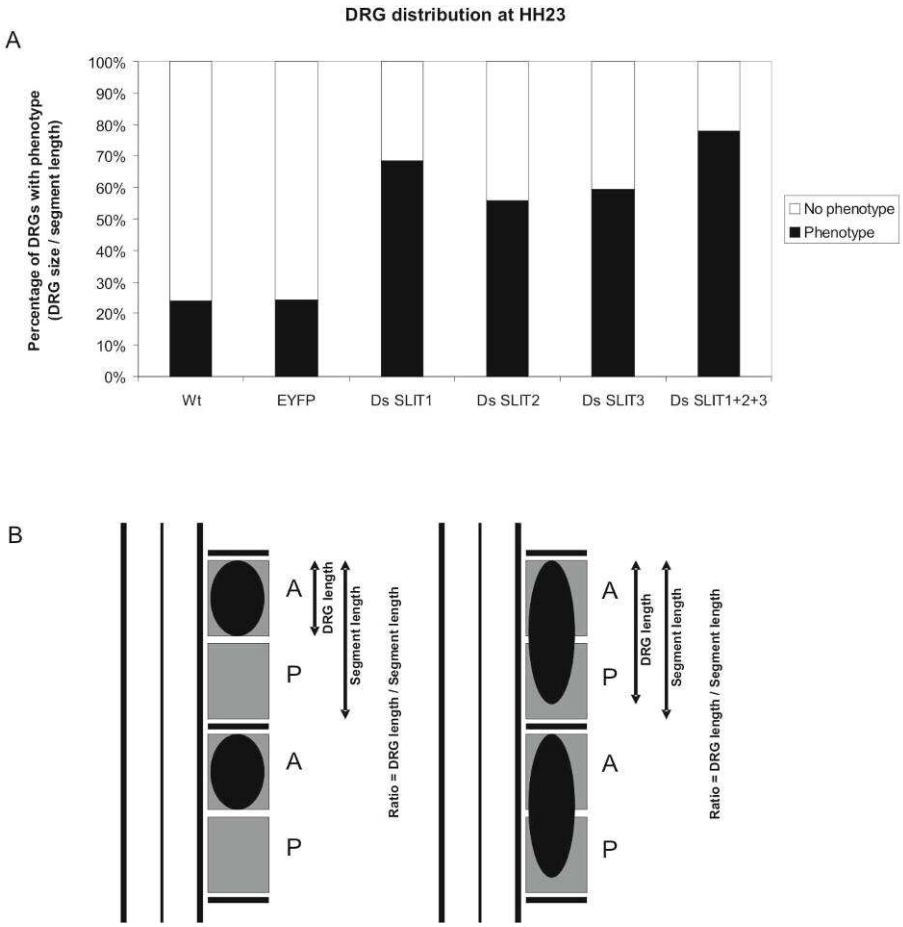

Figure 43 Quantification of the phenotypes observed in embryos where Slits were silenced. (A) Compared to control embryos (wild-type, YFP-injected or embryos lacking Robo3/Rig1), Slit1, Slit2 and Slit3 deficient embryos showed a significantly increased number of DRGs with phenotype. (B) Schematic model with wild-type situation on the left side and experimental situation on the right side. A DRG was counted as phenotypic if the ratio of DRG length / segment length differed more than one standard deviation from the value obtained for YFP-injected control embryos. Nine DRGs (6 trunk and LS1-LS3) were measured per embryo. For each target gene two non-overlapping fragments were used to generate dsRNA. Values for aberrant DRGs did not differ significantly in any case. Therefore, the results for the two different fragments are pooled.

	Percentage of DRGs with phenotype	n embryos	n DRGs	p values compared to wildtype:	compared to YFP:	compared to dsRobo3:
Wildtype	24.10%	15	195		0.386416014	0.137839756
YFP	24.44%	16	135	0.386416014		0.103306611
DsSlit1	68.35%	18	237	1.60595E-22	1.44E-20	3.49E-09
DsSlit2	55.91%	19	254	8.63261E-13	4.26E-12	3.41E-05
DsSlit3	59.51%	16	205	6.19547E-14	2.89E-13	5.04E-06
DsSlit1+2+3	77.78%	6	54	2.03438E-15	1.28E-15	2.52E-10

Table 3 Analysis of DRG segregation in whole-mount preparations. Percentage of embryos with phenotype, number of analysed embryos and DRGs and Student`s t-Test data are shown.

4.9 Peripheral branches of sensory and motor neurons are also guided by the Slit / Robo system

It was shown that Slits are expressed in the limb adjacent to the trajectories of peripheral branches of sensory and motoneurons (Vargesson et al., 2001). We checked the expression of Slits on longitudinal sections in the region where the peripheral branches leave the DRG and start to innervate the limb. Slit1 was expressed at HH20 in the posterior somite (Fig. 44; arrowhead in Fig. 44A) and in the ventro-lateral sclerotome (arrow in Fig. 44A). Slit2 (arrowhead in Fig. 44B) and Slit3 (arrowhead in Fig. 44C) were expressed in somitic boundaries at HH20, Slit3 also in the ventro-lateral sclerotome (arrow in Fig. 44C). The expression in the ventro-lateral sclerotome disappeared after the waiting period of sensory axons at HH23 (data not shown). We therefore investigated the outgrowth of peripheral branches and motoneurons into the limb after downregulation of Robo1 and Robo2, double downregulation of Robo1+2 and after overexpression of mSlit1, hSlit2, hSlit3 and mSlit1 + hSlit2 + hSlit3 triple overexpression. Neurofilament staining on longitudinal cryosections of the proximal initiating part of motoneurons revealed that silencing of Robo1, Robo2 and Robo1+2 led to connected ventral roots initiating along the whole somitic segment compared to segregated ventral roots in wild-type and control conditions (Fig. 44D-G). Due to the lack of specific markers for axons of sensory or motoneurons we did not distinguish in the lateral part between peripheral sensory branches and motor axons and analysed mixed peripheral spinal nerves (Fig. 44L-T). In wild-type (arrowhead in Fig. 44L) and control embryos (arrowheads in Fig. 44M, N) the peripheral sensory branches and motor axons were segregated and fasciculated into one bundle per somitic segment. Robo1 (Fig. 44O), Robo2 (Fig. 44P) and Robo1+2 (Fig. 44Q) deficient peripheral sensory branches and motor axons did not project properly. They left the bundles along the trajectory and entered tissues with Slit expression (arrowheads in Fig. 44O-Q). Furthermore, a reduction of fasciculation was found (arrows in Fig. 44O-Q). The ectopic expression of mSlit1 (Fig. 44R), hSlit2 (Fig. 44S), hSlit3 (Fig. 44T) resulted in too thin and defasciculated peripheral branches (arrowheads in Fig. 44R-T) with an abnormal outgrowth pattern (arrows in Fig. 44R-T). A schematic model shows how motor axons depend on Slit / Robo signalling (Fig. 45). Slit expression in adjacent tissues restricts the trajectory of motor axons to the anterior sclerotome (Fig. 45). Slit expression in the ventral dermomyotome is downregulated after the waiting period at HH23 (data not shown) and allows sensory and motor axon innervation of the periphery (Fig. 45).

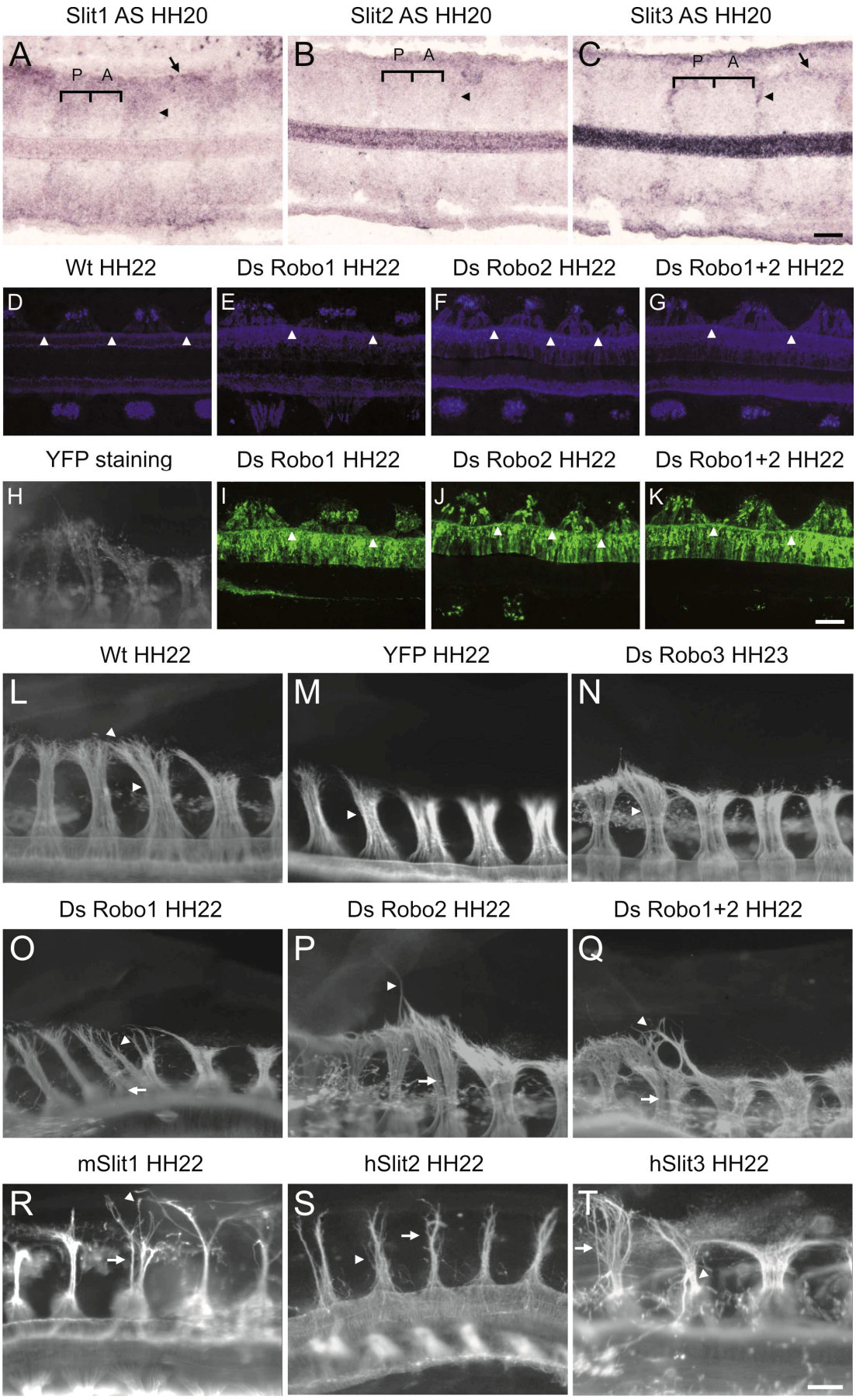

Figure 44. For description, see next page.

Figure 44 Peripheral sensory branches and motoneurons are guided by the Slit / Robo system. Whole-mount preparations of control and experimental chicken embryos and *in situ* hybridizations on longitudinal cryosections on notochord level. (A-C) Expression of Slits on longitudinal sections in the area where peripheral branches and motor axons fuse (between ventral spinal cord and notochord level). (A) Slit1 was expressed at HH20 in the ventral and lateral posterior sclerotome (arrowhead) and in the ventral dermomyotome (arrow). (B and C) Slit2 and Slit3 showed expression in somitic boundaries at HH20 (arrowhead), Slit3 as well in the ventral dermomyotome (arrow). (R-T) Neurofilament immunostaining visualizes peripheral axonal projections including central and peripheral branches of sensory neurons and motor axons. (D-G) Neurofilament staining on longitudinal cryosections through the proximal part of the ventral roots. Silencing of Robo1, Robo2 and Robo1+2 led to connected proximal parts of the ventral roots initiating along the entire somitic segment. (I-K) YFP immunostaining of D-G as transfection control. (L-T) Whole-mount preparations of control and experimental chicken embryos. Downregulation of Robo1 (O), Robo2 (P) and double downregulation of Robo1+2 (Q) resulted in aberrant projections of peripheral sensory- and motoneurons (arrowheads). Axons left the bundles and entered domains of Slit expression. Furthermore, a reduction of fasciculation was found (arrows). (R-T) The ectopic expression / overexpression of mSlit1 (R), hSlit2 (S), hSlit3 (T) resulted in very thin peripheral branches with an abnormal outgrowth pattern (arrowheads). A reduction of fasciculation was found (arrows). (H) YFP immunostaining of P represents an example of transfection. N embryos analysed ≥ 3. A= Anterior somitic compartment, P= posterior somitic compartment. Scale bars: 200µm.

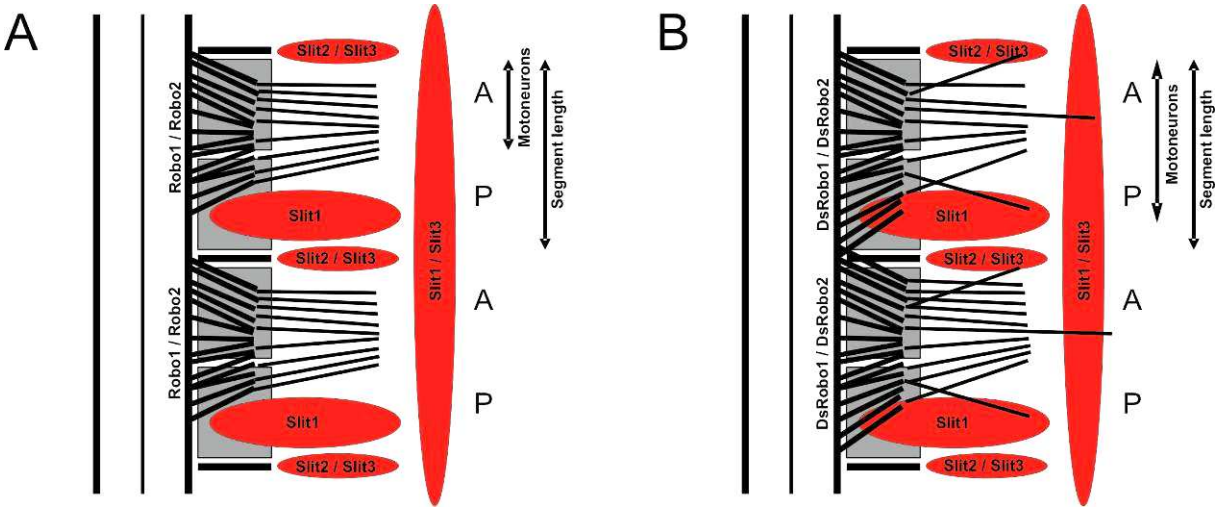

Figure 45 Motoneurons are guided by the Slit / Robo system. (A and B) Schematic model of wild-type (A) and DsRobo situation (B). Silencing of Robo1, Robo2 and Robo1+2 led to connected proximal parts of motor axons initiating along the entire somitic segment. Slit expression in adjacent tissues restricts the trajectory of motor axons to the anterior sclerotome. Slit expression in the ventral dermomyotome is downregulated after the waiting period at HH23 and allows the sensory and motor axon innervation of the periphery. A = Anterior somitic compartment, P = posterior somitic compartment.

4.10 Target layer innervation of nociceptive and proprioceptive afferents within the CNS is perturbed in the absence of Slit or Robo function

The involvement of Slit and Robo in target layer innervation of central projections within the CNS was shown in Robo1 / Robo2 and Slit1 / Slit2 double knock out mice for nociceptive and for proprioceptive sensory collaterals connecting to dorsal layers or to the ventral motor column respectively (Ma and Tessier-Lavigne, 2007). We observed similar phenotypes when we knocked down Robo1, Robo2, Robo1+2 and Slit1 in chicken embryos and analysed their trajectory with the lipophilic dye DiI at HH35 (Fig. 46). Nociceptive and proprioceptive neurons invade the inappropriate target layers after downregulation of Robo1, Robo2, Slit1 and Slit3. A CGRP- and TrkA-positive subpopulation of nociceptive collaterals extended in wild-type and control embryos from the ventral part of the dorsal funiculus towards the dorsal edge of the central canal in a characteristic shape (Fig. 46A-D). In Robo1 (Fig. 46E, F), Robo2 (Fig. 46G, H), Robo1+2 (Fig. 46I, J), Slit1 (Fig. 46M, N), Slit3 (Fig. 46Q, R) and Slit1+2+3 (Fig. 46S, T) deficient embryos, CGRP-positive nociceptive fibres were seen crossing the dorsal midline and invading dorsal layers of the grey matter (arrowheads in Fig. 46E-J; M, N and Q-T). During the time of invasion of collaterals in the grey matter, Slit1 and Slit3 was strongly expressed in the roof plate and dorsal midline (Fig. 23). Lack of Robo3 or Slit2 did not affect nociceptive target layer innervation (Fig. 46K, L and Fig. 46O, P). It is not known how proprioceptive afferents project in any Slit3 deficient vertebrates. For the analysis of their trajectory, we labelled proprioceptive collaterals with the lipophilic dye Fast DiI at HH35 (Fig. 47). In wild type (Fig. 47A, B) or control embryos (Fig. 47C, D) the proprioceptive collaterals stopped before they reached the motor column to connect to dendrites of motoneurons. Robo1, Robo2, Robo1+2, Slit1 and Slit2 deficient embryos exhibited only minor differences compared to control embryos in extension of proprioceptive collaterals. Generally, we observed a reduced number of proprioceptive collaterals on the experimental side of the spinal cord (arrowheads in Fig. 47E-P). Knock down of Slit3 (Fig. 47Q, R) and Slit1+2+3 (Fig. 47S, T) resulted in proprioceptive collaterals that failed to stop before the ventral motor column, grew further and invaded the ventral and medial funiculus. Slit3 was expressed concomitantly in the motor column (Fig. 23).

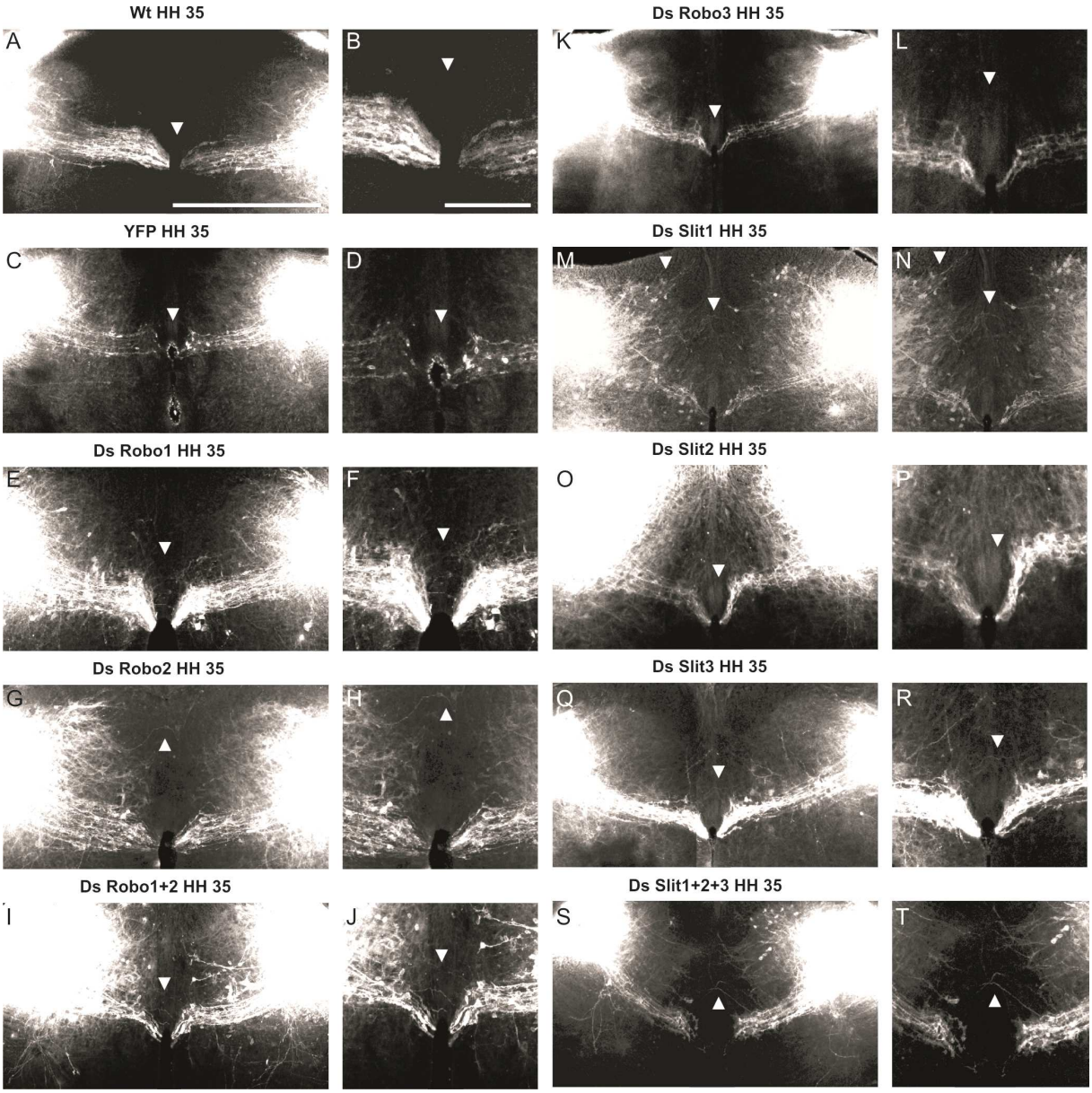

Figure 46 Target layer innervation of nociceptive afferents within the CNS is perturbed in the absence of Slit / Robo signalling. Labelling of a subpopulation of nociceptive collaterals with the lipophilic dye Fast DiI at HH35 in experimental and control chicken embryos. The left half of the spinal cord represents the electroporated side. (A-D) A subpopulation of nociceptive collaterals extended in wild-type and control embryos from the ventral part of the dorsal funiculus towards the dorsal edge of the central canal in a characteristic shape. Knock down of Robo1 (E, F), Robo2 (G, H), Robo1+2 (I, J), Slit1 (M, N), Slit3 (Q, R) and Slit1+2+3 (S, T) resulted in these nociceptive collaterals in invasion of wrong target layers. Overshooting CGRP-/ TrkA-positive collaterals crossed the dorsal midline and invaded dorsal layers of the grey matter (arrowheads). (E-J) Lack of Robo3 (K, L) or Slit2 (O, P) did not alter the trajectory of the collaterals significantly. N embryos ≥ 3. Scale bars: 500µm.

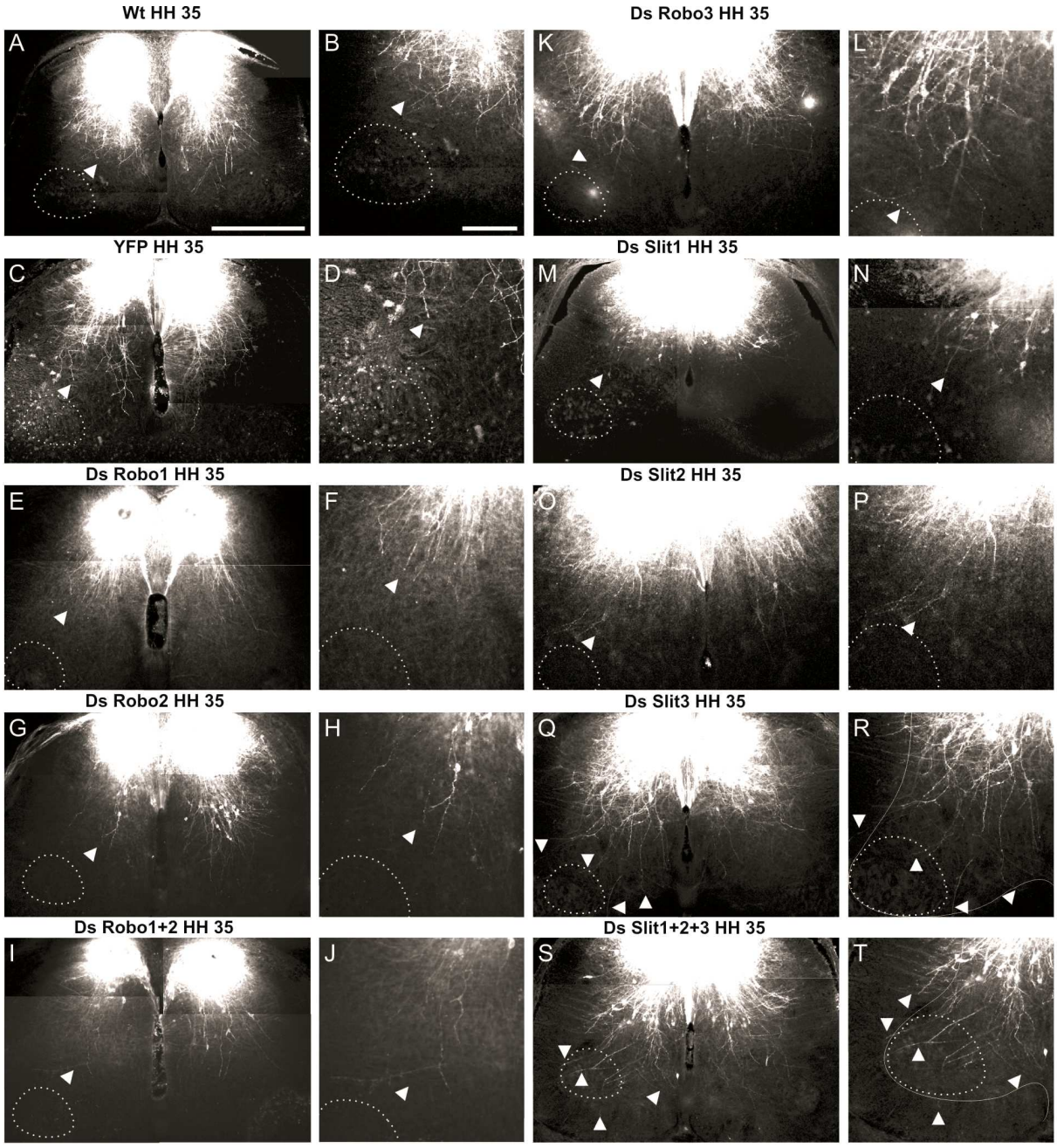

Figure 47 Target layer innervation of proprioceptive Ia muscle afferents within the CNS is perturbed in the absence of Slit3 and Slit1+2+3. The left half of the spinal cord represents the electroporated side. (A-D) Proprioceptive collaterals extended in wild-type and control embryos from the medial dorsal funiculus towards the motor column where they connect to dendrites of motoneurons (arrowheads). (E-L) Lack of Robo1 (E, F), Robo2 (G, H), Robo1+2 (I, J), Robo3 (K, L), Slit1 (M, N) or Slit2 (O, P) did not alter the trajectory of the collaterals significantly although a reduction of collaterals was seen (arrowheads). (Q-T) Knock down of Slit3 (Q, R) and Slit1+2+3 (S, T) resulted in proprioceptive collaterals that failed to stop before the ventral motor column, grew further and invaded the ventral and medial funiculus (arrowheads). Slit3 was expressed concomitantly in the motor column (Fig. 23). N embryos ≥ 3. Scale bars: 500μm.

4.11 More of the repulsive Slit ligands: Slit overexpression confirms their repulsive functions

4.11.1 Expression in COS-7 cells and Western blot analysis

To test whether pcDNA3.1(-)-mSlit1-myc-His A, pSecTagB-hSlit2, pSecTag2B-hSlit3 are expressed *in vitro* I transfected COS-7 cells and checked with immunohistochemistry against the myc tag for expression. All three constructs were strongly expressed (Fig. 48). For *in vivo* analysis, I cloned the constructs into pIRES containing a chicken specific β–actin promoter. These constructs were also tested by expressing them in COS-7 cells and *in vivo* (Fig. 48 and Fig. 53). Expression was detectable although not as strong as the CMV-promoter driven *in vitro* expression (Fig. 48).

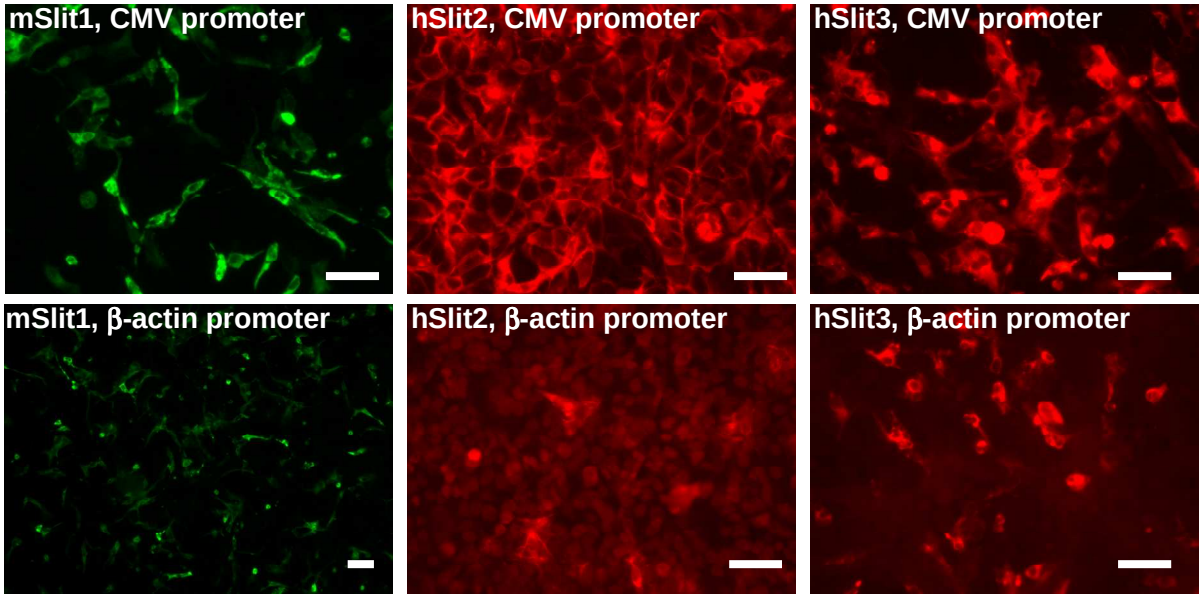

Figure 48 The expression of pcDNA3.1(-)-mSlit1-myc-His A, pSecTagB-hSlit2, pSecTag2B-hSlit3 and their chicken specific β–actin promoter-driven clones are expressed in COS-7 cells. Expression was visualized with anti-Myc immunohistochemistry. Scale bar: 100μm.

To test whether the expressed Slits were secreted into the supernatant / extracellular space I used Western blots. All three Slit constructs were secreted into the supernatant of transfected COS-7 cells (Fig. 49). In Fig. 49A the exposure time was overnight, in Fig. 49B exposure time was 15 minutes. mSlit1, hSlit2 and hSlit3 bands were detected with mouse anti-myc and sheep anti-mouse Peroxidase antibodies running at about 200 kDa (arrows in Fig. 49A). Furthermore hSlit2 was cleaved into a 140 kDa (no myc tag; therefore not detectable) and a 55-60 kDa fragment which is visible in Fig. 49B (arrows; compare also Nguyen Ba-Charvet et al., 2001).

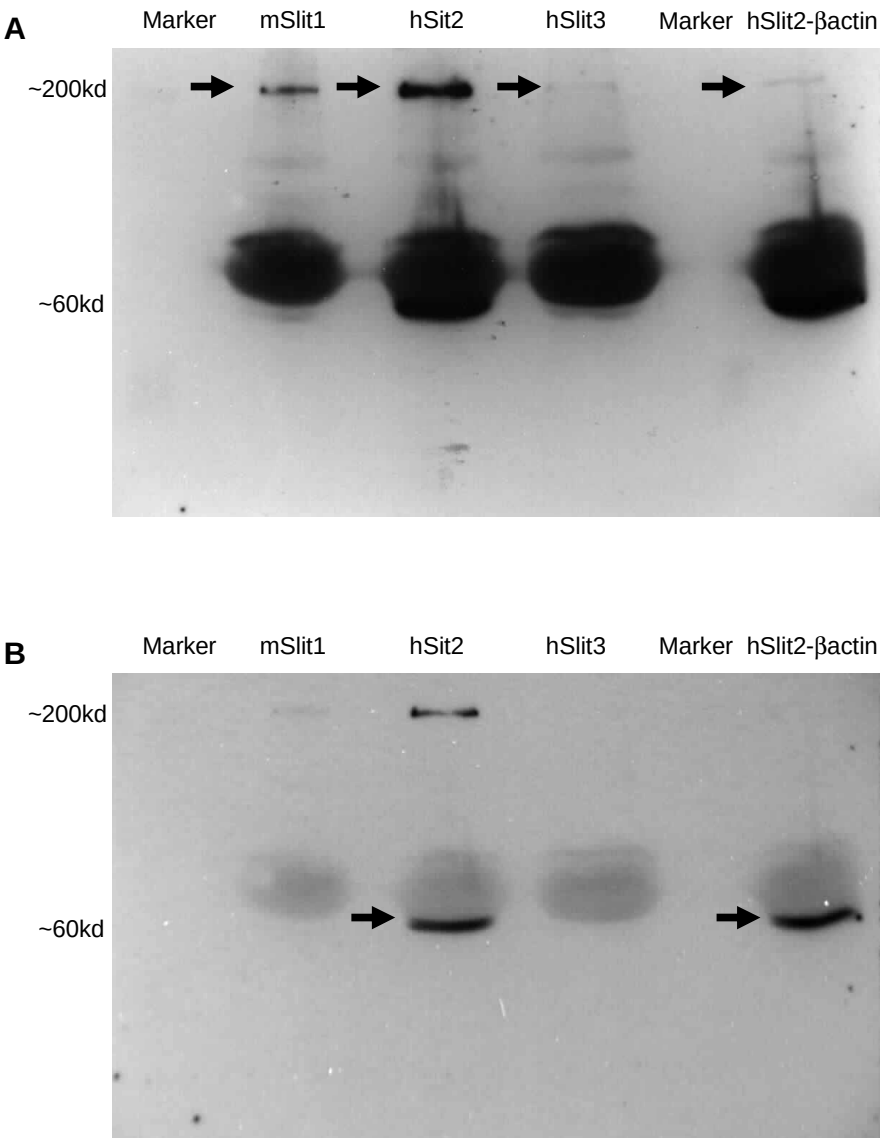

Figure 49 All three Slit constructs are secreted into the supernatant of transfected COS-7 cells. (A) Exposure time overnight, (B) exposure time 15 minutes. mSlit1, hSlit2 and hSlit3 bands are detected with mouse anti myc / sheep anti mouse–Peroxidase antibodies, running at about 200 kDa (arrows in A). Furthermore hSlit2 gets cleaved into a 140 kDa (no myc tag; therefore not detectable) and a 55-60 kDa fragment (arrows in B; compare also Nguyen Ba-Charvet et al., 2001).

4.11.2 DRG neurons get repelled by mSlit1, hSlit2 and hSlit3 in an *in vitro* outgrowth assay

In vitro studies on rat DRG explants or single neuron cultures showed that the Slit proteins have either a branching-, an elongation or a repulsive effect on outgrowing DRG neurons (Wang et al., 1999; Nguyen Ba-Charvet et al., 2001; Ma and Tessier-Lavigne, 2007). Studies focussing on DRG repulsion were done with E12 - E15 rats (developmentally equivalent to E10.5 - E13.5 mice and HH27-35 chicken embryos). E12 rat DRGs express Robo1 only weakly and after E12 they do not express Robo1 (Brose et al., 1999; Wang et al., 1999). In contrast, strong expression of Robo1 and Robo2 was detected in DRGs in the chicken embryo. Therefore, we performed an *in vitro* DRG outgrowth assay where we cultured HH24/25 chicken DRGs on confluent COS-7 cells expressing mSlit1, hSlit2 or hSlit3 (Fig. 50). We counted the number of outgrowing sensory axon bundles per size-normalized

DRG explant and calculated the percentage of outgrowth reduction compared to control DRGs (Fig. 51; Table 4). We only analysed DRG explants on COS-7 cells with equal transfection. Mouse Slit1, human Slit2 and human Slit3 strongly repelled sensory neurons when the culture was analysed after 24 hours (Fig. 50, Fig. 51 and Table 4). 36 hours growth duration led to a radial outgrowth (data not shown), although Slit expressing COS-7 cells were rarely crossed but neurons turned or bifurcated when approaching a Slit-transfected COS-7 cell (arrowheads in Fig. 50A``` - 50D```). These findings are consistent with the results of Ma and Tessier-Lavigne (Ma and Tessier-Lavigne, 2007). In a collapse assay, they found that growth cones collapsed after adding Slit2 but only in a transient manner (after six to 15 minutes) and recovered after 36 minutes. Trypan blue staining of a dissociated DRG neuron culture indicated that DRG cell death was not increased (Fig. 52). Thus, all three Slits have the potential to repress chicken DRG-neuron outgrowth.

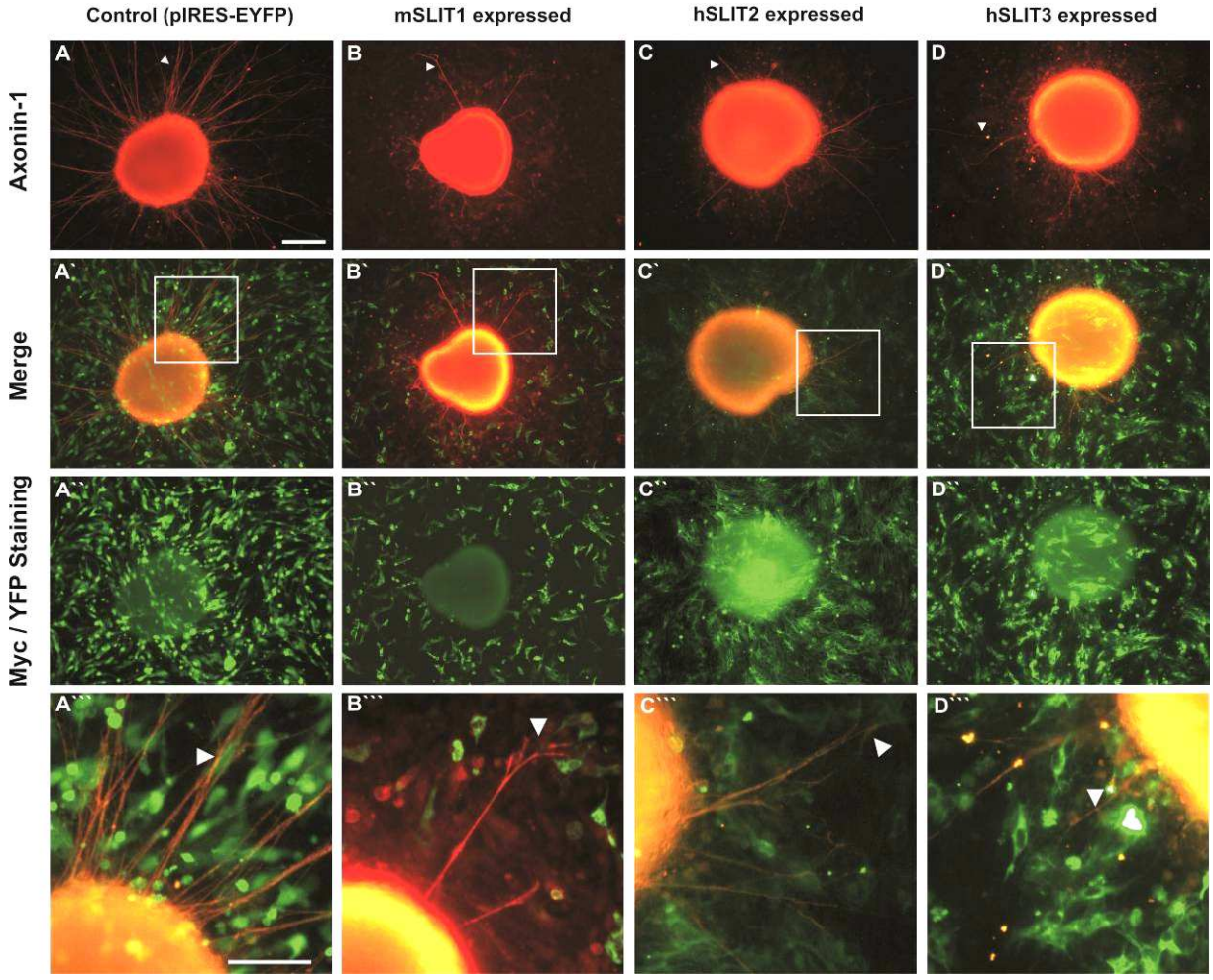

Figure 50 mSlit1, hSlit2 and hSlit3 act repulsively on DRG neurons. (A-D) DRG explant outgrowth assay with cultured HH24-25 chicken DRGs on COS-7 cells expressing mSlit1, hSlit2 or hSlit3. DRGs are visualised with Axonin-1 immunostaining. We counted the number of outgrowing sensory axon bundles per size-normalized DRG explant and calculated the percentage of outgrowth reduction compared to control DRGs. Depending on the duration of DRG outgrowth, mSlit1, hSlit2 and hSlit3 strongly repelled sensory neurons (arrowheads). (A`-D`) Merge of (A-D) and (A``-D``). (A``-D``) Myc immunostaining showed transfection of COS-7 cells with Slit or YFP constructs, respectively. (A```-D```) Higher magnification sections (taken from white sections in A`-D`). DRG neurons avoided Slit expressing cells (arrowheads). Scale bars: 100µm in A-D`` and 50µm in A```-D```.

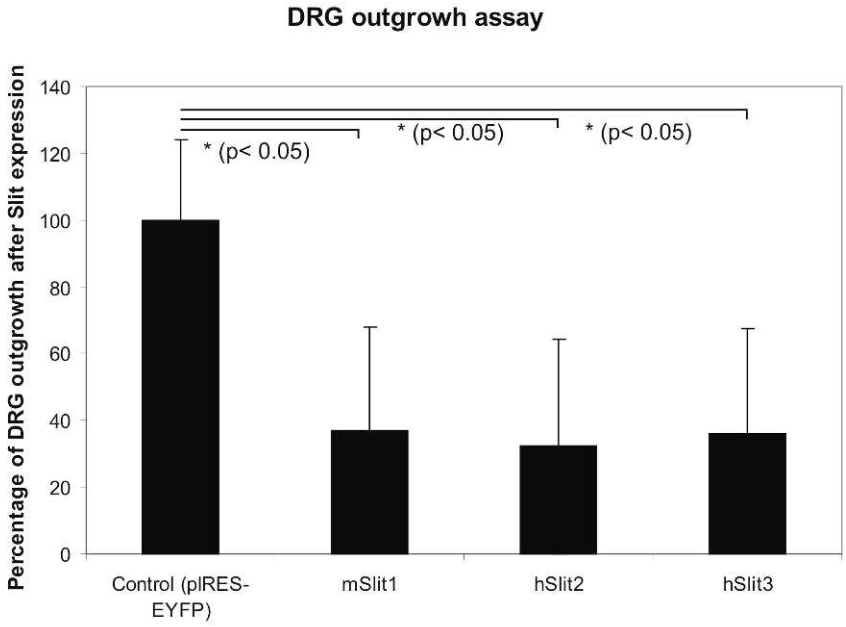

Figure 51 DRG neurons were repelled by mSlit1, hSlit2 and hSlit3. We counted the number of outgrowing sensory axon bundles per size-normalized DRG explant and calculated the percentage of outgrowth reduction compared to control DRGs. The experiment was done at least three times independently, quantification shows pooled data from all experiments. Error bars represent SEM.

Expressed construct	Reduction of outgrowth (in %)	n DRG explants analysed	n experiments	p values
Control (pIRES-EYFP)	100	67		
mSlit1	37.12882635	72	6	0.03741244
hSlit2	32.21506743	61	4	0.032001755
hSlit3	35.82019053	25	3	0.030797342

Table 4 DRG-explant outgrowth assay. The reduction of outgrowth, the number of analysed DRG explants and performed experiments and the probabilities of Student t-tests are shown.

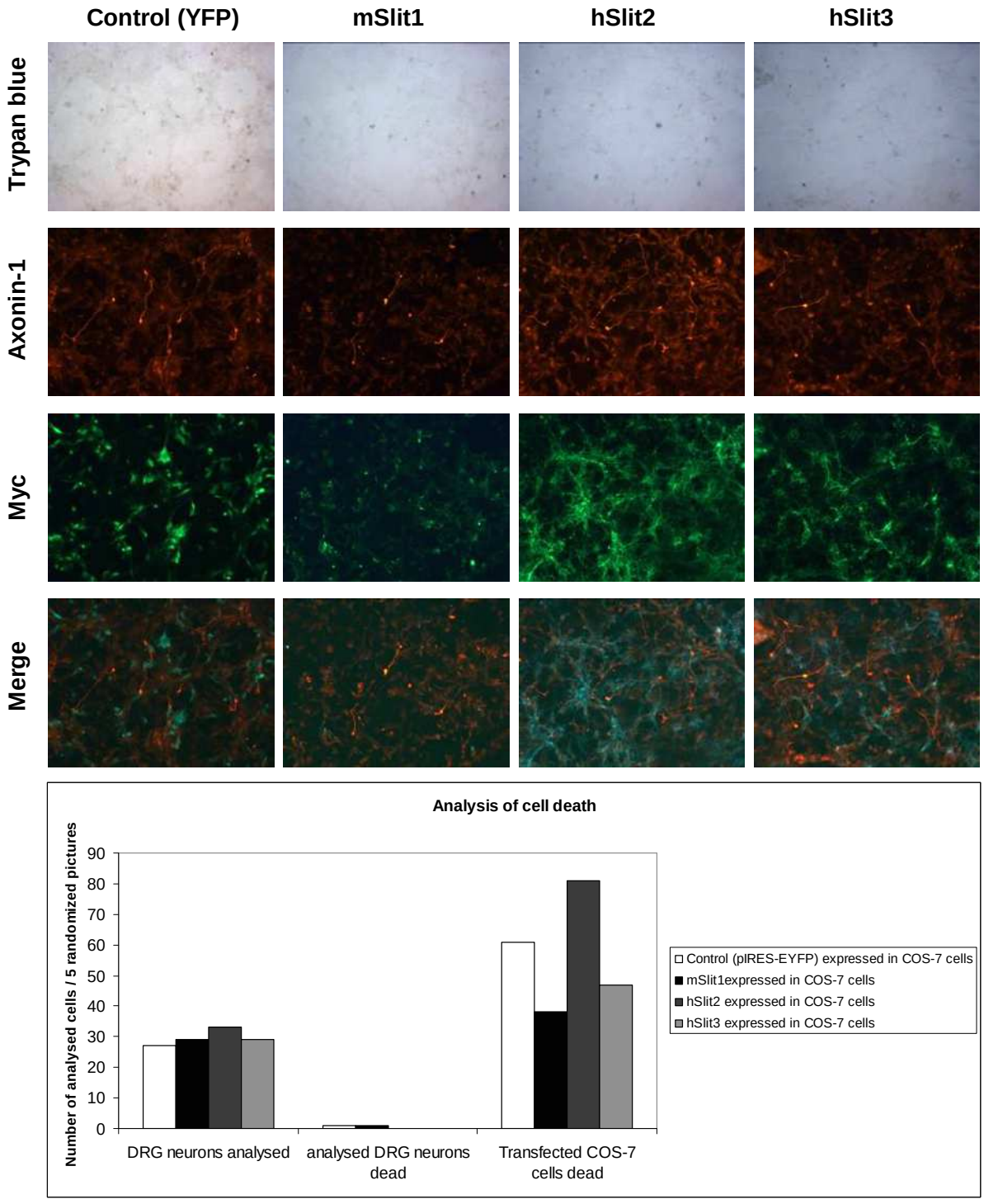

Figure 52 No increase in cell death of dissociated DRG neurons growing on Slit-expressing COS-7 cells. Trypan blue staining was used to visualise dead cells, Axonin-1 immunostaining to label dissociated DRG neurons and Myc immunostaining to visualise transfected COS-7 cells. The experiment was done three times independently. Quantification shows results from one experiment. The shown experiment is representative for three independent experiments.

4.11.3 Overexpression of mSlit1, hSlit2 and hSlit3 leads to a reduction in DRG size and dorsal root number

Slit2 was shown *in vitro* to repel early migrating neural crest cells and to stimulate neural crest cells to migrate further (De Bellard et al., 2003). To further analyse DRG- and dorsal root formation we ectopically expressed mouse and human Slits *in vivo* between HH10 and HH14. To obtain strong *in vivo* expression we cloned myc-tagged Slit plasmids under a constitutively active chicken β–actin promoter and checked for expression by Myc immunostaining (Fig. 53G – 53L). Overexpression of mouse Slit1 (Fig. 54A; n = 18 embryos), human Slit2 (Fig. 54B, n = 10 embryos) and human Slit3 (Fig. 54C; n = 8 embryos) *in vivo* resulted in a strong reduction in DRG size to only a few single neurons and to a loss of almost all dorsal roots (arrowheads in Fig. 54). This indicates that all Slits inhibit the migration of early neural crest cells and the outgrowth of sensory branches *in vivo*. Additionally the bifurcation of central branches into the rostro-caudal axis was perturbed (arrows in Fig. 54A, B and C). Triple overexpression of mSlit1, hSlit2 and hSlit3 did not increase the observed phenotypes indicating that each of the Slit itself is sufficient to impair neural crest cell migration and sensory axon guidance (data not shown).

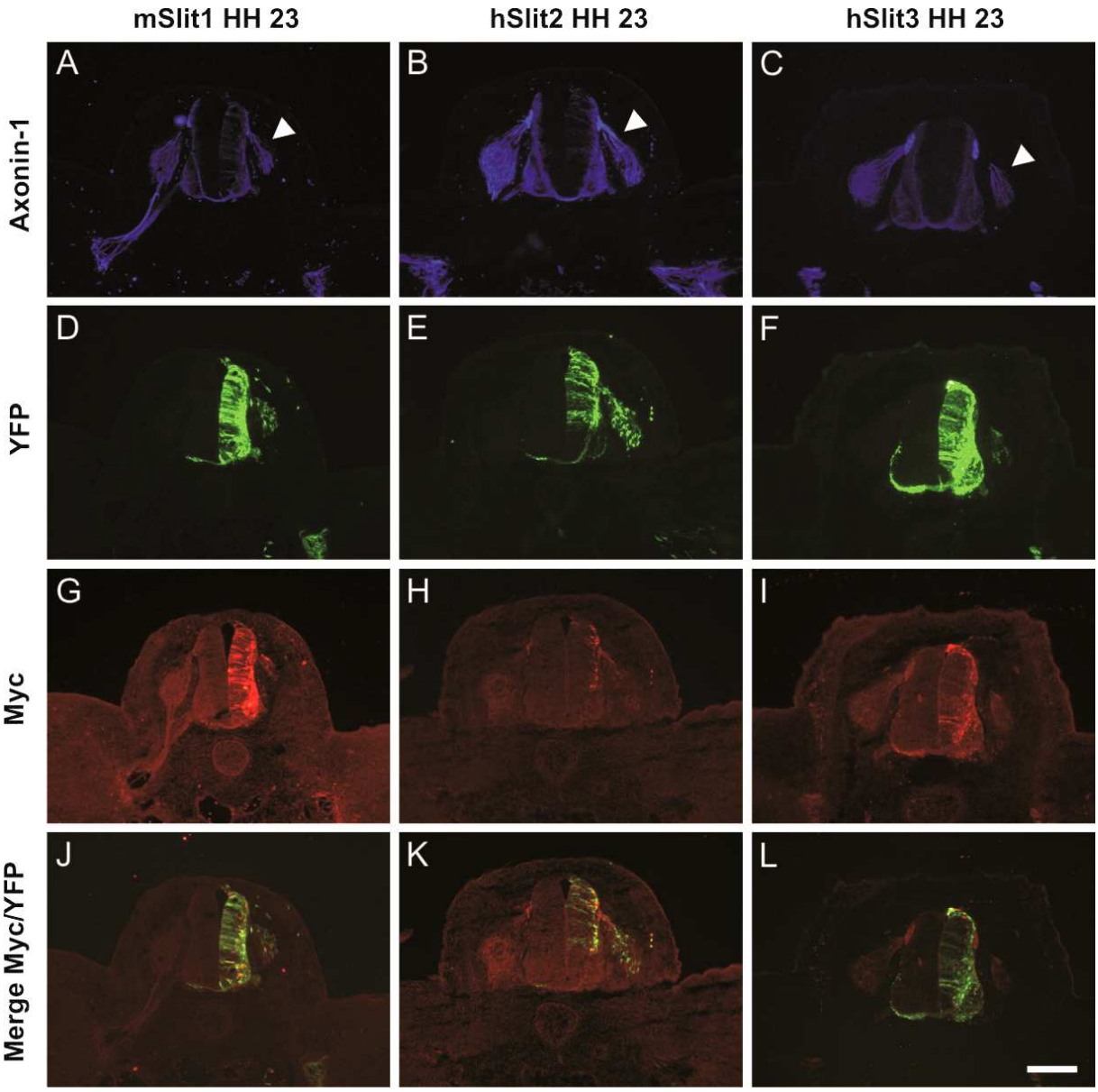

Figure 53 Transversal cryosections of the lumbosacral level of chicken embryos with ectopically expressed Slits. (A-C) Axonin-1 immunostaining visualized peripheral axonal projections including central and peripheral branches of sensory and motor axons. (D-F) YFP immunostaining revealed area of transfection. (G-L) The expression of Slit constructs was approved by myc antibody staining on transversal cryosections. *In vivo* ectopically expressed mouse Slit1, human Slit2 and human Slit3 resulted in a strong reduction in DRG size to only a few single cells and a loss of almost all dorsal roots (arrowheads in A, B and C). Only a few single branches were extending towards the DREZ and the bifurcation into the rostro-caudal axis was perturbed. Scale bars: 200µm.

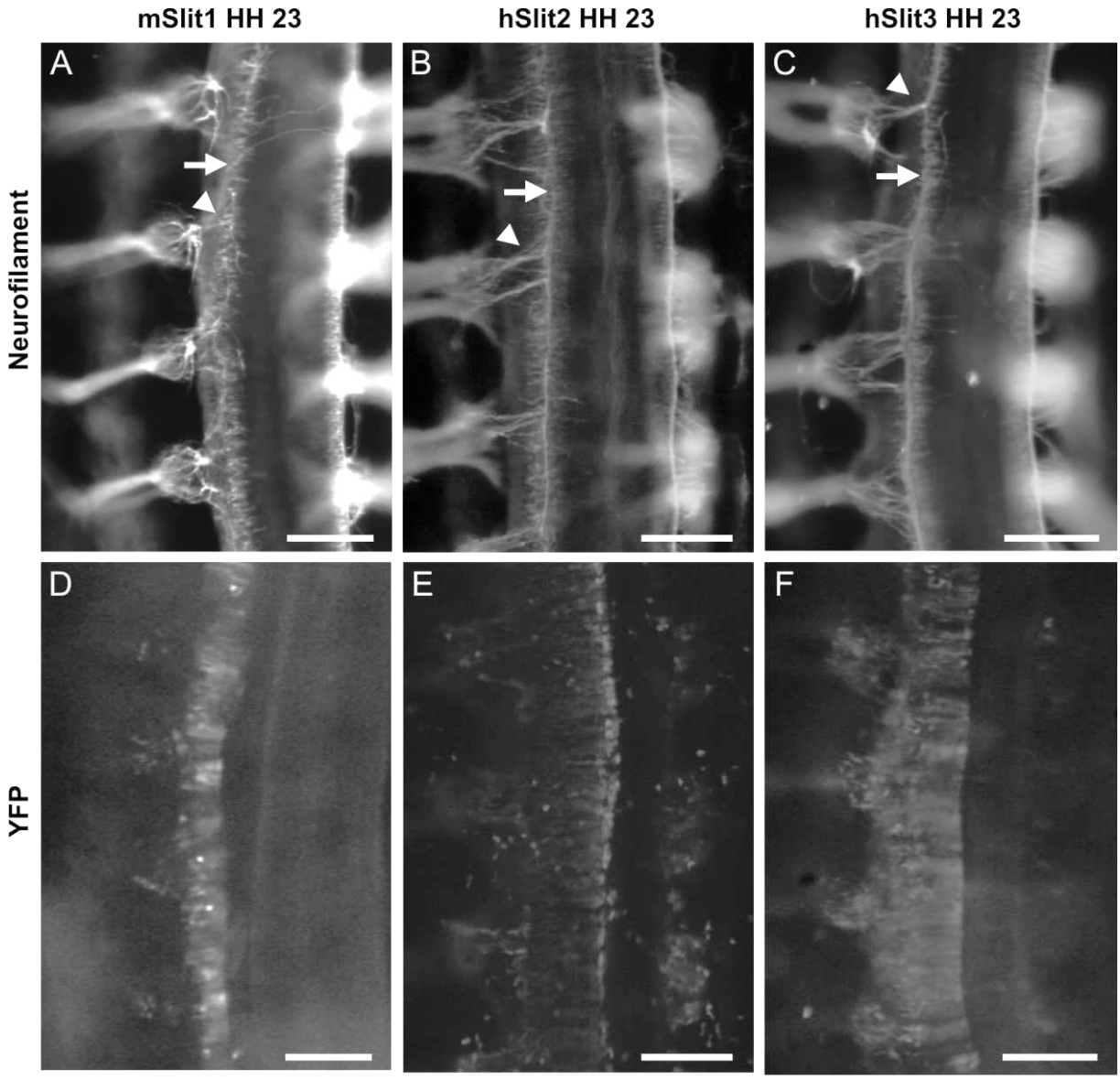

Figure 54 Ectopic expression of Slits leads to a reduction in DRG size and dorsal root number. Whole-mount preparations of control and experimental chicken embryos. (A-C) Neurofilament immunostaining visualized axonal projections including central and peripheral branches of sensory neurons. (D-F) YFP immunostaining revealed area of transfection within the embryo. (A and B) *In vivo* ectopically expressed mouse Slit1 and human Slit2 resulted in a strong reduction in DRG size to few single cells and a loss of almost all dorsal roots (arrowheads). Only a few single branches were extending towards the DREZ and the bifurcation into the rostro-caudal axis was perturbed (arrows in A and B). (C) Slit3 overexpression resulted also in a reduction in DRG size but less strong compared to mSlit1 and Slit2 overexpression. The extension of dorsal roots was affected to the same degree (arrowheads). The bifurcation into the rostro-caudal axis was perturbed (arrow). Scale bars: 200µm.

5. Discussion

A complex system of highly regulated molecular interactions is required for the establishment of a correctly wired and functional nervous system. The analysis of the migration of multipotent neural crest cells within the developing embryo as well as the formation of sensory neural circuits has become a widely studied field (Fraser and Bronner-Fraser, 1991). More and more families of attractive or repulsive guidance molecules and even morphogens have been shown to be implicated in these processes. We analysed the role of the Slit / Robo system in neural crest cell migration as well as in sensory and motor axon guidance. The detailed analysis of the expression patterns of Robos and Slits and their functions revealed new and confirmed previous results.

5.1 The expression patterns of Robo1, Robo2 and all three Slits indicate novel functions during neural crest cell migration and sensory axon guidance

The expression pattern of Robo1 and Robo2 overlap during neural crest cell migration and early phases of sensory axon guidance. It was shown that Robo1 and Robo2 are expressed in HNK-1-positive trunk neural crest cells (but not in vagal neural crest cells that enter the gut) and in the entire DRG (between HH18 and HH20) in chicken embryos (De Bellard et al., 2003, Jia et al., 2005; in mouse: Yuan et al., 1999). We examined their expression in more detail on transverse and longitudinal cryosections and largely confirmed and extended published data (Fig. 20 and 21). Based on their expression patterns a function of Robo1 and Robo2 in neural crest cell migration and sensory axon guidance was very likely.

The expression patterns of Slit1-3 were investigated in tissues adjacent to the trajectory of neural crest cells and sensory as well as motor axons (Yuan et al., 1999; Vargesson et al., 2001; De Bellard et al., 2003; Jia et al., 2005). Our detailed analysis of Slit1-3 expression on transverse and longitudinal cryosections on different levels of the sclerotome largely confirmed published data and additionally showed in more detail that in the chicken embryo Slits were expressed in the dermomyotome, in the posterior sclerotome and at sclerotome boundaries (Fig. 22). These expression patterns indicated a barrier function for neural crest cells and sensory neurons. Therefore, the Slit members were likely to have undescribed functions in restricting early neural crest cells to the anterior sclerotome. Furthermore, it was likely that Slits were also restricting Robo1- and Robo2-positive central and peripheral branches of sensory as well as motor axons to the anterior sclerotome, as the expression of Slits in the posterior sclerotome and in the dermomyotome persisted at the time of axon extension.

5.2 The expression patterns of Slits and Robos at late developmental stages suggest roles in the establishment of the mature connectivity

During and after the establishment of the mature connectivity at around HH39, Robo1 and Robo2 as well as Slit1 and Slit3 expression was still clearly detectable in the spinal cord, the PNS and adjacent tissues. This raised the question about functions of Robos and Slits after the wiring of the neuronal network was completed? The expression profiles of Robo1 and Robo2 at this late time point of

neuronal development could be explained with a function in synaptic target recognition or synapse formation. Sensory neurons but also their potential targets, interneurons and motoneurons, express Robo1 and Robo2.

Furthermore, Robo2 and Slit1 could function in the development of the Hofmann nucleus as their expression was detected in this structure during its development between HH38 and HH42. Additionally, Robo1 and Slit1 were expressed adjacent to the MEP. These expressions indicate an unknown Robo1 and Slit1 function, probably in retaining cell bodies of motoneurons inside the spinal cord. Emigration of motoneuron-cell bodies in embryos lacking Robo1 or Slit1 does not occur before HH25 (data not shown) and further experiments are needed to reveal the function of Slit / Robo signalling in cells adjacent to the MEP.

The observable expression of Slit1 in the ventral and dorsal horn and in Schwann cells ensheathing the ventral and dorsal roots from HH38 to HH42 could result in a repellent function so that sensory and motoneuron-cell bodies do not enter or exit the spinal cord, respectively. Chong and colleagues showed that aberrant sprouting of neurons after peripheral nerve injuries almost never occurred with invasion through the DREZ that is believed to prevent sensory afferent invasion in adult animals (Chong et al., 1999). Slit1, expressed in this region during the development between HH38 and HH42, could also be the responsible repulsive molecules in adult animals after nerve injuries. Therefore, expression of Slit in adult animals has to be investigated. Furthermore, there is evidence that Slits are expressed in CNS lesions sites (Wehrle et al., 2005)). In the injured mouse spinal cord, Slit1 and Slit3 are expressed at the lesion site eight days after CNS injury (Wehrle et al., 2005). Thus, Slits and their receptors may contribute to the regenerative failure of axons in the adult CNS by inhibiting axon outgrowth (Wehrle et al., 2005). Repulsive Slit / Robo signalling may therefore be implicated in negative regulation of regeneration after peripheral and central nerve injuries. Treatment with function-blocking antibodies against Slits as reported for NogoA (Buchli et al., 2007; Maier et al., 2009) could be a promising starting point for clinical therapies to cure nerve injuries.

5.3 Robo3 could not be detected in the peripheral nervous system - Expression is restricted to commissural and other interneurons

The most divergent member of the Robo family, Robo3/Rig1, was shown to be involved in ventral midline crossing of commissural axons in mice (Sabatier et al., 2004). The analysis of the expression pattern of Robo3 in chicken embryos using *in situ* hybridization did not reveal any expression in the PNS as well as the functional analysis did not show any role in the formation of the PNS (Fig. 20, 29 and 34). It was shown by qRT-PCR that Robo3 is expressed in early and late neural crest cells but no function has been described and no data is available about the strength of expression (Jia et al., 2005). However, we were not able to confirm these data using *in situ* hybridization. Probably expression of Robo3 in the PNS is below the detection level of *in situ* hybridization. Thus, we propose no role for Robo3 in the formation of the PNS.

5.4 Impaired early neural crest cell migration in absence of Slit or Robo function

We demonstrated that Robo1 and Robo2, but not Robo3, as well as Slit1 and Slit2 guide neural crest cells towards the correct target position in the anterior sclerotome (Fig. 29 and 30). Ectopic HNK-1 and Islet-1-positive cells were found in the posterior sclerotome and in the dermomyotome in embryos where Robo1, Robo2 (but not Robo3) or Slit1 and Slit2 (but not Slit3) were downregulated (Fig. 29). Ligand (Slits) and receptor (Robos) downregulation resulted in the same phenotypes confirming their function in this process. Furthermore, counting cells in DRGs indicated that DRGs of Robo1-, Robo2-, Slit1- or Slit2-deficient embryos contained a significantly smaller number of cells (Fig. 30). The most likely explanation is the additional migration into the posterior sclerotome / dermomyotome and the dorso-lateral pathway and therefore a reduction of cells in the DRGs.

These data are consistent with the reported functions for Robo1 in confining early neural crest cells to the ventro-medial pathway (Jia et al. 2005). Jia and coworker demonstrated that a dominant-negative Robo1 receptor induces early neural crest cells to migrate ectopically into the dorso-lateral pathway where normally only late neural crest cells enter (Jia et al., 2005). Additionally, our data are consistent with reported *in vitro* and *in vivo* functions for Slit1 and Slit2 (De Bellard et al., 2003, Jia et al., 2005). Work of De Bellard and colleagues and of Jia and coworker demonstrated that Slit1 and Slit2 have an effect on migrating early neural crest cells *in vitro* and *in vivo* (De Bellard et al., 2003; Jia et al., 2005). Migrating early neural crest cells get repelled in presence of Slit2 but, at the same time, migrate further *in vitro* (De Bellard et al., 2003, Jia et al., 2005). Slit2 is proteolytically cleaved into two different fragments, Slit2N and Slit2C that may have distinct functional properties. The N-terminal fragment of Slit2 that is not only secreted, but also incorporated into the cell membrane is thought to mediate the repulsion while secreted soluble Slit2 mediates the enhanced migration (De Bellard et al., 2003).

The function of Slit3 in neural crest cell migration has not been tested and our results provide first evidence that Slit3 is involved in migration of boundary caps cells, a subpopulation of neural crest cells (Fig. 29O-U; see also chapter 5.5). Early neural crest cells that migrate into the anterior sclerotome and give rise to DRGs were not affected in Slit3-deficient embryos. Although downregulation of Slit3 resulted in HNK-1-positive cells along the connected dorsal roots (arrowhead in Fig. 29N), there were no HNK-1 or Islet-1 positive cells found in the posterior sclerotome or the dermomyotome (Fig. 29G/N). Therefore, we concluded that these cells might represent Schwann cells ensheathing the dorsal roots extending erroneously into the DREZ in the posterior sclerotome.

What consequences may result from erroneous neural crest cell migration in absence of Slit or Robo? The positioning of neurons within the forming DRG may be altered. Due to the lack of precise subpopulation-specific markers for sensory neurons, this question may be difficult to answer. Additionally the formation of the posterior sclerotome could be perturbed as differentiating neurons within the posterior sclerotome could interfere with formation of cartilage, vertebrae or blood vessels. More likely, as the polarity of the sclerotome is not changed after perturbance of Slit or Robo (Fig. 30), the normal induction of genes in the posterior sclerotome, for instance those used for the development of cartilage, might still be normal and aberrantly positioned neurons might be eliminated by apoptosis. The analysis of chicken embryos or knockout mice lacking Robo or Slit after cartilage development

could answer this question. Indeed, the analysis at HH35 of embryos lacking Robos or Slits revealed no severe cartilage or vertebrae malformation (data not shown).
Slit / Robo signalling may act in parallel to Neuropilin2 / Semaphorin3F signalling because Neuropilin2 knockout mice show the same phenotype (early neural crest cells that migrate non-segmentally into both, the anterior and posterior sclerotome; Gammill et al., 2006; Roffers-Agarwal and Gammill, 2009; Schwarz et al., 2009). Another point supporting this hypothesis is that only a fraction of the pool of targeted early neural crest cells showed the phenotype indicating redundant functions of different guidance molecules.

5.5 Are boundary cap cells involved in Slit / Robo-dependent segmentation of dorsal roots?

We analysed the distribution of the boundary cap cell clusters at the DREZ formed by dorsal boundary cap cells, a 1E8-positive subpopulation of late-migrating early neural crest cells, on longitudinal cryosections (Fig. 29O-29U). In all experimental embryos (except embryos lacking Robo3), we found that the boundary cap cell clusters were smaller and positioned at the DREZ in the anterior and posterior sclerotome. Because dorsal boundary cap cells reach the DREZ before the first primary sensory afferents reach it (Golding and Cohen, 1997), there are different explanations for the observed phenotypes. Either the boundary cap cells migrate aberrantly to the DREZ in the posterior sclerotome or they initially migrate to their correct target but subsequently move erroneously to the DREZ in the posterior sclerotome due to the absence of Robo-mediated Slit repulsion. Another explanation would be that Robo receptors, expressed on the dorsal roots that extended erroneously into the posterior sclerotome, attract Robo-positive boundary cap cells via homo- or heterophilic interactions in a Slit-independent way. Further experiments may help to answer these questions. *In vivo* time-lapse analysis of neural crest cell migration in absence of Slits or Robos could help to distinguish between the different possibilities.
The initial outgrowth of motor axons is also perturbed in absence of Robo1 or Robo2 (Fig. 44E, F). Furthermore, the overexpression of Slits leads to a reduction in the size of ventral roots (Fig. 44R-T). Ventral boundary cap cells reach their target after motor axons have started to exit the spinal cord (Fraher et al., 2007; Mauti et al., 2007). Therefore, the ventral boundary cap cells may not be implicated in the segregated outgrowth of ventral roots and the complementary expression pattern of all three Slits and other repulsive molecules (e.g. Semaphorin3A and 3F; Gammill et al., 2006; Roffers-Agarwal and Gammill, 2009) may be sufficient to generate the metameric ventral root organisation.

5.6 Guidance of central branches of DRG neurons is severely affected in the absence of Robo or Slit

We report that the Slit / Robo system guides the extending central branches to the correct entrance position at the DREZ along the spinal cord. In embryos lacking Robo1, Robo2, Slit1, Slit2 or Slit3 central branches extended into both, the anterior and posterior sclerotome and entered the DREZ all along the spinal cord (Fig. 35 -37 and Fig. 39 - 42). The inability to segregate properly along the

anteroposterior axis most likely results from a failure of sensory axons to sense Slit1-3 in the posterior sclerotome. A small number of axons extended towards the dorsal posterior sclerotome and dermomyotome (Fig. 35 -37 and Fig. 39 - 42). Incompetence of the Robo1/2-deficient central branches to sense Slit in the dorsal posterior sclerotome and dorsal dermomyotome and Slit2 / Slit3 in the entire dermomyotome might be the explanation. Silencing of the receptors (Robo1 and Robo2) and the ligands (Slit1-3) resulted in the same phenotypes in accordance with the hypothesis.

Is formation of dorsal roots also affected in absence of Slit / Robo signalling, when neural crest cells migrate correctly? The separation of the analysis of neural crest cell migration and sensory axon guidance by injection of dsRNA at later stages (>HH14) when neural crest cells already migrated into the anterior sclerotome showed that dorsal root formation is affected to the same degree in these embryos (data not shown). Therefore, Robo1 and Robo2 control neural crest cell migration and sensory axon guidance independently and sequentially.

Additionally, it was shown that central branches of sensory DRG axons in mice lacking Robo1 and Robo2 or Slit1 and Slit2 fail to bifurcate properly at the DREZ (Ma and Tessier-Lavigne, 2007). One daughter branch of the central branch continues to grow towards the dorsal midline (Ma and Tessier-Lavigne, 2007). Additional evidence that Slits and Robos are involved in the guidance of central branches of sensory axons does not exist. F11/Contactin was shown to have a function in the fasciculation of dorsal roots (Perrin et al., 2001). Notably, Neuropilin1 and Semaphorin3A signalling is required for metameric DRG and dorsal root segregation *in vivo* (Gammill et al., 2006; Roffers-Agarwal and Gammill, 2009; Schwarz et al., 2009).

The partial redundancy of the expression and function of Robo1 and Robo2 in neural crest cells and sensory DRG neurons and of Slit1-3 in adjacent tissues as well as other cooperating guidance molecules might be a backup system to ensure correct wiring of the PNS. Additionally, the separation of the restriction of neural crest cells and sensory dorsal roots to the anterior sclerotome (both mediated by Slit / Robo signalling in independent and sequential steps) might be another backup mechanism to ensure functional wiring. Loss of a functional PNS would lead to erroneously processed sensory information. Given the fact, that sensory input processing is crucial to react on environmental factors, it seems logical that evolution creates such backup redundancies.

It was shown that commissural axons bring Robo1 to the surface of growth cones after entering the floor plate in a Rab GDP dissociation inhibitor (RabGDI) dependent manner (Philip et al., in revision). Does RabGDI also traffic Robo to the surface of sensory neurons? RabGDI is strongly expressed in DRGs during the development of the sensory neural circuits (data not shown) and functional analysis might connect a function of RabGDI and Robo1 in sensory neurons too.

5.7 Peripheral branches are also guided by the Slit / Robo signalling: a widely used repulsive system to ensure functional wiring

The fact that Slits are expressed in the posterior sclerotome, in intersomitic boundaries and in developing limb buds along the trajectories of peripheral sensory and motor axons indicated a role of Robo1 and Robo2 in peripheral sensory and motor axon innervation (Fig. 44A-C). Indeed, we found errors in the outgrowth pattern of peripheral sensory and motor axons in embryos after silencing

Robo1 or Robo2: the peripheral nerve bundles were defasciculated and single axons left the fascicles and entered the posterior sclerotome where Slits are expressed (Fig. 44O-Q). Furthermore, motor axons left the spinal cord all along the anteroposterior axis (Fig. 44E-G). In embryos where mSlit1, hSlit2 or hSlit3 was ectopically expressed, peripheral branches and motoneurons were strongly reduced in size and the remaining fibres were extending in an uncontrolled manner in all directions (Fig. 44R-T). Thus, these results indicate that Robo1, Robo2, and all three vertebrate Slits guide peripheral sensory and motor axons *in vivo*.

Additionally, it was shown that EphrinAs and EphAs are expressed in developing limb buds and could have a function in guiding sensory and motor axons in the limb bud (Eberhart et al., 2000). However, knockout mice lacking EphA3 do not show any motor axon pathfinding defects (Vaidya et al., 2003). Notably, Neuropilin1 and 2 and Semaphorin3A and 3F are necessary for segmented peripheral nerve outgrowth (Huber et al., 2005; Roffers-Agarwal and Gammill, 2009; Schwarz et al., 2009). Therefore, molecules from different axon guidance families may cooperate to achieve proper peripheral nerve innervation.

Slit2 and Slit3 were not only expressed in regions adjacent to the trajectory of peripheral nerves, they were also strongly expressed in motor neurons themselves (Fig. 22). This raised the question why repulsive guidance molecules were expressed by the neurons themselves that were guided by the same guidance molecules expressed in adjacent tissues. An explanation might be that secretion of intrinsic Slit2/3 from motoneurons might enhance migration while extrinsic Slit2/3 might actually guide motor axons. Alternatively, intrinsic Slit2 could be required to detach or slightly defasciculate neighbouring axons from each other to facilitate extension. To address this question embryos lacking Slit either in motoneurons or in the periphery should be analysed. Embryos that lack Slit only in motor neurons should therefore show reduced outgrowth and no guidance errors. Discrete somite electroporation might be used (Scaal et al., 2004) for the analysis of embryos that lack Slits only in the periphery (Scaal et al., 2004). Further experiments are needed to answer these questions.

5.8 Slit / Robo signalling controls target layer innervation of sensory collaterals

In order to analyse the trajectory of nociceptive and proprioceptive collaterals in absence of Robo or Slit function we silenced all Robos and Slits in chicken embryos and traced the collaterals with the lipophilic dye Fast DiI at HH35 (Fig. 46). Nociceptive collaterals invaded the inappropriate target layers and crossed the dorsal midline after downregulation of Robo1, Robo2, Slit1 and Slit3 (Fig. 46). This may be a consequence of the misguidance of these axons along their initial trajectory, because of the failure to sense Slit1 and Slit3 expressed in the dorsal midline and spinal cord, and due to less homo- and heterophilic Robo1 and Robo2 interactions on the growth cones (Fig. 46). Ma and Tessier-Lavigne observed similar phenotypes in Robo1/Robo2 and Slit1/Slit2 double-knockout mice. The trajectory of nociceptive sensory collaterals connecting to dorsal layers was slightly altered (Ma and Tessier-Lavigne, 2007). The observed invasion of inappropriate target layers in embryos lacking Robo or Slit might have dramatic outcomes in adult animals since nociceptive information erroneously transmitted to wrong target neurons might result in chronic pain syndromes.

Additionally, we analysed proprioceptive sensory collaterals in embryos lacking Robo1-3, Robo1+2, Slit1-3 or all Slits by labelling them with the lipophilic dye Fast DiI at HH35. The analysis of Slit3- and Slit1+2+3-deficient embryos revealed that the trajectory of the proprioceptive collaterals was altered (Fig. 47Q-T). In wild-type or control embryos, proprioceptive collaterals stopped when they reached the motor column and connected to dendrites of motoneurons. However, in embryos deficient for Slit3 or all Slits the collaterals failed to stop before the ventral motor column, grew further and invaded the ventral and medial funiculus. This is consistent with the expression of Slit3 in the motor column at that time that may provide a stop signal for these collaterals (Fig. 23). Robo1-, Robo2-, Robo1+2-, Slit1- and Slit2-deficient embryos exhibited only minor differences compared to control embryos. Generally, we observed a reduced number of proprioceptive collaterals on the experimental side of the spinal cord (Fig. 47), most probably due to misprojections and pathfinding errors on the trajectory before the invasion of the grey matter of the spinal cord. Thus, Slit / Robo signalling controls target layer invasion of central collaterals.

5.9 All three Slit members repel DRG neurons *in vitro* and *in vivo*

We performed a DRG repulsion assay where HH24-25 chicken DRG explants were cultured for 36 hours on a COS-7-cell monolayer that expresses mSlit1, hSlit2 or hSlit3. The outgrowth of sensory neurons was not affected significantly (data not shown) confirming previous analyses in mouse and rats. Nguyen Ba-Charvet and coworker have shown that Slit2 does not act repulsively on E15 rat DRGs *in vitro* (Nguyen Ba-Charvet et al., 2001). Likewise, Ma and Tessier-Lavigne demonstrated that Slit2N does not repel E12 rat DRGs in a chronic repulsive coculture assay (Ma and Tessier-Lavigne, 2007). Robo1 and Robo2 expression in the DRG slightly differs in rodents and chicken. Whereas chicken DRGs strongly express Robo1, DRGs in rat and mouse show only weak expression during the formation of early sensory neural circuits. However, when we analysed DRG repulsion after 24 hours, we found that all three Slits strongly repelled DRG neurites (Fig. 50 and 51). This confirmed the transient collapse assay, Ma and Tessier-Lavigne performed (Ma and Tessier-Lavigne, 2007). They demonstrated that Slit2N induces growth cone collapse of DRG neurons in a transient manner (Ma and Tessier-Lavigne, 2007). We then turned to *in vivo* analyses and ectopically expressed the three Slit constructs in chicken embryos. All of them strongly repelled central and peripheral branches of sensory neurons (Fig. 53 and 54). Thus, the *in vitro* data and the *in vivo* analysis confirm our model and previous *in vitro* studies in mice and rats.

5.10 Model

The data I collected during this dissertation led to the following model: Slit / Robo signalling guide early neural crest cells into the ventro-medial pathway (Fig. 55A; Jia et al., 2005). Additionally, Slit / Robo signalling restricts the path of migration to the anterior sclerotome by expressing Slit in adjacent tissues (Fig. 55B; Fig. 22 and 29). Furthermore, after aggregation and formation of DRGs, Slit / Robo function guides the central branches of sensory neurons towards the DREZ (Fig. 55A, B; see also Fig. 32-42). Slit expression in the posterior sclerotome, the entire dermomyotome, the lateral spinal cord and the epidermis restricts the trajectory to the anterior sclerotome (Fig. 55A, B; see also Fig. 22). The bifurcation into the longitudinal axis in the DREZ is Slit / Robo dependent (Ma and Tessier-Lavigne, 2007). Later in development, Slit / Robo signalling is necessary for target layer innervation of central collaterals (Fig. 46 and 47). Additionally, Slit / Robo signalling is necessary for the proper formation of peripheral sensory and motor axon projections (Fig. 55A, B; see also Fig. 44). Thus, repulsive Slit / Robo signalling is necessary to achieve correct wiring of the peripheral nervous system in vertebrate development.

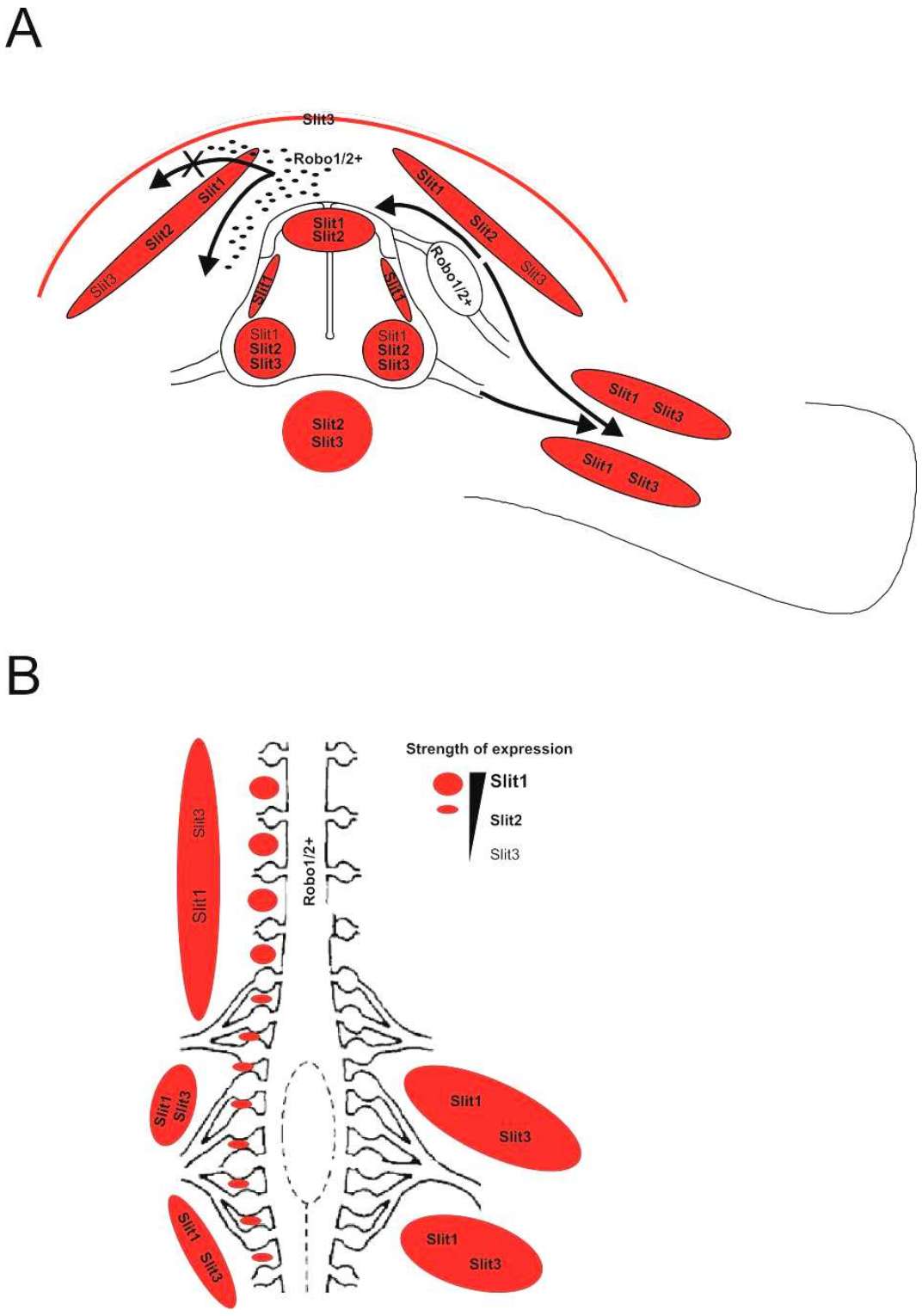

Figure 55 Schematic model of the involvement of the Slit / Robo system in neural crest cell migration and sensory and motor axon guidance. (A) The migration of neural crest cells is shown on the left side of the schematic spinal cord. Central and peripheral sensory and motor axon projections are shown on the right side. (B) Dorsal view of schematic drawing in A. The repulsive Slits form migration/projection boarders for Robo1/2-positive migrating neural crest cells, central and peripheral sensory DRG projections and motoneurons.

5.11 Conclusion

We investigated the function of the Slit / Robo system in neural crest cell migration and in the guidance of central and peripheral branches of sensory as well as motor neurons. We found that Slit / Robo signalling negatively regulated and restricted both, migration of neural crest cells and guidance of sensory and motor axons to the anterior sclerotome in early phases of sensory and motor circuit development. Notably, several other guidance molecules cooperate in this process indicating a certain redundancy. This backup mechanism seems to be necessary to achieve proper functional wiring of the PNS, as it is crucial for survival to properly process sensory information from external environmental stimuli. Later in development, Slit / Robo signalling is necessary for target-specific innervation of central collaterals of sensory neurons in the grey matter. Additionally, the expression patterns of Slits and Robos, observed during and after the finalization of the mature connectivity, indicate functions in synaptic target recognition, synaptogenesis, and in negative regulation of regeneration after peripheral and central nerve injuries. However, future experiments will have to address whether Slit / Robo signalling are crucial during late development and in regeneration processes.

6. Materials and methods

6.1 Plasmids and cloning of constructs

Robo1-2 and Slit1-3 plasmids were kindly provided by the Laufer Lab (Columbia University, New York):

Robo1 (AF364047), 1.9 kb insert at EcoR1 cloning site of pBluescript SK+.

Robo2 (AF364048), 2.1 kb insert at EcoR1 cloning site of pBluescript SK+.

Slit1 (AF364044), 1.7 kb insert at EcoR1 cloning site of pBluescript SK+.

Slit2 (AF364045), 3.5 kb insert at EcoR1 cloning site of pBluescript SK+.

Slit3 (AF364046), 1.9 kb insert at EcoR1 cloning site of pBluescript SK+.

Robo3/Rig1 (XM425794), 550bp insert at EcoR1 cloning site of pBluescript KS+ was kindly provided by Dr. A. Klar (The Hebrew University, Israel).

Full length clones of pSecTagB-hSlit2, pSecTag2B-hSlit3 were kindly provided by Dr. A. Chédotal (Centre National de la Recherche Scientifique, UMR7102, 9 Quai Saint-Bernard, Paris F-75005, France).

A full -length clone of mouse pYX-Asc-mSlit1 was obtained from ImaGenes GmbH (Berlin, Germany). From this vector the mSlit1 open-reading frame was cloned in frame into pcDNA3.1/myc-His(-) A to obtain a Myc tagged version of mSlit1. mSlit1-myc-His tagged was then cloned into pIRES-β-actin.

pIRES-β-actin-EYFP was used as a control plasmid and to visualise targeted areas within the embryo (Pekarik et al., 2003).

6.1 .1 Cloning of pcDNA3.1(-)-mSlit1-myc-His A and pIRES-β–actin-mSlit1-myc-His

The mouse Slit1 full-length sequence was inserted into pcDNA3.1/myc-His(-) A to obtain a myc-tagged CMV promoter-driven version of mSlit1 for *in vitro* studies. mSlit1 tagged with myc/His was then cloned into pIRES-β-actin to get a chicken β-actin promoter driven vector for *in vivo* studies.
5` and 3` mSlit1 PCR primers with flanking restriction enzymes sites were designed with Vector NTI software. Primer were as follows:

Forward: 5` CGGCTAGCACCATGGCGCTAACGCCCCAGCG 3`
Reverse: 5` CGGATATCTGCGCACTGGGCACAGCCACACTT 3`

PCR was carried out in 50 µl with the following conditions and the Phusion Polymerase and buffer (Finnzymes OY, Espoo, Finland): 98℃ for 30 sec, then 30 cycles of 98℃ for 10 sec, 62℃ for 30 sec, 72°C for 150 sec and finally 70° for 5 min followed by 4°C hold. The PCR product was digested with NheI (NEB) and EcoRV (NEB) for three hours, extracted from a 1% agarose gel and purified with the Promega extraction kit according to the manufacturer`s protocol.
pcDNA3.1/myc-His(-) A was digested with NheI (NEB) and EcoRV (NEB) for three hours, the empty vector (with Myc and His tag) extracted from a 1% agarose gel and purified with the Promega extraction kit according to the manufacturer`s protocol. Then the purified vector was dephosphorylated with shrimp Alkaline Phosphatase (Roche) for one hour. Ligation of the vector and the mSlit1 insert was done with T4 DNA Ligase (Promega) at 15℃ overnight at a ratio of 1:3 (vector / insert). PcDNA3.1(-)myc-HisA-mSlit1 was digested with AflII (NEB) for three hours, blunted with T4 DNA Polymerase (Promega) for 5 min before double digestion with NheI (NEB) and DraI (NEB, multiple restriction sites in the backbone of the vector to facilitate the separation of the bands during gel electrophoresis) for three hours. The mSlit1-myc-His insert was extracted from a 1% agarose gel and purified with the Promega extraction kit according to the manufacturer`s protocol. An empty pIRES-β–actin was digested with NotI (NEB) for three hours, blunted with T4 DNA Polymerase (Promega) for 5 min before digestion with NheI (NEB) for three hours. The backbone was dephosphorylated with shrimp Alkaline Phosphatase (Roche) for one hour, extracted from a 1% agarose gel and purified with the Promega extraction kit according to the manufacturer`s protocol. mSlit1-myc-His was ligated into the pIRES-β–actin backbone with T4 DNA Ligase (Promega) at a ratio of 1:3 (vector / insert) at 15℃ overnight.

6.1.2 Cloning of pIRES-β–actin-hSlit2-myc-His

5` and 3` hSlit2 PCR primers with flanking restriction enzymes sites were designed with Vector NTI software. Primer were as follows:

Forward: 5` GCTCTAGA ACCATGGAGACAGACACACT 3`
Reverse: 5` TTGCGGCCGC TCAATGATGATGATGATGATGGTCGA 3`

PCR was done on pSecTagB-hSlit2 in 50 µl with the following conditions and the *Pfu* DNA Polymerase and buffer (Promega, Madison, USA): 94℃ for 5 min, then 40 cycles of 94°C for 30 sec, 60℃ for 30 sec, 68℃ for 6 min and finally 68° for 10 min followed by 4°C hold. The PCR product was digested with XbaI (NEB) and NotI (NEB) for three hours, extracted from a 1% agarose gel and purified with the Promega extraction kit according to the manufacturer`s protocol. An empty pIRES-β–actin was digested with XbaI (NEB) and NotI (NEB) for three hours, the backbone dephosphorylated with shrimp Alkaline Phosphatase (Roche) for one hour, extracted from a 1% agarose gel and purified with the Promega extraction kit according to the manufacturer`s protocol. The hSlit2-myc-His PCR product was ligated into the pIRES-β–actin backbone with T4 DNA Ligase (Promega) at a ratio of 1:3 (vector / insert) at 15℃ overnight.

6.1.3 Cloning of pIRES-β–actin-hSlit3-myc-His

pSecTag2B-hSlit3 was digested with PmeI (NEB), NheI (NEB) and EagI (NEB, multiple restriction sites in the backbone of the vector to facilitate the separation of the bands during gel electrophoresis) for three hours, hSlit3-myc-His extracted from a 1% agarose gel and purified with the Promega extraction kit according to the manufacturer`s protocol. An empty pIRES-β–actin was digested with NheI (NEB) and NotI (NEB) for three hours, the backbone dephosphorylated with shrimp Alkaline Phosphatase (Roche) for one hour, extracted from a 1% agarose gel and purified with the Promega extraction kit according to the manufacturer`s protocol. The hSlit3-myc-His insert was ligated into the pIRES-β–actin backbone with T4 DNA Ligase (Promega) at a ratio of 1:3 (vector / insert) at 15℃ overnight.

6.1.4 Subcloning of cRobo1, cRobo2, cRobo3/RIG1, cSlit1, cSlit2 and cSlit3

To show the specificity of downregulation of the target genes we used two independent, non-overlapping fragments of cDNA for the generation of dsRNA and *in situ* probes. The subcloning strategy with used sequences, length of fragments and a short summary of the subcloning procedure is described in the following chapter.

6.1.4.1 Subcloning strategy

cRobo1

1. fragment:
bp 568-770 of Robo1 (XM_416673)
Length of fragment: 201
In pBluescript SK+
Subcloning strategy: SacI (NEB) single digest, extract vector, religate

2. fragment:
bp 878-1789/3061-3348 of Robo1 (XM_416673)
Length of fragment: 1298
In pBluescript SK+
Subcloning strategy: HindIII (NEB) single digest, extract vector, religate

cRobo2

1. fragment:
bp 79-626 of Robo2 (AF364048)
Length of fragment: 547
In pBluescript SK+
Subcloning strategy: BamHI (NEB) single digest, extract vector + short part of insert (still on vector), religate

2. fragment:
bp 626-1565 of Robo2 (AF364048)
Length of fragment: 943
In pBluescript KS+
Subcloning strategy: BamHI (NEB) single digest, extract long part of insert, ligate into empty pBluescript SK+ plasmid

cRIG1/cRobo3

1.fragment:
bp 569-807 of Rig1 (XM_425794)
Length of fragment: 238
In pBluescript KS+
Subcloning strategy: SpeI / SmaI (NEB, SmaI in insert) double digest, extract vector, religate

2. fragment:
bp 808-1018 of Rig1 (XM_425794)
Length of fragment: 210
In pBluescript KS+
Subcloning strategy: EcoRV / SmaI (NEB, SmaI in insert) double digest, extract vector, religate

cSlit1

1.fragment:
bp 2142-2541 of Slit1 (XM_421715)
Length of fragment: 396
In pBluescript SK+
Subcloning strategy: EcoRV (NEB) single digest, extract vector, religate
(Or EcoRV / XhoI (NEB) double Digest, extract vector, religate)

2.fragment:
bp 2541-3995 of Slit1 (XM_421715)
Length of fragment: 1458
In pBluescript SK+
Subcloning strategy: BamHI/ EcoRV (NEB) double digest, extract longer insert, ligate into empty pBluescript SK+ plasmid

cSlit2

1.fragment:
bp 3155-3946 of Slit2 (XM_001232040)
Length of fragment: 841
In pBluescript SK+
Subcloning strategy: BamHI (NEB) single digest, extract vector, religate

2. fragment:
bp 5892-6394 of Slit2 (XM_001232040)
Length of fragment: 503
PCR primer on pBluescript SK+ cSlit2 plasmid:
T7 primer:
5` GGG TAC CCT GGG TTT TAC TGA 3`
T3 primer:
5` AGC ATG TCG TCT TGG GGT AA 3`
Subcloning strategy: Ligate blunt PCR product into empty blunt and dephosphorylated pBluescript SK+ plasmid

cSlit3

1.fragment:
bp 3832-4572 of Slit3 (XM_414503)
Length of fragment: 745
In pBluescript SK+
Subcloning strategy: BamHI (NEB) single digest, extract vector, religate

2.fragment:
bp 3159-3832 of Slit3 (XM_414503)
Length of fragment: 673
In pBluescript SK+
Subcloning strategy: BamHI (NEB) single digest, extract smaller insert, ligate into empty pBluescript SK+ plasmid

6.2 Production of single-stranded DIG-labelled RNA *in situ* probes and dsRNA

For the production of single-stranded DIG-labelled RNA *in situ* probes ten µg plasmid DNA were digested for three hours to overnight at 37℃. For plasmid linearization following restriction enzymes were used for T7 and T3 promoters, respectively (all from NEB, Ipswich, USA): BamH1 and Xho1 for Robo1, Spe1 and Xho1 for Robo2, EcoR1 and Spe1 for Rig1, BamH1 and Xho1 for Slit1, Spe1 and Xho1 for Slit2, Spe1 and HindIII for Slit3. Afterwards, the DNA was purified by adding 150µl diethylpyrocarbonate (DEPC, 1: 1000 (vol/vol)) treated double-distilled water (ddH_2O) and 200 µl phenol (pH >7):chloroform:isoamyl alcohol (25:24:1 vol/vol/vol), spun down at 10`000 rpm in an Eppendorf centrifuge for 10 min at 4℃ and precipitated with 0.1 volumes 3 M sodium acetate and 2.5 volumes 100% ethanol overnight. Tubes were centrifuged at 13500 rpm for 15 min at 4℃ in an Eppendorf centrifuge. The pellet was washed with 500 µl 70 % ethanol in DEPC-treated ddH_2O, centrifuged at 13500 rpm for 8 min at 4℃ in an Eppendorf centrifuge, dried and dissolved in 20 µl DEPC-treated ddH_2O. One µl of the purified DNA was loaded on a 1% agarose gel for quality control. The concentration of the DNA was measured using a spectrophotometer (NanoDrop®, ND-1000

Spectrometer, Witec AG, Littau, Switzerland). For *in vitro* transcription, the following components were mixed and the tubes were incubated at 37℃ for 3 hours:

4 µg linearized plasmid DNA
3 µl DIG RNA Labeling mix 10x (Roche)
6 µl 5x Transcription buffer (Promega)
3 µl RNA polymerase (15 U/µl, Promega)
0.8 µl RNasin (30 U/µl, Promega)
3 µl 100 mM DTT (Promega)
and DEPC-treated ddH_2O was added to a final volume of 30 µl

In vitro transcription was done with T7 and T3 RNA polymerases (Promega, Madison, USA). Subsequently 3 µl DNaseI (Roche, DNase1, recombinant, RNase-free, [10 U/µl]) were added to remove the template DNA. Incubation was for 15 min at room temperature. Then, 17 µl 7.5 M ammonium acetate and 170 µl of ice-cold 100% ethanol were added and the single-stranded RNA was precipitated for two hours to overnight at –70 ℃. The tubes were spun down at maximal speed for 15 min at 4℃ in an Eppendorf centrifuge, the pellet was washed with 100 µl of ice-cold 70 % ethanol in DEPC-treated ddH_2O, spun down at maximal speed for 15 min at 4℃ and the dry pellets were resuspended in 150 µl of DEPC-treated ddH_2O and stored at –70 ℃. For quality control, one µl sample of the reaction mix was loaded on a 1% agarose gel. The concentration of the ssRNA was measured using a spectrophotometer (NanoDrop®, ND-1000 Spectrometer, Witec AG, Littau, Switzerland).

To produce double-stranded RNA, plasmid linearization, purification and *in vitro* transcription was as described for the production of *in situ* probes, except that the following components were mixed for *in vitro* transcription:

3 µg linearized plasmid DNA
2 µl 100mM rNTP (25mM of each rNTP)
1 µl RNasin (30 U/µl, Promega)
3 µl RNA polymerase (15 U/µl, Promega)
8 µl 5x Transcription buffer (Promega)
4 µl 100 mM DTT (Promega)
and DEPC-treated ddH_2O was added to a final volume of 40 µl

After incubation of the reaction mix at 37℃ for four hours, 3 µl DNaseI (Roche, DNase1, recombinant, RNAse-free, [10 U/µl]) were added (to remove template DNA). The reaction mix was incubated for 20 min at room temperature, followed by purification and precipitation: the DNaseI digest and 40 µl DEPC-treated ddH_2O, 4 µl 0.5 M EDTA (pH 8.0), 50 µl 7.5 M ammonium acetate and 100 µl phenol (pH 4):chloroform:isoamyl alcohol (25:24:1 vol/vol/vol) were mixed and spun down for 10 min at

10`000 rpm at 4℃ in an Eppendorf centrifuge. The supernatant was transferred to a new RNase-free Eppendorf tube and 130 µl of chloroform:isoamyl alcohol (24:1 vol/vol) were added. Tubes were centrifuged for 10 min at 10`000 rpm in an Eppendorf centrifuge at 4℃ and the supernatant transferred to new RNase-free Eppendorf tubes. For precipitation of the single-stranded RNA overnight at -70℃, 2.5 volumes of 100% ethanol were added. The tubes were centrifuged at 13`500 rpm for 15 min at 4℃ in an Eppendorf centrifuge, the pellet washed with 50 µl ice-cold 70 % ethanol/DEPC-treated $ddH_2O$ an spun down at 13`500 rpm for 8 min at 4℃ in an Eppendorf centrifuge. The dry pellets were resuspended in 20 µl DEPC-treated ddH_2O and stored at –70℃ until further use. For quality control, a 0.5 µl sample of the ssRNA was loaded on a 1% agarose gel and the concentration of the single stranded RNA was measured using a spectrophotometer (NanoDrop®, ND-1000 Spectrometer, Witec AG, Littau, Switzerland). To anneal the antisense and sense strands, equal nanogram amounts were mixed in DEPC-treated ddH_2O and denatured for 10 min at 95℃. Then the heating block was switched off to allow for the antisense and sense RNA to anneal overnight. For quality control, 1 µl of the annealed RNA mix was loaded on a 1% agarose gel. The concentration of the dsRNA was measured using a spectrophotometer (NanoDrop®, ND-1000 Spectrometer, Witec AG, Littau, Switzerland).

6.3 Bacterial transformation

Fifty µl of competent XL-1 Blue E. coli bacteria were thawed on ice and 100-300 ng plasmid DNA or 10-20 µl of ligation reaction were gently mixed, cooled for 15 min on ice, heat-shocked for 1.5 min at 42℃ and again shortly cooled on ice. Five hundred µl of LB-Medium were added, shaken for 45 min at 37℃. The suspension was streaked on agar plates (room temperature) containing ampicillin (100µg/ml). Subsequently the plates were incubated overnight at 37℃. No more than 18 hours later, the plates were put at 4℃. For Maxi culture, 200 µl ampicillin (100 µg/ml) were added to 200 ml LB-medium, one colony of each agar plate was picked and the pipet tip was put into the Erlenmeyer containing the LB-medium. The cultures were shaken overnight at 37℃ at 180 rpm. Thereof 850 µl were mixed with 150 µl glycerine for long term storage at –70℃. The remaining 199 ml were transferred in four 50 ml Falcon tubes and centrifuged at 4℃ for 15 min at 4500 rpm in an Eppendorf centrifuge. The supernatant was discarded and the pellets stored at -70℃ until further use.

6.4 *In situ* hybridization

In situ hybridizations with HH14-32 embryos were carried out as described earlier (Mauti et al., 2006). Due to the difficulties to access the mRNA at later developmental stages, a different treatment was used for older stages (HH33-42). Sections from older stages were subject to a proteinase K step. After fixation for 30 min in 4% PFA in autoclaved and DEPC-treated PBS, the cryosections were washed 3 times in PBS for 5 min and then incubated in 10mg/ml proteinase K in proteinase K buffer for 10 min. Subsequently they were washed two times in PBS and again fixed in 4% PFA for 15 min, washed two times in PBS and once in ddH_2O for 5 min each. The following procedure is as described earlier (Mauti

et al., 2006). For *in situ* hybridizations demonstrating the downregulation of the targeted mRNAs, 200 ng of probe per ml hybridization solution was used, the anti-Digoxigenin-AP antibody was diluted 1:10`000 and used overnight and the colour reaction was stopped as soon as a signal was detected.

6.5 *In ovo* RNA interference

For a detailed protocol of *in ovo* RNAi see Pekarik et al., 2003. The volume of 0.5 µl of a mix containing 300-500 ng/µl dsRNA, 100 ng/µl pIRES-β-actin-EYFP plasmid and 0.05% (w/v) Fast Green FCF (AppliChem) as visual injection control, dissolved in sterile PBS, were injected with a glass microcapillary into the central canal of the spinal cord. Embryos were injected at HH10-14, when neural crest cells or the developing somite and the dermomyotome were targeted and at HH11-16, when DRGs were transfected. Subsequently the embryos were electroporated *in ovo* with an Electro Square Porator ECM 830 (BTX, Genetronics Inc.). For this purpose, the electrodes were placed parallel to the embryo in the area of the developing limb buds. Then 7 pulses for DRGs and neural crest cells or 10-12 pulses for the developing somite and the dermomyotome with 22 Volt and with a duration of 50 milliseconds were applied. The volume of 0.2 ml sterile PBS were added to the embryo. The eggshell was closed with Scotch tape for further incubation at 39 ℃.

6.6 *In vivo* overexpression studies

The volume of 0.5 µl of a mix containing 1000-3000 ng/µl of pIRES-β–actin-mSlit1-myc-His, pIRES-β–actin-hSlit2-myc-His or pIRES-β–actin-hSlit3-myc-His and 100 ng/µl pIRES-β-actin-EYFP plasmid and 0.05% (w/v) Fast Green FCF as visual injection control, dissolved in sterile PBS, were injected with a glass microcapillary into the central canal of the spinal cord. Embryos were injected at HH10-14, when neural crest cells or the developing somite and the dermomyotome were targeted and at HH11-16, when DRGs were transfected. Subsequently the embryos were electroporated *in ovo* with an Electro Square Porator ECM 830 (BTX, Genetronics Inc.). For this purpose, the electrodes were placed parallel to the embryo in the area of the developing limb buds. Then 7 pulses for DRGs and neural crest cells or 10 -12 pulses for the developing somite and the dermomyotome with 22 Volt and with a duration of 50 milliseconds were applied and 0.2ml sterile PBS were added to the embryo. The eggshell was closed with Scotch tape for further incubation at 39 ℃.

6.7 Immunohistochemistry

Monoclonal antibodies HNK-1 (not diluted), 40.2D6 recognizing Islet-1 (not diluted), IE8 recognizing P0 (not diluted) and 9E10 binding to Myc tag (diluted 1:80) were obtained from the Developmental Studies Hybridoma Bank, University of Iowa, Iowa City, IA. Furthermore we used rabbit anti-neurofilament (diluted 1:250; Millipore, Billerica, MA), RMO270 (diluted 1:1500; Zymed, Carlsbad, CA, diluted 1:1,500) and a FITC-labelled goat anti-GFP antibody (diluted 1:500; Rockland, Gilbertsville, PA, diluted 1:400). Rabbit anti-axonin-1 was described earlier (diluted 1:1000; Perrin et al., 2001). Secondary antibodies were: goat anti-mouse IgG Cy3 (diluted 1:250; Jackson ImmunoResearch

Laboratories, Newmarket, Suffolk, UK), goat anti-rabbit Alexa350 (diluted 1:250; Invitrogen/Molecular Probes, Carlsbad, CA), donkey anti-rabbit Cy3 (diluted 1:250; Jackson ImmunoResearch Laboratories, Newmarket, Suffolk, UK), goat anti-mouse Alexa488 (diluted 1:250; Jackson ImmunoResearch Laboratories, Newmarket, Suffolk, UK) and goat anti-rabbit Alexa488 (diluted 1:250; Molecular Probes, Carlsbad, CA).

6.8 Sections and tissue preparation

Fertilized eggs were incubated at 38-39 ℃ and sacr ificed at various stages (Hamburger and Hamilton, 1951) .The embryos were pinned down in a Sylgard dish (Dow Corning Corporation) and the internal organs were removed. According to the stage of the embryos, they were fixed in 4 % paraformaldehyde (PFA) at 25 ℃ for one to two hour s or at 4℃ overnight. After fixation, they were cryoprotected overnight by incubation in 25% sucrose in 0.1 M sodium phosphate buffer (pH 7.4). Then they were embedded in Tissue-Tek O.C.T. compound and frozen in isopentane (cooled on dry ice). Transverse sections from the lumbosacral level (25μm) and longitudinal (20μm) sections were cut with a Leica cryocut CM 3000 and collected on Super Frost Plus microscope slides (Menzel-Gläser), dried for 30 min at 30 ℃ and stored at -20℃ until further use.

6.9 Whole-mount preparations and their quantification

Chicken embryos were sacrificed between HH22 and HH26 and the internal organs removed carefully to avoid nerve injuries. They were pinned down in a Sylgard dish (Dow Corning Corporation), checked for YFP expression under a binocular equipped with fluorescence optics (Olympus) and fixed in 4% PFA in PBS for one to two hours at room temperature or overnight at 4℃. Subsequently they were washed in PBS, transferred to a 24-well plate containing 1% Triton in PBS and permeabilized for two hours with constant shaking (for all following steps) at room temperature. Further steps were done as described earlier (Mauti et al., 2007). The antibody used to monitor transfected areas within the embryo was a FITC-labelled goat anti-GFP antibody (diluted 1:500; Rockland, Gilbertsville, PA). To visualise outgrowing neurons the monoclonal antibody RMO270 was used (diluted 1:1500, Zymed) together with the secondary antibody goat anti-mouse Cy3 (diluted 1:250; Jackson ImmunoResearch Laboratories, Newmarket, Suffolk, UK). Quantification was done by measuring the ratio between DRG width (at the DREZ) / segment length of all trunk and LS1-LS3 DRGs. DRGs were considered as phenotypic when the ratio differed more than a standard deviation from the pIRES-β–actin-EYFP-injected control embryos (ratio of control embryos: > 0.599 / <0.723).

6.10 Quantitative real time PCR

Control and experimental embryos were sacrificed between HH28 and HH30 and the DRGs and the spinal cord were removed (for DRG removal see 6.11), transferred into RNA later (Ambion) and immediately frozen in liquid nitrogen. The total RNA was extracted with the RNAeasy Mini extraction kit (Promega) according to the manufacturer`s protocol. Quantitative RT-PCR was carried out with the

SuperScript III Platinum Two-step qRT-PCR kit (Invitrogen) on AB 7900 HT from Applied Biosystems using SYBR green PCR master mix (Applied Biosystems) to monitor double stranded DNA. The primers were designed with Primer3 (freeware) as following: Robo1 forward: 5`- AGT GAC TTT CCA GTG TGA AGC AAC -3`, Robo1 reverse: 5`- GTG ATG GTG AGG TCT CCT GTC TG -3`. PCR products were about 200 bp long. PCR was carried out in 10 µl with the following conditions: 50℃ for 2 min, followed by 95℃ for 10 min, then 40 cycles of 95℃ for 15 sec, 60℃ for 60 sec and finally one cycle of 95° for 15 sec, 60° for 15 sec and 95° for 15 sec. Robo1 levels were normalized to levels of GAPDH, 18s RNA and β-Actin. The control reaction mixes lacking reverse transcriptase resulted in no detectable products. RNA was prepared from three independent experiments and measurements were performed in triplicates two separate times for each sample.

6.11 DRG removal

Control and experimental embryos were sacrificed at HH24/25, pinned down in a Sylgard dish and the internal organs were removed. A ventral laminectomy was performed to facilitate the removal of the DRGs. On both sides of the spinal cord, an intersection was cut with tungsten needles and the spinal cord was removed. A second intersection was performed with tungsten needles to cut the dorsal roots. Then the DRGs were caught at the ventral roots with forceps and extracted.

6.12 *In vitro* assay

6.12.1 Transfection of COS-7 cells

One day before transfection $2x10^5$ COS-7 cells were plated in 500 µl of DMEM (Invitrogen)+ 5% foetal calf serum (FCS) per well (4-well dishes) so that they were >95% confluent at the time of transfection. The amount of 2 to 4 µg plasmid DNA were diluted in 50 µl of Opti-MEM (Invitrogen) and gently mixed. At the same time, two µl Lipofectamine 2000 (Invitrogen) were diluted in 50 µl of Opti-MEM, gently mixed and incubated at room temperature. After 5 min incubation, the DNA sample and the Lipofectamine 2000 solution were mixed and incubated for 20 min at room temperature. Then the 100 µl DNA/Lipofectamine 2000 complexes were added to the wells containing the COS-7 cells in 300 µl DMEM + 5% FCS and slightly rocked back and forth. The transfection mixture was incubated in a 5% CO_2 incubator at 37℃ for at least 6 hours to overnigh t.

6.12.2 DRG explant cultures

COS-7 cells, plated in four-well plates for two days, were transfected for 24 hours with 2 to 4 µg of pcDNA3.1(-)/myc-His A-mSlit1, pSecTagB-hSlit2, pSecTag2B-hSlit3 or pIRES-β-actin-EYFP (control) using Lipofectamine 2000 in DMEM plus 5% FCS. DRGs were removed from HH24/25 embryos (see 6.11) and collected in a drop of DRG medium (DMEM plus 5% FCS, NGF, N3 and Albumax). Twelve DRGs from three embryos were pipetted into a four-well plate with transfected COS-7 cells in DRG

medium (Prior to DRG adding, transfected COS-7 cells were incubated in DRG medium for 24 hours to achieve secretion of Slits into the DRG medium) and incubated for 24h.
They were fixed for 20 min in 4% PFA in PBS, washed once with PBS and perforated in 1% Triton in PBS for 5 min. After three washes in PBS for 5 min each, they were blocked in 10% FCS in PBS for 10 min followed by incubation for three hours at 25℃ or overnight at 4℃ with rabbit-anti Axonin-1 (diluted 1:1000) and 9E10 recognizing the Myc tag (diluted 1:80) or goat anti-GFP FITC (diluted 1:1500) in 10 % FCS in PBS. After three washes of 5 min in PBS, they were again blocked for 10 min in 10% FCS in PBS and afterwards incubated with donkey anti-rabbit Cy3 (diluted 1:250; Jackson ImmunoResearch Laboratories, Newmarket, Suffolk, UK) and goat anti-mouse Alexa488 (diluted 1:250; Jackson ImmunoResearch Laboratories, Newmarket, Suffolk, UK) diluted in 10 % FCS in PBS for one hour. The cultures were then analysed after extensive washing in PBS with an inverted microscope equipped with fluorescence optics (Olympus) and finally mounted with Immu-Mount (Thermo Scientific). All experiments were done at least three times independently with 12 DRGs collected from three embryos for each condition. Quantification was done with all experiments and finally pooled into one histogram.

6.12.3 Dissociated DRG neuron cultures to examine the rate of cell death

For dissociated DRG neuron cultures 20-30 DRGs were removed as described in 6.11. The DRGs were trypsinized for 20 min at 37℃. Glass capillar ies were prepared with the appropriate aperture to disrupt the DRGs. The trypsinized DRG cell suspension was pipetted 6 times up and down. Thereof, 10`000 single DRG neurons were transferred into one LabTek compartment onto transfected (EYFP, mSlit1, hSlit2 and hSlit3) confluent COS-7 cells. After 24 hours, the growth was stopped by fixing with 4% PFA in PBS. DRG neurons were stained with rabbit-anti Axonin-1 (diluted 1:1000) and donkey anti-rabbit Cy3 (diluted 1:250), transfection was visualised with mouse anti-Myc (9E10, diluted 1:80) recognizing the tagged Slit proteins and goat anti-GFP FITC (diluted 1:500) for pIRES-β-actin-EYFP controls. Cell death was examined by Trypan blue staining (0.04% Trypan blue (Gibco) in PBS) before fixation.

6.13 DRG cell counting

Five DRGs per embryo (the two most ventral trunk DRGs and three lumbar DRGs (LS1-LS3)) were removed as described in 6.11 and trypsinized as described in 6.12.3. A drop of the trypsinized DRG-cell suspension was used to fill the Neubauer chamber and four areas in two different count chambers were enumerated.

6.14 Western Blotting

COS-7 cells were transfected with Lipofectamine 2000 in four-well plates with 4µg of pcDNA3.1(-)-mSlit1-myc-His A, pSecTagB-hSlit2 and pSecTag2B-hSlit3 according to the manufacturer`s protocol. The supernatant was collected for three days. Subsequently the proteins were precipitated (after

Wessel and Flügge, 1984) and used for wet Western blot analysis. The samples were dissolved in SDS-PAGE loading buffer (see 6.16), run on a SDS-PAGE gel (7%) using the Biorad MiniProtean Tetra Cell system and Western blotted by standard methods using the Western blotting system Biorad MiniProtean Tetra Cell system and the ECL™ Western Blotting Detection Kit from Amersham (RPN 2109).

6.14.1 Protein Precipitation

The proteins were precipitated according to Wessel and Flügge, 1984. The volume of 500 µl protein sample were mixed with 2 ml Methanol and 500 µl Chloroform and vortexed. The volume of 1.5 ml ddH_2O was added. The mixture was again vortexed and centrifuged for 1 min at full speed at room temperature with an Eppendorf table centrifuge. The upper organic phase was removed, 1.5 ml Methanol was added and thoroughly vortexed. Then the mixture was centrifuged for 5 min at full speed at room temperature with an Eppendorf table centrifuge. The supernatant was removed and the pellet dried at room temperature followed by dissolving in PBS.

6.14.2 Protein Gel Electrophoresis

For protein gel electrophoresis, a 4% stacking gel and a 7% separating gel was used. The Biorad MiniProtean Tetra Cell system was assembled, filled with running buffer (see 6.16) and cooled with ice in a tray. Protein samples were mixed with loading buffer (see 6.16) and heated for 10 min at 95°C. The volume of 30 µl of the mixture was load onto the gel, as well as 10 µl of Kaleidoscope protein marker (Biorad, Hercules, USA) and run at 100V and constant 0.030 Amp for two hours. Then the gel was quickly stored in transfer buffer (see 6.16) until the transfer block was assembled.

6.14.3 Protein transfer

First, the sponge, the filter paper and the membrane was soaked in transfer buffer (see 6.16). Then the transfer block was assembled to the following order: Sponge, filter paper, gel, membrane, filter paper and sponge. The air bubbles between gel and membrane were removed by rolling a 15ml Falcon tube over the assembled transfer block. The assembled sandwich was put into the transfer tank filled with transfer buffer (see 6.16) and the gel blotted for 35 min at 75 Volt. The nitrocellulose membrane was removed followed by washing 2 times with 0.1% Tween20 in PBS (PBT). Subsequently the membrane was blocked for one hour in 5% milk powder (low fat) in PBT, followed by primary antibody (9E10, diluted 1:250 in 5% milk powder (low fat) in PBT) incubation overnight at 4°C. The next day the membrane was washed 5 times with PBT for 10 min each, then incubated for three hours at room temperature with the secondary antibody goat anti-mouse horseradish peroxidase, diluted 1:8000 in 5% milk powder (low fat) in PBT. After intensive washing (at least 5 times with PBT for 10 min each, the membrane was dried by pressing one edge of the membrane against a tissue and processed for detection.

6.14.4 Protein Detection

The signal was detected with ECL™ Western Blotting Detection Kit from Amersham (RPN 2109). One ml of detection solution 1 (ECL™ Western Blotting Detection Kit from Amersham (RPN 2109)) was mixed with 1 ml of detection solution 2 (ECL™ Western Blotting Detection Kit from Amersham (RPN 2109)). The blot was incubated with the detection solution mix for one min at room temperature and then packed into a transparent map, sealed (without air bubbles inside the map) and developed using standard techniques for 10 min up to overnight.

6.15 Anterograde labelling

Injections of the lipophilic dye FAST DiI were done as described earlier (Perrin et al., 2001). FAST DiI was injected with a glass microcapillary into the ventral (to hit nociceptive afferents) and medial (to target proprioceptive fibres) part of the dorsal funiculus in 250μm thick vibratome sections.

6.16 Solutions

Transformation of competent bacteria

LB-Medium (Luria-Bertani Medium): Bacto-Tryptone 10g, Bacto-yeast extract 5g, NaCl 10g, ddH_2O

Agar plates with or without ampicillin (100μg/ml) for selection
Glycerine for long-term storage of transformed bacteria.

Genotype of used bacteria:

XL1 –Blue MRF´: Δ(mcrA)183 Δ(mcrCB-hsdSMR-mrr)173 endA1 supE44 thi-1 recA1 gyr A96 relA1 lac[F´proAB laqIq ZΔM15 Tn10(TETr)

Plasmid preparation and linearization

Restriction enzyme buffer (from NEB and Roche)
1% BSA (Bovine serum albumin, NEB; 10mg/ml)
Restriction enzyme (20-30 U)
Phenol (pH >7):chloroform:isoamyl alcohol (25:24:1 vol/vol/vol)
3 M sodium acetate
Ice cool 70 % and 100 % ethanol

Production of single-stranded DIG-labelled RNA *in situ* probes

DIG RNA Labeling Mix 10x (Roche)

Transcription buffer 5x (Promega)
T3, T7 or SP6 RNA polymerase (15 U/µl, Promega)
RNasin (30 U/µl, Promega)
DTT 100 mM (Promega)
DNaseI (Roche, DNase1, recombinant, RNAse-free, [10 U/µl])
7.5 M Ammonium acetate
Ice cool 70 % and 100 % ethanol

Production of double-stranded RNA

100 mM rNTP
RNasin (30 U/µl, Promega)
T3, T7 or SP6 RNA polymerase (15 U/µl, Promega)
Transcription buffer 5x (Promega)
DTT 100 mM (Promega)
DNaseI (Roche, DNase1, recombinant, RNAse-free, [10 U/µl])
0.5 M EDTA (pH 8.0)
7.5 M ammonium acetate
Phenol (pH 4):chloroform:isoamyl alcohol (25:24:1 vol/vol/vol)
Chloroform:isoamyl alcohol (24:1 vol/vol)
Ice cool 70 % and 100 % ethanol

***In situ* hybridization**

PFA	Paraformaldehyde, 10% PFA in DEPC-treated ddH_2O, 1mM NaOH added and heated on stirrer at 55°C; used as 4% PFA in autoclaved and DEPC-treated PBS.
Sucrose	25 % Sucrose in 0.1 M sodium phosphate buffer (pH 7.4)
Sodium phosphate	0.1 M sodium phosphate buffer (pH 7.4).
20x PBS	NaCl 160g/l KCl 4g/l Na_2HPO_4 x $2H_2O$ 28,8g/l KH_2PO_4 4g/l Volume was made up to 1L with DEPC-treated ddH_2O and adjusted to pH 7.4.
20x SSC	Sodium saline citrate: 3 M NaCl, 0.3 M trisodium citrate dihydrate, pH 7.0
1% Triethanolamine	dissolved in DEPC-treated ddH_2O
0.25% acetic anhydride	dissolved in DEPC-treated ddH_2O
7.5% H_2O_2	dissolved in DEPC-treated ddH_2O

Prehybridization solution	40% Formamide, 5x SSC, 5x Denhardt`s, 500µg/ml herring sperm DNA, 250µg/ml yeast total RNA, dissolved in ddH_2O
Hybridization solution	Prehybridization solution, containing 300-500 ng/ml DIG labelled antisense or sense cRNA probe
Detection buffer	0.1 M Tris-base, 0.15 M NaCl, pH 7.5
Blocking buffer	3% milk powder in 1x detection buffer
Anti-DIG-AP	Anti-digoxigenin antibody conjugated with alkaline phosphatase (Roche), diluted 1:5000 in blocking buffer
AP buffer	0.1 M Tris-base, 0.1 M NaCl, 0.05 M $MgCl_2$, pH 9.5
TE buffer	10 mM Tris, 1 mM EDTA, pH 8.0
Development solution	4.5µl/ml NBT, 3.5µl/ml BCIP and 10µl/ml levaminisole in 1x AP buffer
NBT	nitroblue tetrazolium, 337.5 µg/ml (Roche)
BCIP	5-bromo-4-chloro-3-indoyl-phosphate, 175 µg/ml (Roche)
Levamisole	240 µg/ml (Sigma)
Celvol	100g celvol dissolved in 400 ml PBS, mixed overnight, 200 ml glycerol and 6 ml 5% sodium acide added, again mixed 16 hours and centrifuged at 12000 rpm in a Eppendorf centrifuge. Protect from light.
Proteinase K	10mg/ml in proteinase K buffer
Proteinase K buffer	20ml 1 M Tris-base pH 7.5 and 2ml 0.5M EDTA, filled up to 1litre with DEPC-treated ddH_2O

***In vivo* injection of plasmids and double-stranded RNA probes and *in ovo* electroporation**

Injection solution:	dsRNA (300 - 400 ng/µl) pIRES-β-actin-EYFP plasmid (100 ng/µl) 0.05% Fast Green FCF (Applichem) or Trypan Blue (Invitrogen, Carlsbad) Filled up with sterile PBS to 10 µl

Whole-mount preparations

FCS	Foetal calf serum, 10% FCS in PBS
Lysine	20 mM Lysine in 0.1 M sodium phosphate (pH 7.4)
Triton	1% Triton in PBS
Primary antibodies:	
RMO270	monoclonal mouse anti-neurofilament (160kD) antibody, Zymed, diluted 1:1500 in 10% FCS in PBS
RbαGFP	polyclonal rabbit anti-GFP antibody, Abcam, diluted 1:500 in 10% FCS

	in PBS
GαGFP-FITC	Goat anti-GFP-FITC labelled antibody, Abcam, diluted 1:500 in 10% FCS in PBS

Secondary antibodies:

GαM Cy3	goat anti-mouse Cy3, Jackson ImmunoResearch, diluted 1:250 in 10% FCS in PBS
GαRb Alexa 488	Goat anti-rabbit Alexa 488, Molecular Probes, diluted 1:250 in 10% FCS in PBS

Clearance of tissue:

Methanol	25%, 50%, 75% and 100% methanol
BBBA	Benzyl benzoate / benzyl alcohol, mixed 2:1

Antibody staining of 250µm-thick vibratome sections and antibody staining of 20-25 µm-thick cryosections

Primary antibodies:

GαAxonin-1	polyclonal goat anti-Axonin-1 antibody, diluted 1:1000 in 10% FCS in PBS (Perrin et al., 2001)
RMO270	monoclonal mouse anti-neurofilament (160kD) antibody, Zymed, diluted 1:1500 in 10% FCS in PBS
RbαGFP	polyclonal rabbit anti-GFP antibody, Abcam, diluted 1:500 in 10% FCS in PBS

Secondary antibodies:

DαG Cy3	Donkey anti-goat Cy3, Jackson ImmunoResearch, diluted 1:250 in 10% FCS in PBS
GαRb Cy3	Goat anti-rabbit Cy3, Jackson ImmunoResearch, diluted 1:250 in 10% FCS in PBS
GαM Cy3	goat anti-mouse Cy3, Jackson ImmunoResearch, diluted 1:250 in 10% FCS in PBS
GαRb Alexa488	Goat anti-rabbit Alexa488, Molecular Probes, diluted 1:250 in 10% FCS in PBS

***In vitro* assays**

COS-7 cells

DMEM	Dulbecco's Modified Eagle Medium, Invitrogen
Opti-MEM	Reduced Serum Medium, Invitrogen

Lipofectamine 2000	Invitrogen
DRG medium:	DMEM plus 5% FCS (vol/vol)
	0.2% NGF (Nerve Growth Factor 7S, murine, natural; 10μg/ml, (w/vol), Invitrogen)
	2 % Albumax (200 mg/ml, Gibco (w/vol))
	1 % N3 (vol/vol))
N3 in PBS:	Albumax (10 mg/ml)
	Transferrin (50 mg/ml)
	Putrescine (80 mg/ml)
	Corticosterone (2 mg/ml)
	Sodium Selenite (104 μg/ml)
	Triiodothyronine (200 μg/ml)
	Insulin (12.5 mg/ml)
	Progesterone (125 μg/ml)
PFA	4% in PBS (vol/vol)
Triton	1% in PBS (vol/vol)
FCS	foetal calf serum, 5% (for DRG medium) and 10% (for COS-7 cells) in PBS (vol/vol), Gibco
Trypsin	0.25% in PBS (vol/vol), Gibco
Trypan blue	0.04% Trypan blue (Gibco) in PBS (vol/vol)

Labelling of nociceptive and proprioceptive sensory afferents

L. m. agarose	6.5% low-melting agarose (Sigma), used as embedding medium
Fast DiI	5mg/ml, dissolved in 100% methanol (Molecular Probes, Eugene, OR)

Western Blotting

Protein Precipitation

100% Methanol
Chloroform
ddH_2O

Protein Gel Electrophoresis

Biorad MiniProtean Tetra Cell system

4 % stacking gel:
3 ml ddH_2O

0.67 ml Acrylamide-Bis (Biorad)
1.25 ml 4x Upper Tris buffer
75 µl APS (100mg/ml)
5 µl TEMED (Biorad)

7 % SDS-PAGE separating gel:
5 ml ddH_2O
2.33 ml Acrylamide-Bis (Biorad)
2.5 ml 4x Lower Tris buffer
150 µl APS (100mg/ml)
10 µl TEMED (Biorad)

10x Running Buffer (pH 8.3):

Tris-base	0.25 M
Glycine	2.0 M
SDS	1 % (w/v)

4x Gel-loading Buffer:

Tris-base, pH 6.8	0.25 M
SDS	6 % (w/v)
Sucrose	40 % (w/v)
Bromophenolblue	0.04 % (w/v)

For a working volume of 10 ml: 5 ml 4x Upper Tris Buffer, 0.6 g SDS, 4 g Sucrose, 4 mg Bromophenolblue. Fill up to 8 ml with ddH_2O, aliquot and store at -20℃. Prior to use, add β-Mercaptoethanol to a final concentration of 20 % (1/5 volume).

4x Lower Tris Buffer (pH to 8.8; Separation gel buffer):

Tris-base	1.5 M
SDS	0.4 % (w/v)

4x Upper Tris Buffer (pH 6.8; Stacking gel buffer):

Tris-base	0.5 M
SDS	0.4 % (w/v)

Semi-dry Transfer Buffer (pH 8.3):

Glycine	150 mM
Tris-base	25 mM
Methanol	10 % (v/v)

0.1% Tween20 in PBS (PBT)

TEMED	stock solution (Biorad)
Acrylamide-Bis (29:1)	stock solution (Biorad)
Isopropanol	
APS	10 % (w/v; 100 mg/1 ml ddH_2O)

Kaleidoscope protein marker (Biorad, Hercules, USA)

Protein transfer

Transfer system: Biorad MiniProtean Tetra Cell system
Nitrocellulose membrane (Biorad)
0.1% Tween20 in PBS (PBT)

Transfer buffer:

Tris-base	25 mM
Glycine	192 mM
20% Methanol	200 ml/l (vol/vol), add immediately before use

Protein Detection

9E10	recognizing the Myc tag; diluted 1:250 in 5% milk powder (low fat) in PBT (from the Developmental Studies Hybridoma Bank, University of Iowa, Iowa City, IA)
SαM HRP	Sheep anti-mouse horseradish peroxidase diluted 1:8000 in 5% milk powder (low fat) in PBT (Sigma).

ECL™ Western Blotting Detection Kit from Amersham (RPN 2109)

7. References

Bagri, A., Cheng, H. J., Yaron, A., Pleasure, S. J. and Tessier-Lavigne, M. (2003). Stereotyped pruning of long hippocampal axon branches triggered by retraction inducers of the semaphorin family. *Cell* **113**, 285-99.

Bagri, A., Marin, O., Plump, A. S., Mak, J., Pleasure, S. J., Rubenstein, J. L. and Tessier-Lavigne, M. (2002). Slit proteins prevent midline crossing and determine the dorsoventral position of major axonal pathways in the mammalian forebrain. *Neuron* **33**, 233-48.

Bandtlow, C. E. and Zimmermann, D. R. (2000). Proteoglycans in the developing brain: new conceptual insights for old proteins. *Physiol Rev* **80**, 1267-90.

Barnea, G., Grumet, M., Milev, P., Silvennoinen, O., Levy, J. B., Sap, J. and Schlessinger, J. (1994). Receptor tyrosine phosphatase beta is expressed in the form of proteoglycan and binds to the extracellular matrix protein tenascin. *J Biol Chem* **269**, 14349-52.

Battye, R., Stevens, A., Perry, R. L. and Jacobs, J. R. (2001). Repellent signaling by Slit requires the leucine-rich repeats. *J Neurosci* **21**, 4290-8.

Behar, O., Golden, J. A., Mashimo, H., Schoen, F. J. and Fishman, M. C. (1996). Semaphorin III is needed for normal patterning and growth of nerves, bones and heart. *Nature* **383**, 525-8.

Bossing, T. and Brand, A. H. (2002). Dephrin, a transmembrane ephrin with a unique structure, prevents interneuronal axons from exiting the Drosophila embryonic CNS. *Development* **129**, 4205-18.

Bourikas, D. Molecular mechanisms of axon guidance. Diss. Univ. Zürich, 2005

Bourikas, D., Pekarik, V., Baeriswyl, T., Grunditz, A., Sadhu, R., Nardo, M. and Stoeckli, E. T. (2005). Sonic hedgehog guides commissural axons along the longitudinal axis of the spinal cord. *Nat Neurosci* **8**, 297-304.

Brent, A. E. and Tabin, C. J. (2002). Developmental regulation of somite derivatives: muscle, cartilage and tendon. *Curr Opin Genet Dev* **12**, 548-57.

Brose, K., Bland, K. S., Wang, K. H., Arnott, D., Henzel, W., Goodman, C. S., Tessier-Lavigne, M. and Kidd, T. (1999). Slit proteins bind Robo receptors and have an evolutionarily conserved role in repulsive axon guidance. *Cell* **96**, 795-806.

Brown, C. B., Feiner, L., Lu, M. M., Li, J., Ma, X., Webber, A. L., Jia, L., Raper, J. A. and Epstein, J. A. (2001). PlexinA2 and semaphorin signaling during cardiac neural crest development. *Development* **128**, 3071-80.

Brummendorf, T., Hubert, M., Treubert, U., Leuschner, R., Tarnok, A. and Rathjen, F. G. (1993). The axonal recognition molecule F11 is a multifunctional protein: specific domains mediate interactions with Ng-CAM and restrictin. *Neuron* **10**, 711-27.

Buchli, A. D., Rouiller, E., Mueller, R., Dietz, V. and Schwab, M. E. (2007). Repair of the injured spinal cord. A joint approach of basic and clinical research. *Neurodegener Dis* **4**, 51-6.

Caldero, J., Prevette, D., Mei, X., Oakley, R. A., Li, L., Milligan, C., Houenou, L., Burek, M. and Oppenheim, R. W. (1998). Peripheral target regulation of the development and survival of spinal sensory and motor neurons in the chick embryo. *J Neurosci* **18**, 356-70.

Castellani, V., De Angelis, E., Kenwrick, S. and Rougon, G. (2002). Cis and trans interactions of L1 with neuropilin-1 control axonal responses to semaphorin 3A. *EMBO J* **21**, 6348-57.

Cauthen, C. A., Berdougo, E., Sandler, J. and Burrus, L. W. (2001). Comparative analysis of the expression patterns of Wnts and Frizzleds during early myogenesis in chick embryos. *Mech Dev* **104**, 133-8.

Challa, A. K., Beattie, C. E. and Seeger, M. A. (2001). Identification and characterization of roundabout orthologs in zebrafish. *Mech Dev* **101**, 249-53.

Chiquet-Ehrismann, R. and Chiquet, M. (2003). Tenascins: regulation and putative functions during pathological stress. *J Pathol* **200**, 488-99.

Chong, M. S., Woolf, C. J., Haque, N. S. and Anderson, P. N. (1999). Axonal regeneration from injured dorsal roots into the spinal cord of adult rats. *J Comp Neurol* **410**, 42-54.

Christ, B., Huang, R. and Scaal, M. (2004). Formation and differentiation of the avian sclerotome. *Anat Embryol (Berl)* **208**, 333-50.

Christ, B., Jacob, H. J. and Jacob, M. (1972). [Experimental analysis of somitogenesis in the chick embryo]. *Z Anat Entwicklungsgesch* **138**, 82-97.

Christ, B., Jacob, H. J. and Jacob, M. (1979). Differentiating abilities of avian somatopleural mesoderm. *Experientia* **35**, 1376-8.

Christ, B., Schmidt, C., Huang, R., Wilting, J. and Brand-Saberi, B. (1998). Segmentation of the vertebrate body. *Anat Embryol (Berl)* **197**, 1-8.

Coles, E. G., Gammill, L. S., Miner, J. H. and Bronner-Fraser, M. (2006). Abnormalities in neural crest cell migration in laminin alpha5 mutant mice. *Dev Biol* **289**, 218-28.

Cowan, C. A. and Henkemeyer, M. (2002). Ephrins in reverse, park and drive. *Trends Cell Biol* **12**, 339-46.

Crowley, C., Spencer, S. D., Nishimura, M. C., Chen, K. S., Pitts-Meek, S., Armanini, M. P., Ling, L. H., McMahon, S. B., Shelton, D. L., Levinson, A. D. et al. (1994). Mice lacking nerve growth factor display perinatal loss of sensory and sympathetic neurons yet develop basal forebrain cholinergic neurons. *Cell* **76**, 1001-11.

Davis, B. M., Frank, E., Johnson, F. A. and Scott, S. A. (1989). Development of central projections of lumbosacral sensory neurons in the chick. *J Comp Neurol* **279**, 556-66.

Davy, A. and Soriano, P. (2005). Ephrin signaling in vivo: look both ways. *Dev Dyn* **232**, 1-10.

De Bellard, M. E., Rao, Y. and Bronner-Fraser, M. (2003). Dual function of Slit2 in repulsion and enhanced migration of trunk, but not vagal, neural crest cells. *J Cell Biol* **162**, 269-79.

Debby-Brafman, A., Burstyn-Cohen, T., Klar, A. and Kalcheim, C. (1999). F-Spondin, expressed in somite regions avoided by neural crest cells, mediates inhibition of distinct somite domains to neural crest migration. *Neuron* **22**, 475-88.

Delaire, S., Billard, C., Tordjman, R., Chedotal, A., Elhabazi, A., Bensussan, A. and Boumsell, L. (2001). Biological activity of soluble CD100. II. Soluble CD100, similarly to H-SemaIII, inhibits immune cell migration. *J Immunol* **166**, 4348-54.

Dickson, B. J. and Gilestro, G. F. (2006). Regulation of commissural axon pathfinding by slit and its Robo receptors. *Annu Rev Cell Dev Biol* **22**, 651-75.

Dours-Zimmermann, M. T. and Zimmermann, D. R. (1994). A novel glycosaminoglycan attachment domain identified in two alternative splice variants of human versican. *J Biol Chem* **269**, 32992-8.

Dutt, S., Kleber, M., Matasci, M., Sommer, L. and Zimmermann, D. R. (2006). Versican V0 and V1 guide migratory neural crest cells. *J Biol Chem* **281**, 12123-31.

Dutt, S., Matasci, M., Sommer, L. and Zimmermann, D. R. (2006). Guidance of neural crest cell migration: the inhibitory function of the chondroitin sulfate proteoglycan, versican. *ScientificWorldJournal* **6**, 1114-7.

Eberhart, J., Barr, J., O'Connell, S., Flagg, A., Swartz, M. E., Cramer, K. S., Tosney, K. W., Pasquale, E. B. and Krull, C. E. (2004). Ephrin-A5 exerts positive or inhibitory effects on distinct subsets of EphA4-positive motor neurons. *J Neurosci* **24**, 1070-8.

Eberhart, J., Swartz, M., Koblar, S. A., Pasquale, E. B., Tanaka, H. and Krull, C. E. (2000). Expression of EphA4, ephrin-A2 and ephrin-A5 during axon outgrowth to the hindlimb indicates potential roles in pathfinding. *Dev Neurosci* **22**, 237-50.

Eickholt, B. J., Mackenzie, S. L., Graham, A., Walsh, F. S. and Doherty, P. (1999). Evidence for collapsin-1 functioning in the control of neural crest migration in both trunk and hindbrain regions. *Development* **126**, 2181-9.

Englund, C., Steneberg, P., Falileeva, L., Xylourgidis, N. and Samakovlis, C. (2002). Attractive and repulsive functions of Slit are mediated by different receptors in the Drosophila trachea. *Development* **129**, 4941-51.

Ernfors, P., Lee, K. F. and Jaenisch, R. (1994). Mice lacking brain-derived neurotrophic factor develop with sensory deficits. *Nature* **368**, 147-50.

Ernfors, P., Lee, K. F. and Jaenisch, R. (1994). Target derived and putative local actions of neurotrophins in the peripheral nervous system. *Prog Brain Res* **103**, 43-54.

Ernfors, P., Lee, K. F., Kucera, J. and Jaenisch, R. (1994). Lack of neurotrophin-3 leads to deficiencies in the peripheral nervous system and loss of limb proprioceptive afferents. *Cell* **77**, 503-12.

Erskine, L., Williams, S. E., Brose, K., Kidd, T., Rachel, R. A., Goodman, C. S., Tessier-Lavigne, M. and Mason, C. A. (2000). Retinal ganglion cell axon guidance in the mouse optic chiasm: expression and function of robos and slits. *J Neurosci* **20**, 4975-82.

Evanko, S. P., Tammi, M. I., Tammi, R. H. and Wight, T. N. (2007). Hyaluronan-dependent pericellular matrix. *Adv Drug Deliv Rev* **59**, 1351-65.

Fan, C. M., Porter, J. A., Chiang, C., Chang, D. T., Beachy, P. A. and Tessier-Lavigne, M. (1995). Long-range sclerotome induction by sonic hedgehog: direct role of the amino-terminal cleavage product and modulation by the cyclic AMP signaling pathway. *Cell* **81**, 457-65.

Fan, C. M. and Tessier-Lavigne, M. (1994). Patterning of mammalian somites by surface ectoderm and notochord: evidence for sclerotome induction by a hedgehog homolog. *Cell* **79**, 1175-86.

Fire, A., Xu, S., Montgomery, M. K., Kostas, S. A., Driver, S. E. and Mello, C. C. (1998). Potent and specific genetic interference by double-stranded RNA in Caenorhabditis elegans. *Nature* **391**, 806-11.

Fitzli, D., Stoeckli, E. T., Kunz, S., Siribour, K., Rader, C., Kunz, B., Kozlov, S. V., Buchstaller, A., Lane, R. P., Suter, D. M. et al. (2000). A direct interaction of axonin-1 with NgCAM-related cell adhesion molecule (NrCAM) results in guidance, but not growth of commissural axons. *J Cell Biol* **149**, 951-68.

Fraher, J. P., Dockery, P., O'Donoghue, O., Riedewald, B. and O'Leary, D. (2007). Initial motor axon outgrowth from the developing central nervous system. *J Anat* **211**, 600-11.

Fraser, S. E. and Bronner-Fraser, M. (1991). Migrating neural crest cells in the trunk of the avian embryo are multipotent. *Development* **112**, 913-20.

Fricke, C., Lee, J. S., Geiger-Rudolph, S., Bonhoeffer, F. and Chien, C. B. (2001). astray, a zebrafish roundabout homolog required for retinal axon guidance. *Science* **292**, 507-10.

Fu, S. Y., Sharma, K., Luo, Y., Raper, J. A. and Frank, E. (2000). SEMA3A regulates developing sensory projections in the chicken spinal cord. *J Neurobiol* **45**, 227-36.

Fujii, T., Nakao, F., Shibata, Y., Shioi, G., Kodama, E., Fujisawa, H. and Takagi, S. (2002). Caenorhabditis elegans PlexinA, PLX-1, interacts with transmembrane semaphorins and regulates epidermal morphogenesis. *Development* **129**, 2053-63.

Gale, N. W., Holland, S. J., Valenzuela, D. M., Flenniken, A., Pan, L., Ryan, T. E., Henkemeyer, M., Strebhardt, K., Hirai, H., Wilkinson, D. G. et al. (1996). Eph receptors and ligands comprise two major specificity subclasses and are reciprocally compartmentalized during embryogenesis. *Neuron* **17**, 9-19.

Gammill, L. S., Gonzalez, C., Gu, C. and Bronner-Fraser, M. (2006). Guidance of trunk neural crest migration requires neuropilin 2/semaphorin 3F signaling. *Development* **133**, 99-106.

George, S. E., Simokat, K., Hardin, J. and Chisholm, A. D. (1998). The VAB-1 Eph receptor tyrosine kinase functions in neural and epithelial morphogenesis in C. elegans. *Cell* **92**, 633-43.

Giniger, E., Jan, L. Y. and Jan, Y. N. (1993). Specifying the path of the intersegmental nerve of the Drosophila embryo: a role for Delta and Notch. *Development* **117**, 431-40.

Ginzburg, V. E., Roy, P. J. and Culotti, J. G. (2002). Semaphorin 1a and semaphorin 1b are required for correct epidermal cell positioning and adhesion during morphogenesis in C. elegans. *Development* **129**, 2065-78.

Giordano, S., Corso, S., Conrotto, P., Artigiani, S., Gilestro, G., Barberis, D., Tamagnone, L. and Comoglio, P. M. (2002). The semaphorin 4D receptor controls invasive growth by coupling with Met. *Nat Cell Biol* **4**, 720-4.

Golding, J. P. and Cohen, J. (1997). Border controls at the mammalian spinal cord: late-surviving neural crest boundary cap cells at dorsal root entry sites may regulate sensory afferent ingrowth and entry zone morphogenesis. *Mol Cell Neurosci* **9**, 381-96.

Hamburger, V. and Hamilton, H. L. (1992). A series of normal stages in the development of the chick embryo. 1951. *Dev Dyn* **195**, 231-72.

Harris, K. L. and Whitington, P. M. (2001). Pathfinding by sensory axons in Drosophila: substrates and choice points in early lch5 axon outgrowth. *J Neurobiol* **48**, 243-55.

He, Z. and Tessier-Lavigne, M. (1997). Neuropilin is a receptor for the axonal chemorepellent Semaphorin III. *Cell* **90**, 739-51.

He, Z., Wang, K. C., Koprivica, V., Ming, G. and Song, H. J. (2002). Knowing how to navigate: mechanisms of semaphorin signaling in the nervous system. *Sci STKE* **2002**, RE1.

Helenius, I. T. and Beitel, G. J. (2008). The first "Slit" is the deepest: the secret to a hollow heart. *J Cell Biol* **182**, 221-3.

Himanen, J. P., Chumley, M. J., Lackmann, M., Li, C., Barton, W. A., Jeffrey, P. D., Vearing, C., Geleick, D., Feldheim, D. A., Boyd, A. W. et al. (2004). Repelling class discrimination: ephrin-A5 binds to and activates EphB2 receptor signaling. *Nat Neurosci* **7**, 501-9.

Hindges, R., McLaughlin, T., Genoud, N., Henkemeyer, M. and O'Leary, D. D. (2002). EphB forward signaling controls directional branch extension and arborization required for dorsal-ventral retinotopic mapping. *Neuron* **35**, 475-87.

Hivert, B., Liu, Z., Chuang, C. Y., Doherty, P. and Sundaresan, V. (2002). Robo1 and Robo2 are homophilic binding molecules that promote axonal growth. *Mol Cell Neurosci* **21**, 534-45.

Hoang, B. H., Thomas, J. T., Abdul-Karim, F. W., Correia, K. M., Conlon, R. A., Luyten, F. P. and Ballock, R. T. (1998). Expression pattern of two Frizzled-related genes, Frzb-1 and Sfrp-1, during mouse embryogenesis suggests a role for modulating action of Wnt family members. *Dev Dyn* **212**, 364-72.

Holder, N. and Klein, R. (1999). Eph receptors and ephrins: effectors of morphogenesis. *Development* **126**, 2033-44.

Holmes, G. and Niswander, L. (2001). Expression of slit-2 and slit-3 during chick development. *Dev Dyn* **222**, 301-7.

Howitt, J. A., Clout, N. J. and Hohenester, E. (2004). Binding site for Robo receptors revealed by dissection of the leucine-rich repeat region of Slit. *EMBO J* **23**, 4406-12.

Huber, A. B., Kolodkin, A. L., Ginty, D. D. and Cloutier, J. F. (2003). Signaling at the growth cone: ligand-receptor complexes and the control of axon growth and guidance. *Annu Rev Neurosci* **26**, 509-63.

Huber, A. B., Kania, A., Tran, T. S., Gu, C., De Marco Garcia, N., Lieberam, I., Johnson, D., Jessell, T. M., Ginty, D. D. and Kolodkin, A. L. (2005). Distinct roles for secreted semaphorin signaling in spinal motor axon guidance. *Neuron* **48**, 949-64.

Ikeya, M. and Takada, S. (1998). Wnt signaling from the dorsal neural tube is required for the formation of the medial dermomyotome. *Development* **125**, 4969-76.

Jia, L., Cheng, L. and Raper, J. (2005). Slit/Robo signaling is necessary to confine early neural crest cells to the ventral migratory pathway in the trunk. *Dev Biol* **282**, 411-21.

Johnson, R. L., Laufer, E., Riddle, R. D. and Tabin, C. (1994). Ectopic expression of Sonic hedgehog alters dorsal-ventral patterning of somites. *Cell* **79**, 1165-73.

Karlstrom, R. O., Trowe, T., Klostermann, S., Baier, H., Brand, M., Crawford, A. D., Grunewald, B., Haffter, P., Hoffmann, H., Meyer, S. U. et al. (1996). Zebrafish mutations affecting retinotectal axon pathfinding. *Development* **123**, 427-38.

Keleman, K., Rajagopalan, S., Cleppien, D., Teis, D., Paiha, K., Huber, L. A., Technau, G. M. and Dickson, B. J. (2002). Comm sorts robo to control axon guidance at the Drosophila midline. *Cell* **110**, 415-27.

Kidd, T., Bland, K. S. and Goodman, C. S. (1999). Slit is the midline repellent for the robo receptor in Drosophila. *Cell* **96**, 785-94.

Kidd, T., Brose, K., Mitchell, K. J., Fetter, R. D., Tessier-Lavigne, M., Goodman, C. S. and Tear, G. (1998). Roundabout controls axon crossing of the CNS midline and defines a novel subfamily of evolutionarily conserved guidance receptors. *Cell* **92**, 205-15.

Klein, R. (1994). Role of neurotrophins in mouse neuronal development. *FASEB J* **8**, 738-44.

Knoll, B., Zarbalis, K., Wurst, W. and Drescher, U. (2001). A role for the EphA family in the topographic targeting of vomeronasal axons. *Development* **128**, 895-906.

Kolodkin, A. L. and Ginty, D. D. (1997). Steering clear of semaphorins: neuropilins sound the retreat. *Neuron* **19**, 1159-62.

Kolodkin, A. L., Levengood, D. V., Rowe, E. G., Tai, Y. T., Giger, R. J. and Ginty, D. D. (1997). Neuropilin is a semaphorin III receptor. *Cell* **90**, 753-62.

Kramer, S. G., Kidd, T., Simpson, J. H. and Goodman, C. S. (2001). Switching repulsion to attraction: changing responses to slit during transition in mesoderm migration. *Science* **292**, 737-40.

Krull, C. E., Lansford, R., Gale, N. W., Collazo, A., Marcelle, C., Yancopoulos, G. D., Fraser, S. E. and Bronner-Fraser, M. (1997). Interactions of Eph-related receptors and ligands confer rostrocaudal pattern to trunk neural crest migration. *Curr Biol* **7**, 571-80.

Kuhn, T. B., Stoeckli, E. T., Condrau, M. A., Rathjen, F. G. and Sonderegger, P. (1991). Neurite outgrowth on immobilized axonin-1 is mediated by a heterophilic interaction with L1(G4). *J Cell Biol* **115**, 1113-26.

Kullander, K., Croll, S. D., Zimmer, M., Pan, L., McClain, J., Hughes, V., Zabski, S., DeChiara, T. M., Klein, R., Yancopoulos, G. D. et al. (2001). Ephrin-B3 is the midline barrier that prevents corticospinal tract axons from recrossing, allowing for unilateral motor control. *Genes Dev* **15**, 877-88.

Kullander, K. and Klein, R. (2002). Mechanisms and functions of Eph and ephrin signalling. *Nat Rev Mol Cell Biol* **3**, 475-86.

Kullander, K., Mather, N. K., Diella, F., Dottori, M., Boyd, A. W. and Klein, R. (2001). Kinase-dependent and kinase-independent functions of EphA4 receptors in major axon tract formation in vivo. *Neuron* **29**, 73-84.

Kultti, A., Rilla, K., Tiihonen, R., Spicer, A. P., Tammi, R. H. and Tammi, M. I. (2006). Hyaluronan synthesis induces microvillus-like cell surface protrusions. *J Biol Chem* **281**, 15821-8.

Landolt, R. M., Vaughan, L., Winterhalter, K. H. and Zimmermann, D. R. (1995). Versican is selectively expressed in embryonic tissues that act as barriers to neural crest cell migration and axon outgrowth. *Development* **121**, 2303-12.

Legg, J. A., Herbert, J. M., Clissold, P. and Bicknell, R. (2008). Slits and Roundabouts in cancer, tumour angiogenesis and endothelial cell migration. *Angiogenesis* **11**, 13-21.

Liu, Z., Patel, K., Schmidt, H., Andrews, W., Pini, A. and Sundaresan, V. (2004). Extracellular Ig domains 1 and 2 of Robo are important for ligand (Slit) binding. *Mol Cell Neurosci* **26**, 232-40.

Long, H., Sabatier, C., Ma, L., Plump, A., Yuan, W., Ornitz, D. M., Tamada, A., Murakami, F., Goodman, C. S. and Tessier-Lavigne, M. (2004). Conserved roles for Slit and Robo proteins in midline commissural axon guidance. *Neuron* **42**, 213-23.

Lopez-Bendito, G., Flames, N., Ma, L., Fouquet, C., Di Meglio, T., Chedotal, A., Tessier-Lavigne, M. and Marin, O. (2007). Robo1 and Robo2 cooperate to control the guidance of major axonal tracts in the mammalian forebrain. *J Neurosci* **27**, 3395-407.

Ma, L. and Tessier-Lavigne, M. (2007). Dual branch-promoting and branch-repelling actions of Slit/Robo signaling on peripheral and central branches of developing sensory axons. *J Neurosci* **27**, 6843-51.

Maeda, N. and Noda, M. (1996). 6B4 proteoglycan/phosphacan is a repulsive substratum but promotes morphological differentiation of cortical neurons. *Development* **122**, 647-58.

Maier, I. C., Ichiyama, R. M., Courtine, G., Schnell, L., Lavrov, I., Edgerton, V. R. and Schwab, M. E. (2009). Differential effects of anti-Nogo-A antibody treatment and treadmill training in rats with incomplete spinal cord injury. *Brain* **132**, 1426-40.

Mambetisaeva, E. T., Andrews, W., Camurri, L., Annan, A. and Sundaresan, V. (2005). Robo family of proteins exhibit differential expression in mouse spinal cord and Robo-Slit interaction is required for midline crossing in vertebrate spinal cord. *Dev Dyn* **233**, 41-51.

Mann, F., Ray, S., Harris, W. and Holt, C. (2002). Topographic mapping in dorsoventral axis of the Xenopus retinotectal system depends on signaling through ephrin-B ligands. *Neuron* **35**, 461-73.

Margolis, R. K., Rauch, U., Maurel, P. and Margolis, R. U. (1996). Neurocan and phosphacan: two major nervous tissue-specific chondroitin sulfate proteoglycans. *Perspect Dev Neurobiol* **3**, 273-90.

Marti, E., Takada, R., Bumcrot, D. A., Sasaki, H. and McMahon, A. P. (1995). Distribution of Sonic hedgehog peptides in the developing chick and mouse embryo. *Development* **121**, 2537-47.

Masuda, T. and Shiga, T. (2005). Chemorepulsion and cell adhesion molecules in patterning initial trajectories of sensory axons. *Neurosci Res* **51**, 337-47.

Maurel, P., Rauch, U., Flad, M., Margolis, R. K. and Margolis, R. U. (1994). Phosphacan, a chondroitin sulfate proteoglycan of brain that interacts with neurons and neural cell-adhesion molecules, is an extracellular variant of a receptor-type protein tyrosine phosphatase. *Proc Natl Acad Sci U S A* **91**, 2512-6.

Mauti, O., Domanitskaya, E., Andermatt, I., Sadhu, R. and Stoeckli, E. T. (2007). Semaphorin6A acts as a gate keeper between the central and the peripheral nervous system. *Neural Dev* **2**, 28.

Mauti, O., Sadhu, R., Gemayel, J., Gesemann, M. and Stoeckli, E. T. (2006). Expression patterns of plexins and neuropilins are consistent with cooperative and separate functions during neural development. *BMC Dev Biol* **6**, 32.

McMahon, J. A., Takada, S., Zimmerman, L. B., Fan, C. M., Harland, R. M. and McMahon, A. P. (1998). Noggin-mediated antagonism of BMP signaling is required for growth and patterning of the neural tube and somite. *Genes Dev* **12**, 1438-52.

Medioni, C., Astier, M., Zmojdzian, M., Jagla, K. and Semeriva, M. (2008). Genetic control of cell morphogenesis during Drosophila melanogaster cardiac tube formation. *J Cell Biol* **182**, 249-61.

Messersmith, E. K., Leonardo, E. D., Shatz, C. J., Tessier-Lavigne, M., Goodman, C. S. and Kolodkin, A. L. (1995). Semaphorin III can function as a selective chemorepellent to pattern sensory projections in the spinal cord. *Neuron* **14**, 949-59.

Miao, H. Q., Soker, S., Feiner, L., Alonso, J. L., Raper, J. A. and Klagsbrun, M. (1999). Neuropilin-1 mediates collapsin-1/semaphorin III inhibition of endothelial cell motility: functional competition of collapsin-1 and vascular endothelial growth factor-165. *J Cell Biol* **146**, 233-42.

Mjaatvedt, C. H., Yamamura, H., Capehart, A. A., Turner, D. and Markwald, R. R. (1998). The Cspg2 gene, disrupted in the hdf mutant, is required for right cardiac chamber and endocardial cushion formation. *Dev Biol* **202**, 56-66.

Montgomery, M. K. and Fire, A. (1998). Double-stranded RNA as a mediator in sequence-specific genetic silencing and co-suppression. *Trends Genet* **14**, 255-8.

Montgomery, M. K., Xu, S. and Fire, A. (1998). RNA as a target of double-stranded RNA-mediated genetic interference in Caenorhabditis elegans. *Proc Natl Acad Sci U S A* **95**, 15502-7.

Morales, G., Hubert, M., Brummendorf, T., Treubert, U., Tarnok, A., Schwarz, U. and Rathjen, F. G. (1993). Induction of axonal growth by heterophilic interactions between the cell surface recognition proteins F11 and Nr-CAM/Bravo. *Neuron* **11**, 1113-22.

Moreno-Flores, M. T., Martin-Aparicio, E., Martin-Bermejo, M. J., Agudo, M., McMahon, S., Avila, J., Diaz-Nido, J. and Wandosell, F. (2003). Semaphorin 3C preserves survival and induces neuritogenesis of cerebellar granule neurons in culture. *J Neurochem* **87**, 879-90.

Morgelin, M., Paulsson, M., Malmstrom, A. and Heinegard, D. (1989). Shared and distinct structural features of interstitial proteoglycans from different bovine tissues revealed by electron microscopy. *J Biol Chem* **264**, 12080-90.

Muller, T. S., Ebensperger, C., Neubuser, A., Koseki, H., Balling, R., Christ, B. and Wilting, J. (1996). Expression of avian Pax1 and Pax9 is intrinsically regulated in the pharyngeal endoderm, but depends on environmental influences in the paraxial mesoderm. *Dev Biol* **178**, 403-17.

Murai, K. K. and Pasquale, E. B. (2003). 'Eph'ective signaling: forward, reverse and crosstalk. *J Cell Sci* **116**, 2823-32.

Muramatsu, T., Mizutani, Y., Ohmori, Y. and Okumura, J. (1997). Comparison of three nonviral transfection methods for foreign gene expression in early chicken embryos in ovo. *Biochem Biophys Res Commun* **230**, 376-80.

Murray, M. J. and Whitington, P. M. (1999). Effects of roundabout on growth cone dynamics, filopodial length, and growth cone morphology at the midline and throughout the neuropile. *J Neurosci* **19**, 7901-12.

Nakamoto, M. (2000). Eph receptors and ephrins. *Int J Biochem Cell Biol* **32**, 7-12.

Nguyen Ba-Charvet, K. T., Brose, K., Ma, L., Wang, K. H., Marillat, V., Sotelo, C., Tessier-Lavigne, M. and Chedotal, A. (2001). Diversity and specificity of actions of Slit2 proteolytic fragments in axon guidance. *J Neurosci* **21**, 4281-9.

Niederlander, C. and Lumsden, A. (1996). Late emigrating neural crest cells migrate specifically to the exit points of cranial branchiomotor nerves. *Development* **122**, 2367-74.

Niederost, B. P., Zimmermann, D. R., Schwab, M. E. and Bandtlow, C. E. (1999). Bovine CNS myelin contains neurite growth-inhibitory activity associated with chondroitin sulfate proteoglycans. *J Neurosci* **19**, 8979-89.

Oakley, R. A. and Tosney, K. W. (1991). Peanut agglutinin and chondroitin-6-sulfate are molecular markers for tissues that act as barriers to axon advance in the avian embryo. *Dev Biol* **147**, 187-206.

O'Leary, D. D. and Wilkinson, D. G. (1999). Eph receptors and ephrins in neural development. *Curr Opin Neurobiol* **9**, 65-73.

Olivera-Martinez, I., Thelu, J., Teillet, M. A. and Dhouailly, D. (2001). Dorsal dermis development depends on a signal from the dorsal neural tube, which can be substituted by Wnt-1. *Mech Dev* **100**, 233-44.

Orioli, D. and Klein, R. (1997). The Eph receptor family: axonal guidance by contact repulsion. *Trends Genet* **13**, 354-9.

Ozaki, S. and Snider, W. D. (1997). Initial trajectories of sensory axons toward laminar targets in the developing mouse spinal cord. *J Comp Neurol* **380**, 215-29.

Parsons, L., Harris, K. L., Turner, K. and Whitington, P. M. (2003). Roundabout gene family functions during sensory axon guidance in the drosophila embryo are mediated by both Slit-dependent and Slit-independent mechanisms. *Dev Biol* **264**, 363-75.

Pasquale, E. B. (1997). The Eph family of receptors. *Curr Opin Cell Biol* **9**, 608-15.

Pasterkamp, R. J., Peschon, J. J., Spriggs, M. K. and Kolodkin, A. L. (2003). Semaphorin 7A promotes axon outgrowth through integrins and MAPKs. *Nature* **424**, 398-405.

Pekarik, V., Bourikas, D., Miglino, N., Joset, P., Preiswerk, S. and Stoeckli, E. T. (2003). Screening for gene function in chicken embryo using RNAi and electroporation. *Nat Biotechnol* **21**, 93-6.

Perrin, F. E., Rathjen, F. G. and Stoeckli, E. T. (2001). Distinct subpopulations of sensory afferents require F11 or axonin-1 for growth to their target layers within the spinal cord of the chick. *Neuron* **30**, 707-23.

Perris, R., Krotoski, D. and Bronner-Fraser, M. (1991). Collagens in avian neural crest development: distribution in vivo and migration-promoting ability in vitro. *Development* **113**, 969-84.

Pfeffer, S. and Aivazian, D. (2004). Targeting Rab GTPases to distinct membrane compartments. *Nat Rev Mol Cell Biol* **5**, 886-96.

Plump, A. S., Erskine, L., Sabatier, C., Brose, K., Epstein, C. J., Goodman, C. S., Mason, C. A. and Tessier-Lavigne, M. (2002). Slit1 and Slit2 cooperate to prevent premature midline crossing of retinal axons in the mouse visual system. *Neuron* **33**, 219-32.

Poliakov, A., Cotrina, M. and Wilkinson, D. G. (2004). Diverse roles of eph receptors and ephrins in the regulation of cell migration and tissue assembly. *Dev Cell* **7**, 465-80.

Polleux, F., Morrow, T. and Ghosh, A. (2000). Semaphorin 3A is a chemoattractant for cortical apical dendrites. *Nature* **404**, 567-73.

Puschel, A. W., Adams, R. H. and Betz, H. (1996). The sensory innervation of the mouse spinal cord may be patterned by differential expression of and differential responsiveness to semaphorins. *Mol Cell Neurosci* **7**, 419-31.

Rajagopalan, S., Nicolas, E., Vivancos, V., Berger, J. and Dickson, B. J. (2000). Crossing the midline: roles and regulation of Robo receptors. *Neuron* **28**, 767-77.

Rajagopalan, S., Vivancos, V., Nicolas, E. and Dickson, B. J. (2000). Selecting a longitudinal pathway: Robo receptors specify the lateral position of axons in the Drosophila CNS. *Cell* **103**, 1033-45.

Ranscht, B. and Bronner-Fraser, M. (1991). T-cadherin expression alternates with migrating neural crest cells in the trunk of the avian embryo. *Development* **111**, 15-22.

Retzler, C., Gohring, W. and Rauch, U. (1996). Analysis of neurocan structures interacting with the neural cell adhesion molecule N-CAM. *J Biol Chem* **271**, 27304-10.

Retzler, C., Wiedemann, H., Kulbe, G. and Rauch, U. (1996). Structural and electron microscopic analysis of neurocan and recombinant neurocan fragments. *J Biol Chem* **271**, 17107-13.

Rickmann, M., Fawcett, J. W. and Keynes, R. J. (1985). The migration of neural crest cells and the growth of motor axons through the rostral half of the chick somite. *J Embryol Exp Morphol* **90**, 437-55.

Rilla, K., Tiihonen, R., Kultti, A., Tammi, M. and Tammi, R. (2008). Pericellular hyaluronan coat visualized in live cells with a fluorescent probe is scaffolded by plasma membrane protrusions. *J Histochem Cytochem* **56**, 901-10.

Robinson, V., Smith, A., Flenniken, A. M. and Wilkinson, D. G. (1997). Roles of Eph receptors and ephrins in neural crest pathfinding. *Cell Tissue Res* **290**, 265-74.

Roffers-Agarwal, J. and Gammill, L. S. (2009). Neuropilin receptors guide distinct phases of sensory and motor neuronal segmentation. *Development* **136**, 1879-88.

Rovasio, R. A., Delouvee, A., Yamada, K. M., Timpl, R. and Thiery, J. P. (1983). Neural crest cell migration: requirements for exogenous fibronectin and high cell density. *J Cell Biol* **96**, 462-73.

Ruit, K. G., Elliott, J. L., Osborne, P. A., Yan, Q. and Snider, W. D. (1992). Selective dependence of mammalian dorsal root ganglion neurons on nerve growth factor during embryonic development. *Neuron* **8**, 573-87.

Sabatier, C., Plump, A. S., Le, M., Brose, K., Tamada, A., Murakami, F., Lee, E. Y. and Tessier-Lavigne, M. (2004). The divergent Robo family protein rig-1/Robo3 is a negative regulator of slit responsiveness required for midline crossing by commissural axons. *Cell* **117**, 157-69.

Santiago-Martinez, E., Soplop, N. H., Patel, R. and Kramer, S. G. (2008). Repulsion by Slit and Roundabout prevents Shotgun/E-cadherin-mediated cell adhesion during Drosophila heart tube lumen formation. *J Cell Biol* **182**, 241-8.

Scaal, M. and Christ, B. (2004). Formation and differentiation of the avian dermomyotome. *Anat Embryol (Berl)* **208**, 411-24.

Scaal, M., Gros, J., Lesbros, C. and Marcelle, C. (2004). In ovo electroporation of avian somites. *Dev Dyn* **229**, 643-50.

Schmalfeldt, M., Bandtlow, C. E., Dours-Zimmermann, M. T., Winterhalter, K. H. and Zimmermann, D. R. (2000). Brain derived versican V2 is a potent inhibitor of axonal growth. *J Cell Sci* **113 (Pt 5)**, 807-16.

Schwarz, Q., Maden, C. H., Vieira, J. M. and Ruhrberg, C. (2009). Neuropilin 1 signaling guides neural crest cells to coordinate pathway choice with cell specification. *Proc Natl Acad Sci U S A* **106**, 6164-9.

Scully, A. L., McKeown, M. and Thomas, J. B. (1999). Isolation and characterization of Dek, a Drosophila eph receptor protein tyrosine kinase. *Mol Cell Neurosci* **13**, 337-47.

Seeger, M., Tear, G., Ferres-Marco, D. and Goodman, C. S. (1993). Mutations affecting growth cone guidance in Drosophila: genes necessary for guidance toward or away from the midline. *Neuron* **10**, 409-26.

Serini, G., Valdembri, D., Zanivan, S., Morterra, G., Burkhardt, C., Caccavari, F., Zammataro, L., Primo, L., Tamagnone, L., Logan, M. et al. (2003). Class 3 semaphorins control vascular morphogenesis by inhibiting integrin function. *Nature* **424**, 391-7.

Shepherd, I. T., Luo, Y., Lefcort, F., Reichardt, L. F. and Raper, J. A. (1997). A sensory axon repellent secreted from ventral spinal cord explants is neutralized by antibodies raised against collapsin-1. *Development* **124**, 1377-85.

Shiau, C. E., Lwigale, P. Y., Das, R. M., Wilson, S. A. and Bronner-Fraser, M. (2008). Robo2-Slit1 dependent cell-cell interactions mediate assembly of the trigeminal ganglion. *Nat Neurosci* **11**, 269-76.

Shitara, K., Yamada, H., Watanabe, K., Shimonaka, M. and Yamaguchi, Y. (1994). Brain-specific receptor-type protein-tyrosine phosphatase RPTP beta is a chondroitin sulfate proteoglycan in vivo. *J Biol Chem* **269**, 20189-93.

Shoji, W., Isogai, S., Sato-Maeda, M., Obinata, M. and Kuwada, J. Y. (2003). Semaphorin3a1 regulates angioblast migration and vascular development in zebrafish embryos. *Development* **130**, 3227-36.

Simpson, J. H., Bland, K. S., Fetter, R. D. and Goodman, C. S. (2000). Short-range and long-range guidance by Slit and its Robo receptors: a combinatorial code of Robo receptors controls lateral position. *Cell* **103**, 1019-32.

Simpson, J. H., Kidd, T., Bland, K. S. and Goodman, C. S. (2000). Short-range and long-range guidance by slit and its Robo receptors. Robo and Robo2 play distinct roles in midline guidance. *Neuron* **28**, 753-66.

Smeyne, R. J., Klein, R., Schnapp, A., Long, L. K., Bryant, S., Lewin, A., Lira, S. A. and Barbacid, M. (1994). Severe sensory and sympathetic neuropathies in mice carrying a disrupted Trk/NGF receptor gene. *Nature* **368**, 246-9.

Smith, A., Robinson, V., Patel, K. and Wilkinson, D. G. (1997). The EphA4 and EphB1 receptor tyrosine kinases and ephrin-B2 ligand regulate targeted migration of branchial neural crest cells. *Curr Biol* **7**, 561-70.

Snider, W. D. (1994). Functions of the neurotrophins during nervous system development: what the knockouts are teaching us. *Cell* **77**, 627-38.

Snow, D. M., Lemmon, V., Carrino, D. A., Caplan, A. I. and Silver, J. (1990). Sulfated proteoglycans in astroglial barriers inhibit neurite outgrowth in vitro. *Exp Neurol* **109**, 111-30.

Song, H., Ming, G., He, Z., Lehmann, M., McKerracher, L., Tessier-Lavigne, M. and Poo, M. (1998). Conversion of neuronal growth cone responses from repulsion to attraction by cyclic nucleotides. *Science* **281**, 1515-8.

Spassky, N., de Castro, F., Le Bras, B., Heydon, K., Queraud-LeSaux, F., Bloch-Gallego, E., Chedotal, A., Zalc, B. and Thomas, J. L. (2002). Directional guidance of oligodendroglial migration by class 3 semaphorins and netrin-1. *J Neurosci* **22**, 5992-6004.

Stern, C. D., Norris, W. E., Bronner-Fraser, M., Carlson, G. J., Faissner, A., Keynes, R. J. and Schachner, M. (1989). J1/tenascin-related molecules are not responsible for the segmented pattern of neural crest cells or motor axons in the chick embryo. *Development* **107**, 309-19.

Stoeckli, E. T. and Landmesser, L. T. (1995). Axonin-1, Nr-CAM, and Ng-CAM play different roles in the in vivo guidance of chick commissural neurons. *Neuron* **14**, 1165-79.

Suter, D. M., Pollerberg, G. E., Buchstaller, A., Giger, R. J., Dreyer, W. J. and Sonderegger, P. (1995). Binding between the neural cell adhesion molecules axonin-1 and Nr-CAM/Bravo is involved in neuron-glia interaction. *J Cell Biol* **131**, 1067-81.

Tamagnone, L. and Comoglio, P. M. (2000). Signalling by semaphorin receptors: cell guidance and beyond. *Trends Cell Biol* **10**, 377-83.

Tamagnone, L. and Comoglio, P. M. (2004). To move or not to move? Semaphorin signalling in cell migration. *EMBO Rep* **5**, 356-61.

Tessarollo, L., Vogel, K. S., Palko, M. E., Reid, S. W. and Parada, L. F. (1994). Targeted mutation in the neurotrophin-3 gene results in loss of muscle sensory neurons. *Proc Natl Acad Sci U S A* **91**, 11844-8.

Tucker, R. P., Hagios, C., Chiquet-Ehrismann, R., Lawler, J., Hall, R. J. and Erickson, C. A. (1999). Thrombospondin-1 and neural crest cell migration. *Dev Dyn* **214**, 312-22.

Tucker, R. P. and McKay, S. E. (1991). The expression of tenascin by neural crest cells and glia. *Development* **112**, 1031-9.

Tuzi, N. L. and Gullick, W. J. (1994). eph, the largest known family of putative growth factor receptors. *Br J Cancer* **69**, 417-21.

Vaidya, A., Pniak, A., Lemke, G. and Brown, A. (2003). EphA3 null mutants do not demonstrate motor axon guidance defects. *Mol Cell Biol* **23**, 8092-8.

Vargesson, N., Luria, V., Messina, I., Erskine, L. and Laufer, E. (2001). Expression patterns of Slit and Robo family members during vertebrate limb development. *Mech Dev* **106**, 175-80.

Wang, B., Xiao, Y., Ding, B. B., Zhang, N., Yuan, X., Gui, L., Qian, K. X., Duan, S., Chen, Z., Rao, Y. et al. (2003). Induction of tumor angiogenesis by Slit-Robo signaling and inhibition of cancer growth by blocking Robo activity. *Cancer Cell* **4**, 19-29.

Wang, H. U. and Anderson, D. J. (1997). Eph family transmembrane ligands can mediate repulsive guidance of trunk neural crest migration and motor axon outgrowth. *Neuron* **18**, 383-96.

Wang, K. H., Brose, K., Arnott, D., Kidd, T., Goodman, C. S., Henzel, W. and Tessier-Lavigne, M. (1999). Biochemical purification of a mammalian slit protein as a positive regulator of sensory axon elongation and branching. *Cell* **96**, 771-84.

Wang, X., Roy, P. J., Holland, S. J., Zhang, L. W., Culotti, J. G. and Pawson, T. (1999). Multiple ephrins control cell organization in C. elegans using kinase-dependent and -independent functions of the VAB-1 Eph receptor. *Mol Cell* **4**, 903-13.

Wehrle, R., Camand, E., Chedotal, A., Sotelo, C. and Dusart, I. (2005). Expression of netrin-1, slit-1 and slit-3 but not of slit-2 after cerebellar and spinal cord lesions. *Eur J Neurosci* **22**, 2134-44.

Wilkinson, D. G. (2000). Eph receptors and ephrins: regulators of guidance and assembly. *Int Rev Cytol* **196**, 177-244.

Wong, K., Park, H. T., Wu, J. Y. and Rao, Y. (2002). Slit proteins: molecular guidance cues for cells ranging from neurons to leukocytes. *Curr Opin Genet Dev* **12**, 583-91.

Wong, K., Ren, X. R., Huang, Y. Z., Xie, Y., Liu, G., Saito, H., Tang, H., Wen, L., Brady-Kalnay, S. M., Mei, L. et al. (2001). Signal transduction in neuronal migration: roles of GTPase activating proteins and the small GTPase Cdc42 in the Slit-Robo pathway. *Cell* **107**, 209-21.

Xu, Q., Mellitzer, G. and Wilkinson, D. G. (2000). Roles of Eph receptors and ephrins in segmental patterning. *Philos Trans R Soc Lond B Biol Sci* **355**, 993-1002.

Yamada, H., Fredette, B., Shitara, K., Hagihara, K., Miura, R., Ranscht, B., Stallcup, W. B. and Yamaguchi, Y. (1997). The brain chondroitin sulfate proteoglycan brevican associates with astrocytes ensheathing cerebellar glomeruli and inhibits neurite outgrowth from granule neurons. *J Neurosci* **17**, 7784-95.

Yamagata, M. and Sanes, J. R. (2005). Versican in the developing brain: lamina-specific expression in interneuronal subsets and role in presynaptic maturation. *J Neurosci* **25**, 8457-67.

Yamaguchi, Y. (2000). Lecticans: organizers of the brain extracellular matrix. *Cell Mol Life Sci* **57**, 276-89.

Younossi-Hartenstein, A. and Hartenstein, V. (1993). The role of the tracheae and musculature during pathfinding of Drosophila embryonic sensory axons. *Dev Biol* **158**, 430-47.

Yuan, W., Zhou, L., Chen, J. H., Wu, J. Y., Rao, Y. and Ornitz, D. M. (1999). The mouse SLIT family: secreted ligands for ROBO expressed in patterns that suggest a role in morphogenesis and axon guidance. *Dev Biol* **212**, 290-306.

Zako, M., Shinomura, T., Ujita, M., Ito, K. and Kimata, K. (1995). Expression of PG-M(V3), an alternatively spliced form of PG-M without a chondroitin sulfate attachment in region in mouse and human tissues. *J Biol Chem* **270**, 3914-8.

Zallen, J. A., Kirch, S. A. and Bargmann, C. I. (1999). Genes required for axon pathfinding and extension in the C. elegans nerve ring. *Development* **126**, 3679-92.

Zallen, J. A., Yi, B. A. and Bargmann, C. I. (1998). The conserved immunoglobulin superfamily member SAX-3/Robo directs multiple aspects of axon guidance in C. elegans. *Cell* **92**, 217-27.

Zimmermann, D. R. and Dours-Zimmermann, M. T. (2008). Extracellular matrix of the central nervous system: from neglect to challenge. *Histochem Cell Biol* **130**, 635-53.

Zimmermann, D. R. and Ruoslahti, E. (1989). Multiple domains of the large fibroblast proteoglycan, versican. *EMBO J* **8**, 2975-81.

8. Acknowledgements

I am grateful to Prof. Dr. Esther T. Stoeckli for her great support and enthusiasm, her interesting discussions and her help in all kinds of questions during my entire dissertation.

I want to thank my thesis committee members Prof. Dr. Stephan Neuhauss and Prof. Dr. Dieter Zimmermann for giving me inputs and fruitful discussions.

My special thanks go to all the Stoeckli lab members, especially to Dr. Olivier Mauti, for the help and patience to overcome all kinds of problems, for being always ready to answer my questions and for the great atmosphere in and around the lab.

Additionally, I want to thank all the members of the Institute of Zoology for their support in technical and other questions.

Last but not least, my deepest gratitude belongs to my parents, my family and my girl friend, Nibra Habouch, without their support and patience I would not have been able to finish my studies.

9. Curriculum vitae

Surname: DEBRUNNER First name: Marc

Date of birth: 26th of August 1979 Nationality: Swiss

Education

2006 - 2010 PhD Thesis in Developmental Neuroscience, Institute of Zoology, University of Zurich

2004 - 2005 Diploma Thesis in Developmental Neuroscience, Institute of Zoology, University of Zürich
Topic: New roles for Slits and Robos in sensory axon guidance in the chicken embryo
Supervisor: Prof. Dr. Esther Stoeckli

2002 - 2004 Graduate studies in Reproduction Biology, Modern Genetics and Genomics, Developmental Biology and Developmental Neurobiology, University of Zürich

2000 - 2002 Undergraduate studies in Biology, University of Zurich

1992 – 1999 Gymnasium, Rychenberg Winterthur, Typus B

Meetings

2005 ZNZ Symposium in Zurich
2006 ZNZ Symposium in Zurich
2007 SSN meeting in Bern
ZNZ Symposium in Zurich
2008 NCCR meeting in Berlingen
FENS meeting in Geneva
ZNZ Symposium in Zurich
2009 ZNZ Symposium in Zurich

List of publications

Debrunner, M. and Stoeckli, E.T. The Slit / Robo system guides both neural crest cells and sensory axons towards their targets, in preparation.

Philipp, M., Niederkofler, V., Debrunner, M. and Stoeckli, E.T. RabGDI controls axonal midline crossing by regulating Robo1 surface expression, in revision.

Debrunner, M.*, Wacker, W.* and Stoeckli, E. T. Gene silencing by *in ovo* RNAi – an efficient method for functional gene analysis during vertebrate embryonic development, in preparation.